SKIN BLOOD FLOW OSCILLATION STUDIES USING LASER DOPPLER FLOWMETRY

CHI TIANXI

PhD

The Hong Kong Polytechnic University

2020

The Hong Kong Polytechnic University

Department of Mechanical Engineering

Skin Blood Flow Oscillation Studies Using Laser Doppler Flowmetry

CHI Tianxi

A thesis submitted in partial fulfillment of the requirements for the degree

of Doctor of Philosophy

April 2019

Certificate of Originality

I hereby declare that this thesis is my own work and that, to the best of my knowledge and belief, it reproduces no material previously published or written, nor material that has been accepted for the award of any other degree or diploma, except where due acknowledgement has been made in the text.

_____(Signed)

CHI Tianxi (Name of student)

Abstract

Skin blood flow oscillation (SBO) may have considerable implication in the physiology and pathology of the arterial system. It has been well known that there are five frequency bands in skin blood flow oscillation, which are related to cardiac activity (0.6 - 2 Hz), respiration (0.145 - 0.6 Hz), myogenic activity (0.052 - 0.145 Hz), sympathetic activity (0.021 - 0.052 Hz) and endothelial activity (0.0095 - 0.021 Hz), respectively. SBO exists all over the body, but shows different characteristics in different part of the body. The previous findings proved that the abnormal activity of skin blood oscillation on specific part of body could herald the coming of diseases such as hypertension, congestive heart failure and diabetes. Moreover, it also suggested that the skin blood flow oscillation might be related with the acupoints of acupuncture in Traditional Chinese Medicine (TCM) based on the literature reviews. It has been well accepted that the acupuncture could be effective in treating some diseases by stimulating certain acupoints. It have been found that acupuncturing a certain acupoint may change the skin blood flow oscillation activity on another acupoint of the body. We speculate that the skin blood flow oscillation on different acupoints may have intrinsic relationship. The previous studies only focused on the variation of amplitude of skin blood flow oscillation, and the spectral characteristics relationship have not been studied. Thus, the objective of my study is to investigate the spectral characteristics of each acupoint and the interrelationship among these acupoints, particularly on the background noise and signal to noise ratio (SNR).

From mechanical engineering point of view, the flow oscillation should be induced by external force. The external driving force of SBO is from heartbeat, and we wonder if the

variation of heartbeat induces the low frequency oscillation. To verify this assumption, we designed an experiment for simulating the blood flow through the single vessel. The infusion apparatus was regarded as the cardiac beating and the water as blood flow. During the experiment, we control the drip refer to the cardiac heart frequency, which around 1 Hz but varies with time, and use the LDF probe to measure the flow oscillation. In the absence of any biological response, we still detected the low frequency around 0.03 Hz by imitating the flow of blood through a signal vessel at the heart's pulse rate. We suggested that the variation of inlet flow (~ 1 Hz) may induce the lower frequency (0.03Hz) flow oscillation.

Finally, some researcher have created the theoretical models for SBO based on the real biological data. They believed that analysis of these data along with computational modeling of vasomotion would help them to understand physiological mechanism in spectral characteristics. As their assumption, the created theoretical model could be considered as the healthy sample for comparing the real data from patient such as cerebrovascular or diabetes on spectral analysis, so that they could predict the severity of disease based on the spectral differences. Thus, we also believed that creating the theoretical models on different acupoints is an innovate method for deep understanding of TCM and essence of acupuncture. According to the performance of regularity activities shown differently in SBO at different acupoints on forearm, different theoretical models could be produced for assembling a total system.

Acknowledgements

First and foremost, I would like to thank my supervisor, Dr. Y. Liu, first for giving me the opportunity to work in such an interesting field, and with a pioneer in that field, and with a pioneer in that field, and second for his support and guidance during the last three years, which has allowed me to grow not only as a researcher, but also as a person. With his precisely scientific attitude and encouragement, which give me a deep impression and inspired me in my research work.

Secondly, I would like to acknowledge my family, especially my father, encouraged me stick to scientific research. I would also like to thank all the group members involved S.H. Liu and M.R. Liu in the Hong Kong Polytechnic University.

Finally, I would like to particularly acknowledge the funding support from the Hong Kong Polytechnic University and Department of Mechanical Engineering.

Content

List of Figures

List of Tables

Chapter 1 - Introduction & Literature review

1.1 Vascular structure and function

Blood flow, moving through the cardiovascular system, is considered as a critical process of survival. If blood stops flowing, neurons die irreversibly from lack of oxygen, and the brain can survive only three minutes at physiological temperatures without damage (Safar and Kochanek 2000). Other tissues also die after the prolonged hypoperfusion, which is known as ischemia.(Kalogeris, Baines et al. 2012).

Blood serves as a medium that transports nutrients to all cells in the body and collects their waste for removal. Blood consists of a vast variety of cells, of which red blood cells and oxygen carriers take up the largest amount. White blood cells, also known as leukocytes, are also of huge significance to the immune system.

The composition of blood flow is sophisticated. The hemodynamics resulting from large vessels and small vessels depend on several factors (e.g., the speed of the blood, the geometric properties of the vessels as well as the impact of blood vessels on the vessel wall). Though complex, these factors have been employed to develop models capable of accurately recovering the features of the primarily observed arterial blood flow (Olufsen, Peskin et al. 2000). These models are based on the assumption that the container walls are impermeable. Accordingly, it is to be clear why different methods must be used in the case of microcirculation, in which capillaries that must be permeable are considered, allowing the dissolved gases, ions, and solutes to diffuse passively across the vessel wall (Mehta and Malik 2006). This permeability is caused by the arrangement of endothelial cells and varies

with location and function (Mehta and Malik 2006). Given the intrinsic behavior and function of blood vessels, the role of endothelium is considered to be crucial for understanding the regulation of blood flow. Measurements of blood pressure and basal skin blood flow were performed in diabetics and controls to assess the relationship between macrovascular and microvascular hemodynamics (Urbančič-Rovan, Bernjak et al. 2006). They found that, except that systolic blood pressure has a significant positive correlation with endothelial frequency interval in patients with right-sided diabetes, macro- and micro-vascular changes do not occur at the same time. This highlights the requirements for each system-specific macroscopic and microvascular blood flow model.

Arteries carry oxygenated blood away from the heart. There are two exceptions carrying deoxygenated blood, i.e., pulmonary and umbilical arteries. The arterial vasculature is the most stressful as the blood arteries carry a great distance from the heart. Arteries withstand the stress generated by the strong heart muscle wall. Aorta is the largest artery, directly connected to the left heart ventricle. Then, it branches to smaller arteries, small arteries and down to branch capillaries.

The arterial wall has many layers. The outer layer, namely the outer membrane, is a solid outer covering primarily composed of connective tissue, collagen and elastic fibers. These fibers allow the arteries to stretch to withstand overexpansion caused by blood flow pressure. The middle layer, namely the middle membrane, is composed of smooth muscle and elastic fibers. The inner layer, namely the inner membrane, primarily has an elastic membrane liner and a smooth endothelium covered by elastic tissue.

The vein carries the deoxygenated blood back to the heart generating less pressure than the artery. Accordingly, the middle layer of the vein is thinner than that of the artery. Under the lower pressure and the movement of the blood against gravity, the veins have valves, allowing themselves to withstand the backflow of blood. The largest veins are the vena cava, superior vena cava, and inferior vena cava, which carry blood directly to the right atrium. The smaller vein, known as the venule, is also connected to the capillaries.

1.2 The Microvasculature

Harvey's pioneering work also verified that arteries and veins were connected, while how they were connected was not proven. In fact, Leonardo da Vinci observed capillaries that reached this end, whereas he did not associate them with the effect of their connection of arterioles and venules (Pearce 2007).

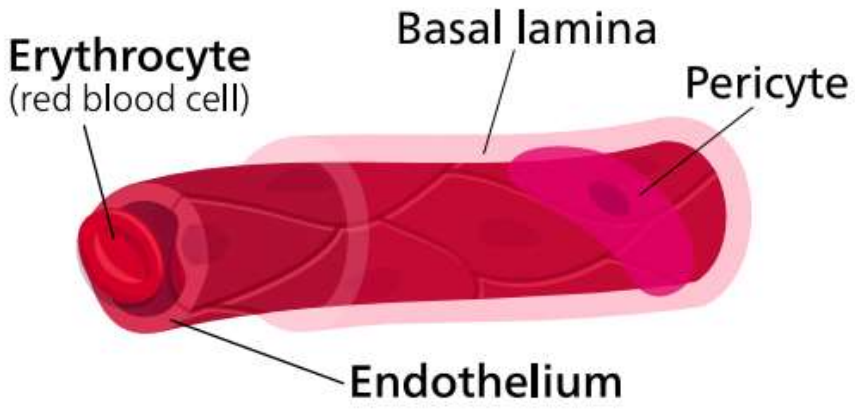

Fig.1.1 Capillary structure (Kelvinsong 2015)

In 1661, Marcello Malpighi clarified the connection between arteries and veins when he observed blood flowing through the small network of lungs and the frog's expanding bladder. He speculated that these capillaries were the connection between the artery and vein (Young 1929, Pearce 2007). Also, Van Leeuwenhoek independently observed red

blood cells and their movement through capillaries in 1688. These findings are collectively the earliest observation of blood flow in micro-vessels (van Leeuwenhoek 1800). Also, capillaries are thought as the smallest blood vessels in the body, usually about 5-10 microns, connecting small arteries and venules to complete the blood transport network.

The blood flow from the arterioles and to the venules through the capillary bed is known as microcirculation. The capillary bed is a collection of capillaries forming an interwoven network. It consists of two types of blood vessels: blood vessel shunts and true capillaries. The real capillaries are the places where material exchange takes place. Blood can bypass the capillary bed through a vascular shunt (namely a fine artery) to carry blood to another area of the body depending on vasomotion nerves and chemical conditions. The smallest capillaries are only composed of a single layer of endothelial cells, allowing the rapid diffusion of water, oxygen, carbon dioxide and other substances through their walls.

1.3 The Endothelium

Originally thought to be tunnels, in the 19th century, Reckinghausen observed that the blood vessels were actually canals filled with cells (Eliseyeva 2013). These cells were identified by William, differentiating the body cavity from the epithelium, and referred to as endothelial cells in 1865 (His 1865, Favero, Paganelli et al. 2014). However, detailed studies of endothelial cells began in the 1950s with Howard Florry's description of endothelial cells. Structures don't realize their significance (Florey 1966).

Jaffe et al. recognized that endothelial cells are the key to clarifying how vascular walls play a role in health and disease. It led to their first culture of human umbilical cord

endothelial cells in 1973 (Jaffe, Nachman et al. 1973), forming the field of vascular biology (Nachman 2012).

A continuous monolayer in all blood vessels generated from vascular endothelial cells was once considered as an inert barrier between blood and tissue, it is now known that this vital organ has a large number of fundamental functions (Vane, Änggård et al. 1990) (e.g., maintaining blood flow, regulating the flow of nutrients and bioactive molecules (Cines, Pollak et al. 1998) and signaling (Cleaver and Melton 2003)). Endothelial cells varies with different sites, and almost every organ regulates the endothelial structure in accordance with the functional requirements (Fishman 1982). The vascular endothelium is also critical for the development of new blood vessels from the existing vasculature in angiogenesis through the differentiation and the migration in response to growth factors, e.g., vascular endothelial growth factor (VEGF) (Frelin, Ladoux et al. 2000). However, the first key role played by the discovered vascular endothelial cells is their impact on vascular tone, which regulating blood flow by releasing vasomotion substances (Cines, Pollak et al. 1998). This was started in 1976 when Moncada et al. found that blood vessels secreted vasodilator prostacyclin (Moncada, Gryglewski et al. 1976). In 1980, Furchgott and Zawadzki (Furchgott and Zawadzki 1980) found that the vasodilator acetylcholine (ACh) is a high effective vasodilator *in vivo* that not always induce the same response *in vitro*. They also discovered the reason was because endothelial cells were accidentally removed during the preparation, and their presence was required for the process of vasodilation using ACh. Moreover, they suggested that acetylcholine stimulates the release of a substance named endothelium-derived relaxing factor (EDRF). Later Ignarro et al. confirmed that EDRF was nitric oxide (NO). In 1987, Vasodilation was still observed after suppressing the production

of NO and prostacyclin, and it was named endothelium-derived hyperpolarizing factor (EDHF) (Félétou and Vanhoutte 1996), which differed from Chen et al.'s EDRF (Chen, Suzuki et al. 1988). In 1989, another endothelium secretion was found, which was a vasoconstrictor this time, known as endothelin (Yanagisawa, Kurihara et al. 1988).

The substances secreted by endothelial cells will induce the reactions in the blood vessel wall, making the blood vessels contract or expand to regulate blood flow as needed. For instance, NO relaxes smooth muscle cells by activating guanylate cyclase, thereby elevating the concentration of cGMP (cGMP) (Pappano and Wier 2012). As a result, cGMP-dependent protein kinase (PKG) activity is increased, and myosin light chain phosphatase (MLCP) (Pappano and Wier 2012) is activated. Relaxation is then induced by reducing the concentration of light chain subunits in vascular smooth muscle by phosphorylated myosin (Pappano and Wier 2012). By detecting blood flow shear stress generated by an anionic polyelectrolyte heparan sulfate proteoglycan (HS-PG), endothelial cells act on smooth muscle cells to cause flow-dependent vasodilatation in response to the accelerated blood flow, and simultaneously a decrease in blood flow will cause vasoconstriction. Siegel (Siegel, Meyer-Rath et al. 2015) first demonstrated this flow-dependent regulation of endothelial cells in vivo in 1986 (Pohl, Holtz et al. 1986). Vascular endothelial dysfunction is primarily reflected by a reduction of vasodilation and an increase in endothelium-derived contractile factor, which has been correlated with a number of pathologies, including atherosclerosis (Steyers and Miller 2014) and other chronic inflammatory diseases, e.g., psoriasis, rheumatoid arthritis and inflammatory bowel disease (Steyers and Miller 2014), hypertension (Endemann and Schiffrin 2004), diabetes (Dolger 1950), renal impairment (Stam, van Guldener et al. 2003), erectile dysfunction (Costa and

Virag 2009), Alzheimer's disease (Tong, Nicolakakis et al. 2005), pre-eclampsia (Germain, Romanik et al. 2007) as well as obesity (Avogaro and de Kreutzenberg 2005). Accordingly, focusing on vascular vasomotion is clearly significant for understanding the development of many diseases, in particular at the level of micro-vessels.

1.4 Vasomotion and Flowmotion

Vasomotion is a rhythmic change in the tone shown by the arteries primarily in the microcirculation (Stergiopulos, Porret et al. 1998) but also in the large muscle arteries (ROSS, Stinson et al. 1980). The mechanism and physiological importance of vascular movement is not fully understood so that it is still an interesting field of research.

In 1852, Jones first observed the vasomotion in the bat wing's circulation (Jones 1852), and it was then broadly observed in humans and animals both *in vivo* and *in vitro*. The first vasomotion study under different conditions *in vivo* employed a living body microscope. It proved that the frequency and amplitude of vasomotion activity were affected by the variations in pH, temperature, oxygen partial pressure (Bouskela and Grampp 1992) and arterial pressure (Slaaf, Tangelder et al. 1987). Another way to indirectly observe vasomotion is to measure the effect of these variations in the vascular wall on the blood flowing through them which will be oscillatory as result, it would be known as flowmotion (Schmidt, Borgström et al. 1993).

Both *in vivo* and *in vitro* methods show their own benefits. The *in vivo* study of vasomotion activity enables the study on the behavior of the vascular wall in its natural environment following the systematic and local regulatory procedures. In contrast, *in vitro* studies present the information about the intrinsic behavior of the blood vessel only and allow fine-

tuning of experimental conditions to directly identify the causes of various phenomena, yet their origin may be less clear *in vivo* due to the difficulties in measurement. *In vivo*, it is a challenge for the direct observation of vascular movement, whereas such observation has been shown to be possible using a living microscope (Kaufman and Intaglietta 1985), namely an optical resolution photoacoustic microscopy (Hu, Maslov et al. 2009). *In vitro*, vasomotion activity in the frequency range from 0.01 to 0.3 Hz was observed in isolated arteries from different species and in blood vessels from different areas of the body (Nilsson and Aalkjaer 2003, Aalkjær, Boedtkjer et al. 2011). It has been observed that the frequency of vasoconstriction observed *in vitro* is consistent with that *in vivo* in the myogenic frequency interval (Bouskela and Grampp 1992, Kvandal, Landsverk et al. 2006), which provides the automated nature of the oscillations observed at myogenic frequencies. The evidence also provides the local *in vivo* regulation that neurogenicity as well as endothelial contribution.

To have vasomotion movements, the macroscopic oscillations of blood vessels must be observed, and the oscillations in each smooth muscle cell (Aalkjaer and Nilsson 2005) must be synchronized. The origin of these individual cell oscillations is controversial and may result from oscillations in membrane potential, cytosolic oscillations or metabolic oscillations (Aalkjaer and Nilsson 2005). At the fully automated level, to respond to the increased blood pressure, vasodilation will work to reduce stress (Söderström, Stefanovska et al. 2003).

Vascular motion occurs in a wide range of frequencies. Colantuoni et al. (Colantuoni, Bertuglia et al. 1984) showed that the frequency of vascular movement varies with the size of blood vessels, and the frequency of arteriole vasomotion is greater than that of hamsters.

These findings were based on the frequency with the largest amplitude in the Fourier transform of the blood vessel diameter time series, so the apparent change was not considered in this frequency. The study also suggested that vascular movement is strongly suppressed during anesthesia (Colantuoni, Bertuglia et al. 1984). This effect was later confirmed in the body by Landsverk et al (S.A. Landsverk et al. 2007).

1.5 Vasomotion Study by using Laser Doppler Flowmetry

Laser Doppler flowmeter (LDF) is the most broadly used technique for assessing skin microvascular blood flow. Based on the Doppler Effect, LDF uses a laser to measure the velocity of red blood cells, which is determined by the frequency of the incident light. Stern et al. employed LDF for the first time to measure *in vivo* blood flow in undisturbed microcirculation of human skin (Stern 1975, Stern, Lappe et al. 1977), and then this technique was applied in rabbit retinal arteries (Boggett, Blond et al. 1985). The resulting signal, blood flow, flux or perfusion not only represented the speed of red blood cells but also its concentration. Since then, its development introduced new areas of non-invasive blood flow testing in the microcirculation of health and disease, and this phenomenon has shown a wide range of variations in various pathologies.

Many studies aiming to assess microvascular function have used LDF to directly measure the characteristics of microcirculatory blood flow (Roustit and Cracowski 2012). The most basic tests include the calculation of average blood perfusion and the comparison between various states of health and disease. However, it has been shown that the basal flux value is highly variable and dependent on many factors, e.g., the recording site and skin temperature (Cracowski, Minson et al. 2006). Even considering these factors,

microvascular blood flow fluctuates in a non-constant manner, so the average blood flow value does not offer a fundamentally accurate representation.

Most of the *in vivo* data on the incidence of vasomotion tone have been obtained by LDF (Aalkjær, Boedtkjer et al. 2011), yet the attention to the interpretation of these results must be paid due to the single nature of LDF and the impossibility of placing basic blood vessels. Most of the existing knowledge about vasomotion is derived from studies on animal. Movement in the human body has been found with a heavy dependence on experimental conditions and pathology. Vasodilation changes are observed in possible pathological states. In Type 2 diabetes (Bocchi, Evangelisti et al. 2010), vasomotion diminutions are observed in obesity (Rossi, Nannipieri et al. 2011) and hypertension (Rossi, Bradbury et al. 2011). In the case of type 2 diabetes, it has been shown that microcirculation can be improved by synchronizing smooth muscle cell activity, thereby promoting vasomotion (Bocchi, Evangelisti et al. 2010). It has also been shown that the vasomotion activity induced by electrical stimulation of the cervical sympathetic nerve is eliminated at high and low temperatures (Sakurai and Terui 2006). The same study provided evidence that vasomotion can boost tissue perfusion and highlight its important role in tissue oxygen delivery. Sheppard et al. studied the impact of body temperature on spontaneous vasomotion in humans. They combined local skin cooling and heating with LDF and then found that local cooling increases the myogenic response but reduces the frequency of vasomotion movements in this interval, whilst heating the skin reduced myogenic activity whilst increasing blood flow, which suggests the maximum sustained vasodilation of local vessels during heating (Sheppard, Vuksanović et al. 2011). Vuksanovic et al. also studied the impacts of different dynamics on temperature changes. They found that the temperature

flow curves obtained during heating and cooling show hysteresis, indicating bi- or blood flow levels for a given temperature stimulus (Vesna Vuksanović 2008).

1.6 Blood flow dynamics for the evaluation of skin microvascular function

Though the LDF study first considered average perfusion values or responses to various stimuli only, it soon became clear that the LDF signal contained much more information than what was first thought. Longer records lead to the conclusion that the data recorded with LDF varies significantly and is not reproducible. In contrast, once these changes are properly handled in healthy skin, sustained oscillations will be observed in the microcirculatory blood flow recorded by LDF (Bracic and Stefanovska 1998). Given this, some studies have been conducted using a Fourier transform to acquire information about these oscillation frequencies, yet this method is not suitable for such time-varying data. When Steanovaska et al. made a breakthrough, the wavelet transform was introduced to the LDF signal (Stefanovska, Bračič et al. 1999) to accurately observe the time and frequency of these biological oscillations and their changing characteristics. Due to the logarithmic scale of the wavelet transform, this method is also ideal for observing low frequency oscillations. Accordingly, a number of studies have attempted to further characterize the oscillations present in the skin's bloodstream and their physiological origin.

Though heart beats obviously have a significant impact on blood flow, in particular in larger blood vessels, hemodynamics is also governed by many other physiological processes. An essential effect, independent of the systemic heart and respiratory influences, is the local vasomotion phenomenon. Besides the intrinsic movement of the blood vessels

and the role played by the vascular endothelium, the amplitude and frequency of vasomotion are affected by neurological factors as well.

Extensive spectral analysis of the signals obtained using LDF helps to gain an insight into the oscillations found in these signals and their physiological origin. For the data, six different frequency intervals have been identified, which include different oscillation processes corresponding to various functions in the body (Shiogai 2010):

Interval I - Cardiac interval (0.6-2 Hz). The dominant oscillation around 1 Hz can be detected at all points of the body and reliably attributed to cardiac function compared with the ECG recorded simultaneously. Depending on the proximity of the LDF probe to large vessels other than capillaries, the effective contribution of the heart will vary. Accordingly, LDF measurements near these large vessels are not recommended as to observe the dynamics of lower frequencies that usually have lower power contributions.

Interval II - Respiratory interval (0.145 - 0.6 Hz). Bollinger et al. also observed slower oscillations at around 0.3 Hz, which were shown to originate from the breathing (Bollinger, Yanar et al. 2015).

Interval III - Myogenic interval (0.052 - 0.145 Hz). As discussed previously in vasomotion, this interval contains oscillations caused by the endogenous myogenic activity of vascular smooth muscle cells. This indicates that oscillations at this frequency are inherent in the vascular wall and have been observed both in vivo and in vitro (Aalkjaer and Nilsson 2005). This classification was demonstrated when oscillations were not changed in the 0.11 Hz range during local and ganglionic nerve blockade (Kastrup, Bülow et al. 1989). Myogenic response is a passive local regulation of blood flow in smooth

muscle cells and a response to the increased blood pressure (Söderström, Stefanovska et al. 2003). One of the current disputes in this field is the observation and description of waves at around 0.1 Hz. These waves are considered different from the myogenic response, originating from the Mayer wave, and observed in the arterial pressure signal. Though these waves are usually enhanced during sympathetic activation, their underlying mechanisms remain unknown (Julien 2006). The origin of oscillation at this frequency remains uncertain and may involve different physiological processes depending on the type of blood vessel.

Interval IV - neurogenic interval (0.021-0.052 Hz). This reflects neurogenic (sympathetic) activity. Soderstrom et al. confirmed that the sympathetic nervous system (SNS) is involved in this interval. LDF recordings were used on skin flaps in which it is known that there is no sympathetic activity compared with LDF records on intact skin (Söderström, Stefanovska et al. 2003). Differences are observed between 0.02-0.05 Hz, which can be therefore attributed to sympathetic activity. As Malpas stated (Malpas 1998), this activity offers another basic mechanism for the control of blood flow through rhythmic discharges and has impacts on the relaxation and contraction of blood vessels (Söderström, Stefanovska et al. 2003). To assess the effect of brachial plexus block on the skin during microcirculation, Landsverk et al. provides further evidence of the origin of oscillations during this period, which is known to cause sympathetic nerve damage (Landsverk, Kvandal et al. 2006). By using LDF and wavelet transforms, they found a reduction in the relative amplitude of oscillations in the frequency range from 0.0095 to 0.021 and 0.021 to 0.052 Hz, indicating the inhibition of endothelial and sympathetic nerve activity (Lehtipalo, Winsö et al. 2000). Bajrovic et al. also proved the origin of this intermittent sympathetic

nerve in rats. When the hindlimb is partially denervated, the relative energy of the neurogenesis interval will be significantly reduced (4 times the frequency) (Bajrovic, Cencur et al. 2000).

Intervals V and VI - Oscillations caused by endothelial activity. This has been tested using various vasoactive substances in the presence of endothelial cells and after removal (Peng, Matchkov et al. 2001). By using the endothelium-dependent vasodilator acetylcholine (ACh) and the endothelium-dependent vasodilator sodium nitroprusside (SNP) (Kvernmo, Stefanovska et al. 1999), it was first found that interval V (from 0.0095 to 0.021 Hz) contained oscillations due to endothelial activity. It was found that this endothelial-active fraction is mediated by nitric oxide (NO) (Kvandal, Stefanovska et al. 2003). In a later study, even lower frequency (Kvandal, Landsverk et al. 2006) oscillations in the frequency range of 0.005 to 0.0095 Hz were observed, forming an interval VI. In contrast to interval V, oscillations in this interval are not caused by NO but by other endothelial mechanisms, e.g., the endothelium-derived hyperpolarizing factor (EDHF) (Kvandal, Landsverk et al. 2006). To prove that these conclusions based on iontophoresis are result of endothelial activity rather than current induced blood flow increases, Veber et al. carried out the original plan concluded by Kvandal et al. (Kvandal, Stefanovska et al. 2003), but the difference was Veber replaced ACh and SNPs with deionized water and NaCl solutions (Veber, Bandrivskyy et al. 2004). They found that while iontophoresis with a low-conducting electrolyte for iontophoresis, the cathodic current simulates more current than the anodic current, whereas this does not affect the specific frequency interval. When using NaCl, a high-conductivity solution for iontophoresis, there was also no difference shown in blood flow. Given the differences observed previously using ACh and SNPs,

these two highly conductive solutions are indeed the result of endothelial activity (Veber, Bandrivskyy et al. 2004).

The complexity of the blood flow signal results from the coupling between all these physiological processes and possibly other additional effects. These show partiality in modulating vascular movement through the contributions discussed above. Stefanovska & Bracic introduced a coupled-oscillator model of the cardiovascular system in 1999 (AnetaStefanovska 1999). This reveals that skin blood flow records can be used to extract information about potential processes that change microvascular regulation by calculating the contribution of oscillations. The frequency separation usually uses time-frequency analysis methods, e.g., wavelet transforms and comparisons between states and subjects. This method has been shown to be reliable and repeatable (Stefanovska, Sheppard et al. 2011). The characterization of blood flow dynamics at rest could be used to investigate the skin microvasculature in a large number of clinical studies, including hypertension, congestive heart failure (Vesna Vuksanović 2008), aging (Shiogai 2010), obesity (Rossi, Nannipieri et al. 2011), athlete (Kvernmo, Stefanovska et al. 2003), diabetes (Berliner 1997) and critical limb ischemia (Ticcinelli, Martini et al. 2014)

1.7 Laser Doppler Flowmetry working principle

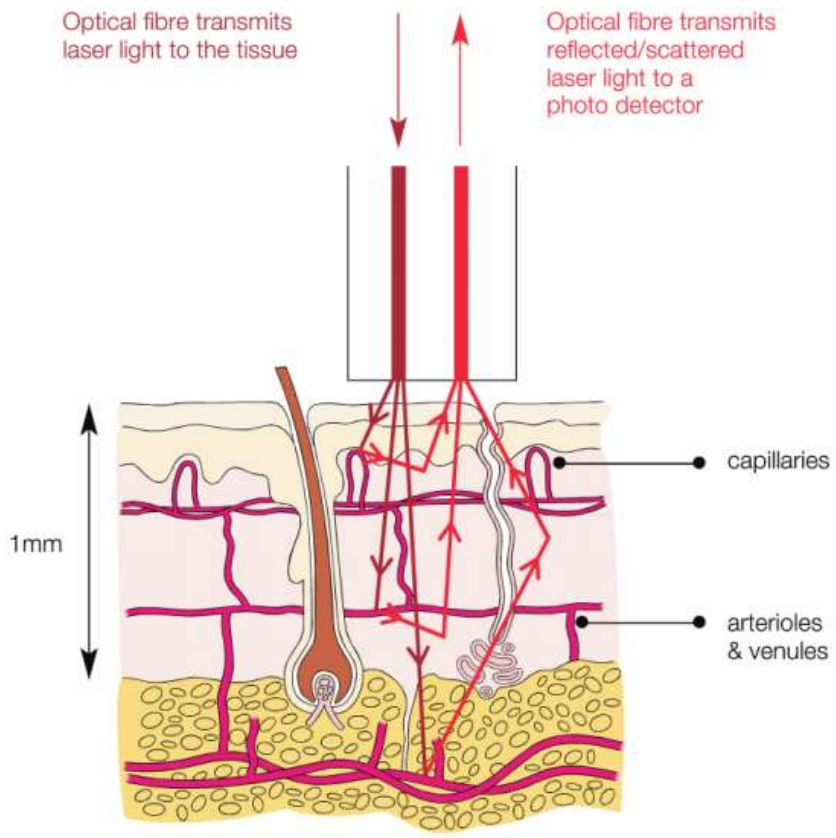

Fig. 1.2 Laser Doppler Flowmetry working principal (Rajan, Varghese et al. 2009)

The laser Doppler flowmeter (LDF) draws upon the Doppler Effect to calculate the blood flow (or flux) of the laser-illuminated microvessels (Fig. 1.2). Photons from light beams directed into the tissue will be scattered by static and dynamic particles. The moving red blood cells give the photon Doppler shift in line with the cell's scattering angle, wavelength as well as velocity vector (Rajan, Varghese et al. 2009). If a wave with a frequency ω is scattered from a dynamic particle with speed v, the Doppler shift is $\Delta\omega$.

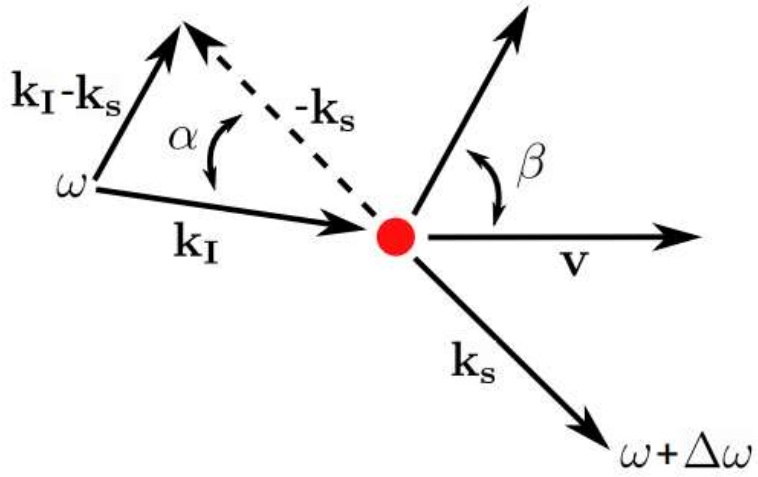

Fig. 1.3 Physical principal of LDF (Rajan, Varghese et al. 2009)

Where k_I denotes the incident wave vector; ks is the wave vector of the scattered wave; β is the angle between the velocity vector and the scattering vector, defined as k_I-ks (Fig. 1.3). If α is the scattering angle and λ is the wavelength of light, the Doppler shift can be expressed as (Rajan, Varghese et al. 2009),

$$\Delta\omega = 2(2\pi/\lambda)|v|\sin(\alpha/2)\cos\beta$$

The large number of blood vessels and dynamic particles in the microcirculation indicates that the photons will inevitably undergo multiple Doppler oscillations and produce a series of motion even if all particles have the same velocity (Rajan, Varghese et al. 2009). Doppler-shifted light will interfere with non-Doppler shift light on the photodetector, creating a dynamic speckle pattern that makes the detector's current signal fluctuate. Subsequently, these fluctuating power spectra provide information on the flux and concentration of red blood cells (Rajan, Varghese et al. 2009) since the first-order or average frequency of the power spectrum has a linear relationship to these values. These methods do not provide an absolute velocity value so that blood flow or flux is measured

in perfusion units (PU). The perfusion signal is the mean concentration multiplied by the mean rms velocity of the moving red blood cells.

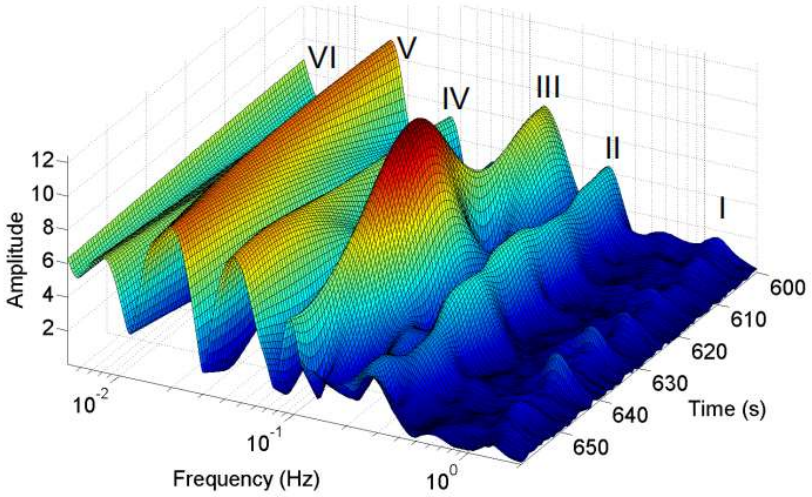

Fig. 1.4 Five intervals in wavelet analysis (Kvandal, Landsverk et al. 2006)

The LDF probe has an optical fiber, through which the laser is propagated, coupled with a transmitter and a probe, depending on the desired depth of penetration. This technique has been broadly used to study microcirculation and gained important insights into the oscillations in the blood stream. It is necessary to find six characteristic peaks in the spectrum of the LDF signal (Kvandal, Landsverk et al. 2006). As mentioned above, these peaks have been reliably attributed to various processes of physiological oscillation. LDF is advantaged in its non-invasiveness and the ability to measure microvascular blood flow in real-time at high sampling rates. Its weakness is that it only provides a single point of measurement so that there is no spatial information from the surrounding tissue.

1.8 Acupoint & Non - acupoint

In 1997, the National Institutes of Health (NIH) Consensus Development Conference concluded: "There is sufficient evidence to show that acupuncture's value is adopted in

conventional medicine and encourages the further study of its physiological and clinical value." The safety in most cases is limited by the low number of experimentally reasonable research studies (Aird, Coyle et al. 2000, Coyle, Aird et al. 2000). Historical literature indicates that acupuncture points are physical locations and the focus of acupuncture needles, acupressure and other surgeries.

In accordance with the theory of acupuncture, there are hundreds of acupuncture points distributed along the "meridians" or "channels" linking these acupuncture points, and there are numerous "extra acupoints" having no correlation with specific meridians. Though acupuncturists have a general consensus on the approximate location of the main acupoints, experimental studies have shown that there is a large difference in the precise positioning across professionals in experimental studies. In addition, there is no scientific evidence to support the difference between acupuncture points and non-acupoints. It is assumed that acupoints have some anatomical correlations (e.g., nerves, connective tissue and gap junctions) and bioelectrical properties, whereas limited systematic studies can be used to support these theories (Ahn, Colbert et al. 2008). This lack of understanding of what an acupuncture point is will affect our ability to explain the results of clinical trials comparing acupuncture and non-acupuncture acupuncture.

1.9 Previous research for acupoint in microvasculature

According to some previous researchers, there is a big difference between acupoints and non-acupoint microcirculation conditions. Hsiu (Hsiu, Hsu et al. 2011) reported that the mean blood flow (MBF) of acupoints (Hoh-Ku, Yang-Tsih, Shu-Ku) was greater than that of the surrounding tissues, which indicates that MBF can serve as a discriminating indicator of the difference between acupoints and surrounding tissue microcirculation. He also drew

the conclusion that MBF has greater electrical conductivity and a higher concentration of vascular components in the acupoint vascular bed than in its surrounding tissue. The differential reflectance of acupuncture points detected with the infrared diffuse reflectance spectroscopy is greater than its surrounding problems, which also suggests that there may be more microvasculature and blood content under skin acupoints (Lo 2002). Since the surface micro-circulation flux is provided by the underlying vascular bed (Shepherd 1990), it is believed that the increase in acupuncture micro-circulation may be attributed to more blood supply in the arterial bed. As Hsiu (Hsiu, Hsu et al. 2011) also proposed, the local physical properties of the acupoint vasculature, e.g., the number of blood vessels, radius or wall elasticity, will affect the perfusion resistance and adjust the microcirculation perfusion following the needs of the tissue. Furthermore, another possibility is that the depth of the vascular bed differs between acupuncture points.

Previous studies have shown that the acupoint microvascular bed has a blood supply greater than non-acupoint blood supply. The findings of this study show a possible link between the basic mechanisms of microcirculatory physiology and acupoint stimulation and introduce objective research methods for the understanding of the mechanisms behind oriental medicine.

Chapter 2 - Methodology

2.1 Frequency domain

Before analyzing the frequency signal, we must consider the frequency range which can be observed based on the data features. The maximum observable frequency in the signal is equal to half of the sampling frequency, known as the Nyquist frequency. This limit prevents aliasing. Aliasing will occur when the sampling frequency is insufficient for the acquisition of accurate information about the system being observed. The lowest observable frequency reaches one over the length of the time series (1 / L), ensuring that at least one oscillation period is possible in the measured time series. It also cannot solve the amplitude of two oscillations with frequency difference less than 1 / L. Practically, it is more reliable to define the minimum observed frequency as 1 / 5L, in particular when dealing with signals from the living system (Keselbrener and Akselrod 1996).

2.2 The Fourier transform

Every physical process can be defined in the time or frequency domain. In the time domain, the value of the quantity f is given as a function of time f (t), while in the frequency domain, the process is defined as the amplitude of the process F as a function of frequency, F (f). Both of them are the representations of the same function offering different types of information. If you measure time in seconds, the frequency unit will be hertz or cycles per second.

The Fourier series represents the periodic function as an infinite sine and cosine.

$$f(t) = a_0 + \sum_{\omega=1}^{\infty} [a_\omega \cos \omega t + b_\omega \sin \omega t],$$

Where ω denotes the angular frequency and a_0, and a_ω and b_ω are Fourier coefficients.

Data resulting from biological recordings will include discrete sampling. Based on the above description, the discrete Fourier transform (DFT) of signal is defined as:

$$F_\omega = \sum_{n=0}^{N-1} f(n) e^{\frac{2\pi i \omega n}{N}}$$

The Fourier transform will show the peak of the periodic frequency included in the time series. The Fourier transform is symmetrical, and the positive and negative frequencies are calculated. Nevertheless, the negative frequency component is usually discarded, and the positive component is doubled for compensation.

The Fourier transform assumes that the signal it performs is fixed, i.e., the frequency components do not change over time. There exists a certain degree of temporal variation in most biological signals, even if the certainty is not distinguishable from random variations in the basic Fourier transform. The sine basis of the Fourier transform may also wrongly represent oscillations with more irregular shapes.

2.3 Continuous wavelet transform

As the characteristics of the blood flow signal change constantly, it is better to apply the wavelet transform for spectrum analysis. A wavelet is a zero-mean function, being local in both time and frequency domains. This feature helps to determine the primary modes of

blood flow oscillations and how these modes change over time. Through the wavelet transform of the signal, a three-dimensional structure is produced on the time-frequency plane. In general, the wavelet amplitude and power spectrum can be defined as the absolute value and the square of the wavelet transform, respectively. Morlet wavelet is a good choice for skin blood flow signals as it offers a favorable balance between time and frequency positioning. The optimal solution to the previously discussed limitations is wavelet transforms. This solution allows the simultaneous detection of time and frequency signals, and good resolution can be achieved using an adaptive window. If this process is performed separately, it is called a Discrete Wavelet Transform (DWT), which yields no overlap between frequency bands. If it is continuous, it is a continuous wavelet transform (CWT). The advantages of CWT for FFT when analyzing linear frequency modulated (LFM) signals are shown in Fig. 2.1. The continuous wavelet transform is given by

$$\mathrm{g}(s,t) = \frac{1}{\sqrt{s}} \int_{-\infty}^{\infty} \psi\left(\frac{u-t}{s}\right) g(u)\,du \,,$$

Where s denotes the scale factor; t is the position of the signal over time; ψ is the wavelet function. The wavelet transform is achieved by moving the wavelet function along all positions of the signal.

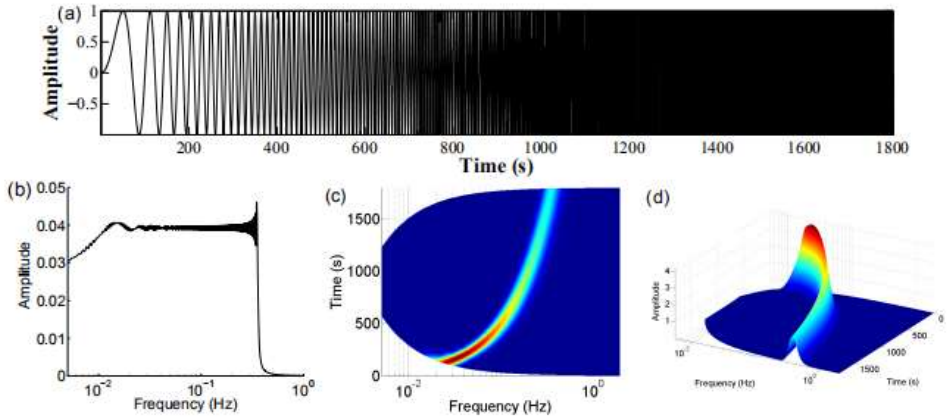

Fig. 2.1 Nonlinear chrip signal has a frequency which increase with time, FFT, CWT

For each position, the full range of the wavelet is used and can be adjusted in accordance with the frequency range to be explored. The value obtained from the convolution of the wavelet function with the signal over these times and frequencies will be large (if the signal has a good match) (if the signal is out of phase, it will still give a large value, yet it will be in real numbers; if a complex wavelet is used, it will be an imaginary part). In such a way, you can create the entire picture of a signal, the time, frequency and amplitude of the axis, which is the transformation value for each scale, as shown in Fig. 2.2. Wavelet power spectrum can be calculated as the square of the wavelet transform integral over frequency (Clemson and Stefanovska 2014),

$$P_{\mathrm{w}}(\omega,t)=\int_{\omega-\frac{d\omega}{2}}^{\omega+\frac{d\omega}{2}}\left|W_T(\omega,t)\right|^2 d\omega$$

The time average of Pw gives a representation of the entire time series that can be employed to compare the power spectra of various signals. Though the Fourier transform function seems to have a reduction, the time-averaged wavelet power provides a higher resolution

for time-varying oscillations at low frequencies due to the logarithmic frequency scale. (As shown in Fig. 2.2).

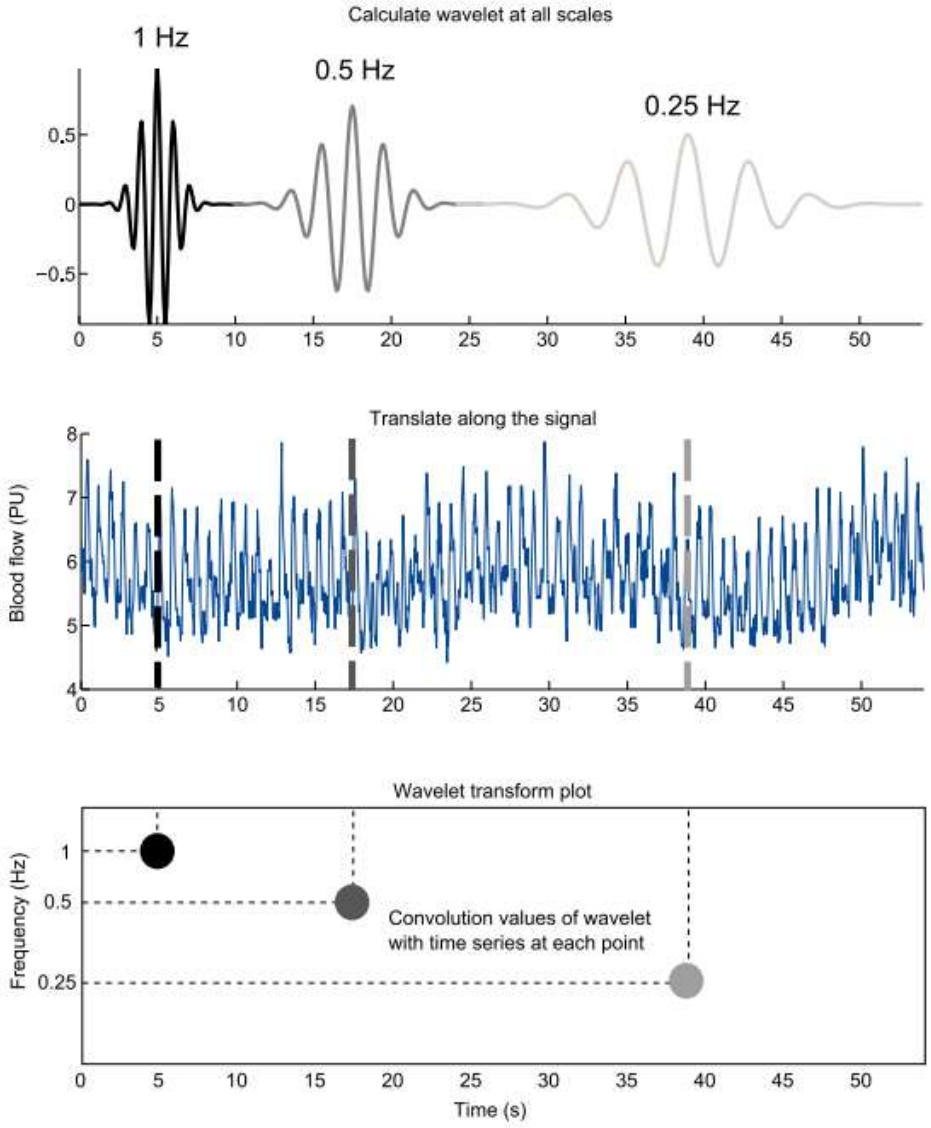

Fig. 2.2 Example of translation of wavelets of different scales

2.4 Wavelet types

There is a vast variety of wavelets, each of which has its own application. Complex wavelet is particularly useful, which allows the separation of the phase and amplitude components

of the signal. Morlet wavelet is employed in this study, which is a complex wave in a Gaussian envelope with unit standard deviation. The phase difference between the actual and the imagined sine curve is a quarter (Addison 2016). The complex Morlet wavelet is expressed as

$$\psi(u) = \frac{1}{\sqrt[4]{\pi}} e^{i2\pi f_0 u} e^{-u^2/2}$$

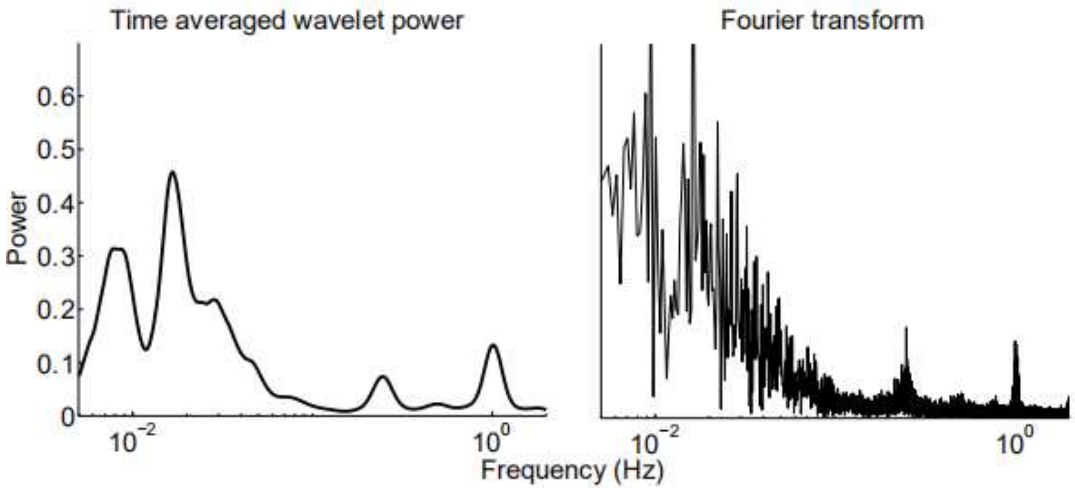

Fig. 2.3 Time average wavelet transform vs FFT (Kaiser, 2011)

Complex numbers are the wavelet coefficients obtained using the complex Morlet, which define the amplitude and instantaneous phase of each frequency and time (Kaiser 2011).

2.5 Cone of influence

CWT integrates unlimited time, whereas the actual length of the data set is limited. As a result, the wavelet transform becomes ambiguous near the time boundary, close to t=0 or when t is close to the length of the time series. To solve this problem, the signal can be 'filled'; i.e., it becomes longer at both ends during the calculation and then trimmed to keep

only the original time period. Various filling mechanisms are adopted (e.g., zero-fill, predictive fill and periodic fill) (Iatsenko, Mcclintock et al. 2015). Even with the padding scheme, since the wavelet runs on the edge of the time series, the border effect can still be observed. The unaffected part of the wavelet transform is known as the cone-of-influence.

2.6 Noise analysis

1/f noise is used in body movement, which is also regarded as 'pink noise' or 'fractal scale', indicating the specific nature of cognition and influence. To understand pink or 1/f noise, it is important to recognize that any signal scale could be represented in two domains, namely time domain and frequency domain. The Figures show how the signal changes over time. These time series can be converted to frequency domain, where the key is how the signal is distributed in different frequency bands. This is shown in the right panel of Fig. 2.4, showing the distribution of amplitude a (intensity or power on the Y axis) as a function of frequency f (on the X axis) on the log plot. The type of noise in the signal can be estimated by the relationship between power and frequency. To be specific, the lack of relationship between amplitude and frequency (i.e., slope = 0, $\alpha \propto f^0$) is a feature of white noise (as shown in Fig. 2.4 (a)). When the slope (namely the spectral slope) is -2 ($\alpha \propto f^{-2}$), brown noise (or fractional Brownian motion) occurs, as shown in Fig.2.4 (b). Pink noise ($\alpha \propto f^{-1}$ or $\alpha \propto 1/f$; as shown in Fig. 2.4 (c)) occurs when there is an inverse relationship between amplitude and frequency. The spectral slopes of the time series in Fig. 2.4 are 0, -1, and -2, representing white noise, pink noise and brown noise, respectively. These time series are prepared from the synthesized data, so the slope is almost perfectly matched to the ideal values for white, pink and brown noise. The slopes of naturalistic time series

rarely follow these idealized values but lie within these boundaries (Holden 2005). As shown above, the nature of the relationship between amplitude and frequency varies with the signal and can serve as an indirect method to infer the "intrinsic" property of the system that produces the signal. White noise is particularly a random system diagnosis where there is no short-term or long-term correlation between observations. In contrast, brown noise is a strong short-term correlation between diagnostic observations (random walking).

Pink noise is particularly interesting as showing short-term and long-term correlations between the extremes of disorder (white noise) and short-term predictability (brown noise) (Holden 2005) (Orden, Kloos et al. 2011)). The 1/f model is of important theoretical and practical significance since the past decade of research shows that any reliable continuous cognitive measure will reveal the "intrinsic" 1 / f fluctuation model. This finding has aroused much interest (Gilden 2001, Wagenmakers, Farrell et al. 2004, Orden, Kloos et al. 2011). For instance, in an experiment that collects repeated response time measurements (e.g., time interval estimates), the fluctuations in this ordered series of responses are not stationary at the mean time for estimation, with a completely random “error” above and below the mean (Orden, Kloos et al. 2011). In contrast, the time series suggest that the peaks and valleys rise and fall between very low frequencies (high amplitude), very high frequencies (low amplitude) and all possible modes (Fig. 2. 4 (c)). This model is consistent with some properties of natural fractals (self-similarity, scale relations, etc.) so that the pink or 1 / f modes are often referred to as fractal scaling (Mandelbrot 1999).

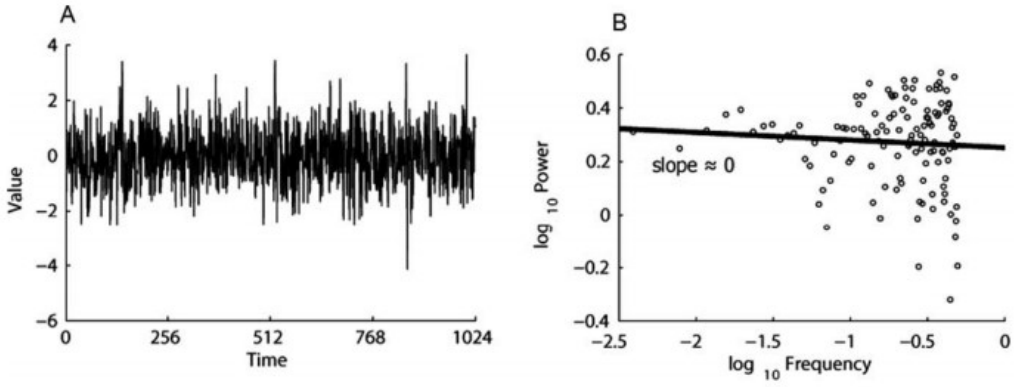

(a)

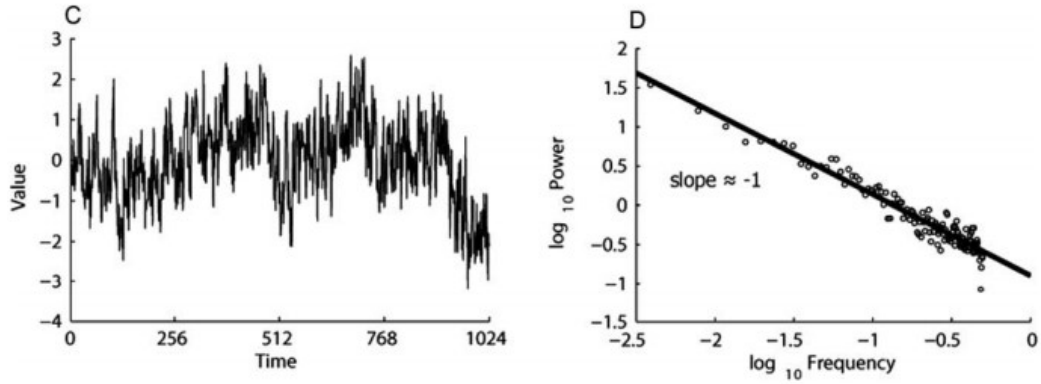

(b)

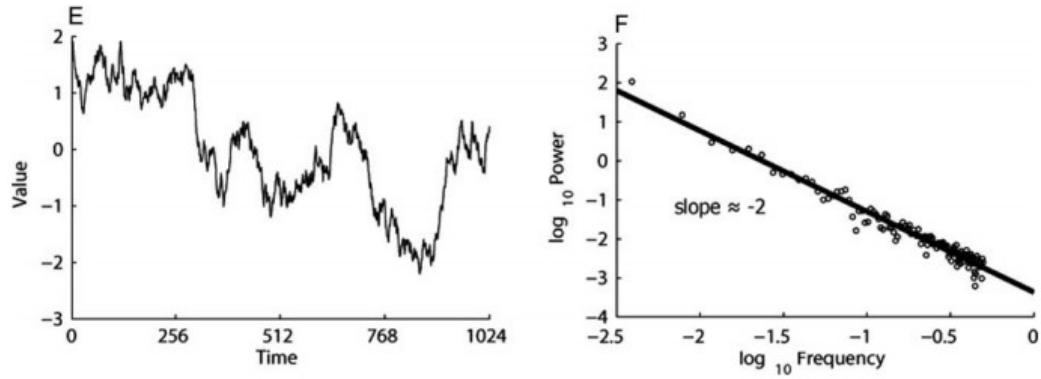

(c)

Fig. 2.4 Different time series changed with time and slope calculated

White noise is a type of noise containing equal amounts of all frequencies. It is said that noise containing an unequal number of all frequencies is considered colored. One type of colored noise is pink noise with lower intensity at higher frequencies. In pink noise, the spectral intensity has an inverse relation with the frequency, resulting in an equal amount of energy per octave.

All octaves (or similar log bundles) have the same amount of energy. In terms of power at a constant bandwidth, pink noise drops at a rate of 3 dB per octave.

$$octaves = \log_2\left(\frac{f_2}{f_1}\right)$$

Where f_1 and f_2 refer to two different frequencies within frequency band

$$s(f) = PD \sim = \frac{1}{f^{\alpha}}$$

$$\frac{PD_2}{PD_1} = \left(\frac{f_2}{f_1}\right)^{-\alpha}$$

Where p_1 and p_2 denote power spectral densities situated on f1 and f2 frequency

$$10 \times \frac{\log_{10} PD_2 - \log_{10} PD_1}{\log_2 f_2 - \log_2 f_1} = \Delta dB$$

$$10 \times \alpha \times \log_{10} \frac{f_2}{f_1} = \Delta dB \times \log_2 \frac{f_2}{f_1}$$

$$\alpha = \frac{\Delta \mathrm{d}B}{10 \times \log_{10} 2} = \frac{\Delta dB}{3}$$

At sufficiently high frequencies, pink noise never dominates. Brown noise contains all frequencies and has lower intensity at higher frequencies (e.g., pink noise) but to a greater extent. In brown noise, the spectral intensity has an inverse relation with the square of the frequency. An increase in single octave causes a 3 dB drop in pink noise and a 6 dB drop in brown noise. In this study, the frequency of each test's signal strength in decibels was plotted, and the change in intensity was measured by one octave.

2. 7 Signal to noise (SNR) analysis

Noise performance and signal-to-noise ratio are the key parameters of any radio receiver. The signal-to-noise ratio or SNR is normally referred to as an indicator of receiver sensitivity performance. The S/N ratio or SNR is a critical specification and widely serves as a measure of receiver sensitivity (Ian Poole 2018). This is of huge importance to all applications ranging from simple broadcast receivers to cellular or wireless communications as well as fixed or mobile radio communications, two-way radio communication systems, satellite broadcasting, etc.

There are plenty of ways to measure noise performance for measuring the sensitivity of a radio receiver. The most obvious method is to compare the signal and noise level of the known signal level, i.e., the greater the S / N ratio or SNR, the better the radio receiver sensitivity performance will be.

The difference is usually expressed as the ratio of signal to noise (S / N), usually expressed

in decibels. As the signal input level obviously impacts this ratio, the input signal level must be given, which is usually expressed in microvolts. In general, the specific input level is required to give a signal-to-noise ratio of 10 dB.

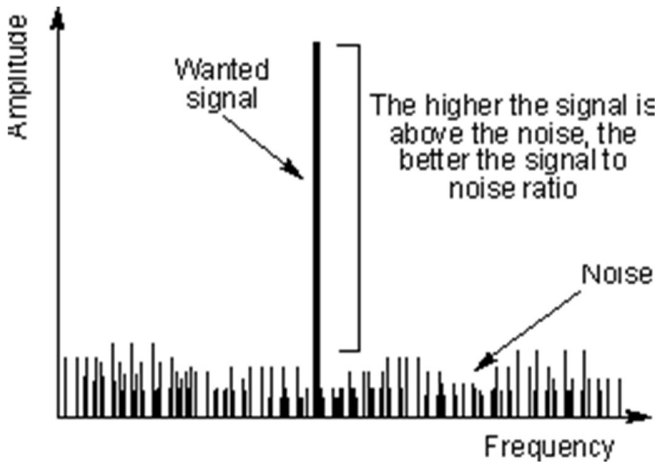

Fig. 2.5 Signal to noise ratio (Ian Poole 2018)

The signal to noise ratio is recognized as the ratio between the wanted signal and the unwanted background noise.

$$SNR = \frac{P_{signal}}{P_{noise}}$$

P denoted the average power. Both signal power and noise power must be measured at the same point in the system and measured in the same system bandwidth. If the variance of the signal and noise is known, and both the signal and the noise are zero means, the SNR is defined as:

$$SNR = \frac{\sigma^2_{signal}}{\sigma^2_{noise}}$$

If the signal and the noise are measured across the same impedance, the SNR can be yielded through the calculation of the square of the amplitude ratio:

$$SNR = \frac{P_{signal}}{P_{noise}} = \left(\frac{A_{signal}}{A_{noise}} \right)^2$$

Where A denotes root mean square (RMS) amplitude.

Since many signals have a very wide dynamic range, signals are often expressed using the logarithmic decibels scale. Based on the definition of decibels (dB), it yields that:

$$P_{signal,dB} = 10 \log_{10}(P_{signal})$$

And

$$P_{\text{noise},dB} = 10 \log_{10}(P_{noise})$$

Likewise, SNR may be expressed in decibels as

$$SNR_{dB} = 10 \log_{10}(SNR)$$

Using the definition of SNR

$$SNR_{\text{dB}} = 10 \log_{10}(\frac{P_{signal}}{P_{noise}})$$

When the signal and noise are measured in Volts or Amperes, which are the measures of amplitudes, they must be squared to be proportional to power in the following:

$$SNR_{\mathrm{d}B} = 10\log_{10}\left[\left(\frac{A_{signal}}{A_{noise}}\right)^2\right] = 20\log_{10}\left(\frac{A_{signal}}{A_{noise}}\right)$$

Chapter 3 - Skin Blood Flow Oscillation at Acupoint & Non-acupoint

3.1 Experimental Method & Procedure

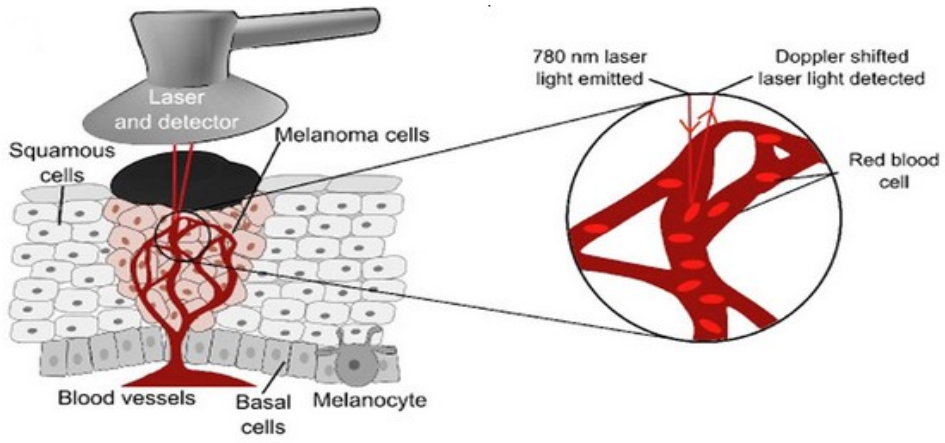

Fig. 5 Laser Doppler Flowmetry Probe working principal (Cracowski and Roustit 2016)

The moorVMS - LDF2 (LDF), recognized as an accurate and dependable tool for detecting microcirculatory condition, is the acceptable signal acquisition apparatus. Two laser probes serve as the main component installed by the Laser Doppler perfusion and temperature monitor. The probes are composed of one transmitting and one receiving optical fibers. When these two probes are attached with the specific skin locations, the probe will receive the Doppler shifted laser light based on the red blood cell activity while flowing through the blood vessels. Fig. 3.1 shows the Laser Doppler Flowmetry probe working principle (Cracowski and Roustit 2016).

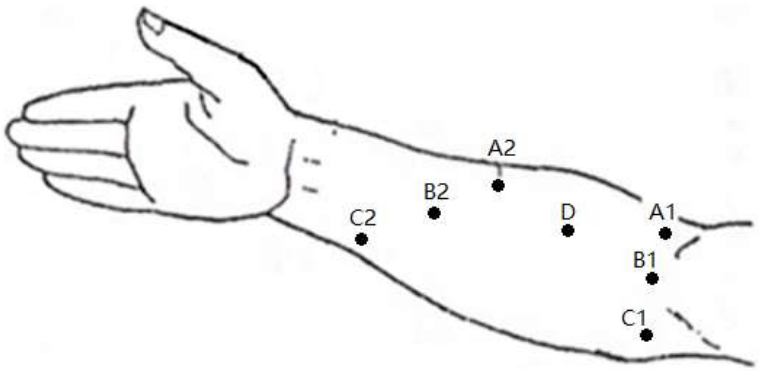

Fig. 3.2 Seven selected Acupoint & Non-Acupoint on Forearm

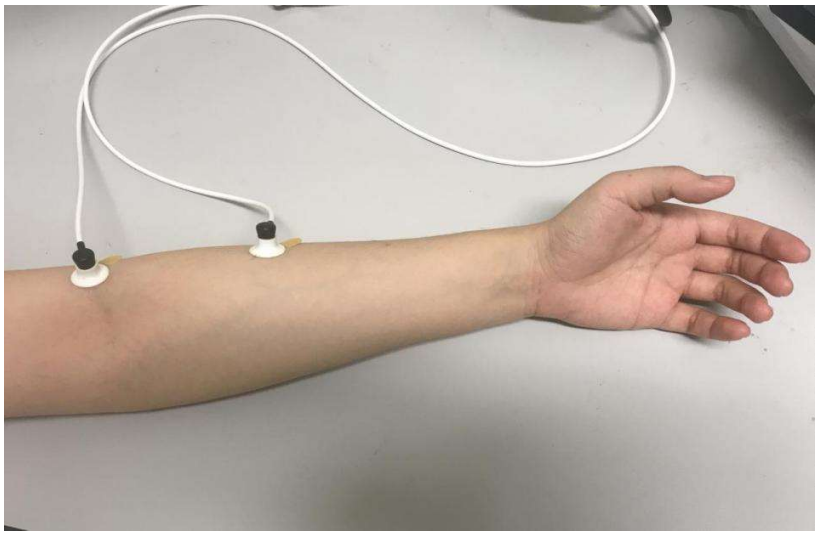

Fig. 3.3 Experiment processing

According to the literature, the researcher has found that the microcirculatory situated on Acupoint (Hoh - Ku) located on hand is extremely active. Accordingly, it is assumed that the skin blood flow oscillation on other Acupoints also has significantly outcomes. This Chapter will focus on the six Acupoints on forearm named Chize (A1), Kongzui (A2), Quze (B1), Xianmen (B2), Shaohai (C1), Lingdao (C2) and one non-acupoint (D) considered as the reference point, respectively. (As shown in Fig. 3.2). The Fig. 3.3 shows that the two Acupoints are detected simultaneously.

Table 1 Six healthy subjects base index

Sample No.	Age	Gender	BMI
1	28	Female	19
2	26	Female	18.3
3	24	Male	24.1
4	25	Male	20.5
5	27	Male	27.6
6	23	Male	20.2

Thus, six healthy subjects (25±3 years old) (4 males and 2 females) were selected in the *in vivo* experiment and asked to avoid taking caffeine within 2 hours before the test and without moving during the collection. The subjects should not take any medicine three days before measurement. The two LDF probes located at two selected points would be detected simultaneously. The ambient temperature is set as 23±1°C, and the sampling rate is 20 Hz, which is equivalent to the 0.05s time interval. Measurement will last for 20 minutes.

3.2 Measured time series

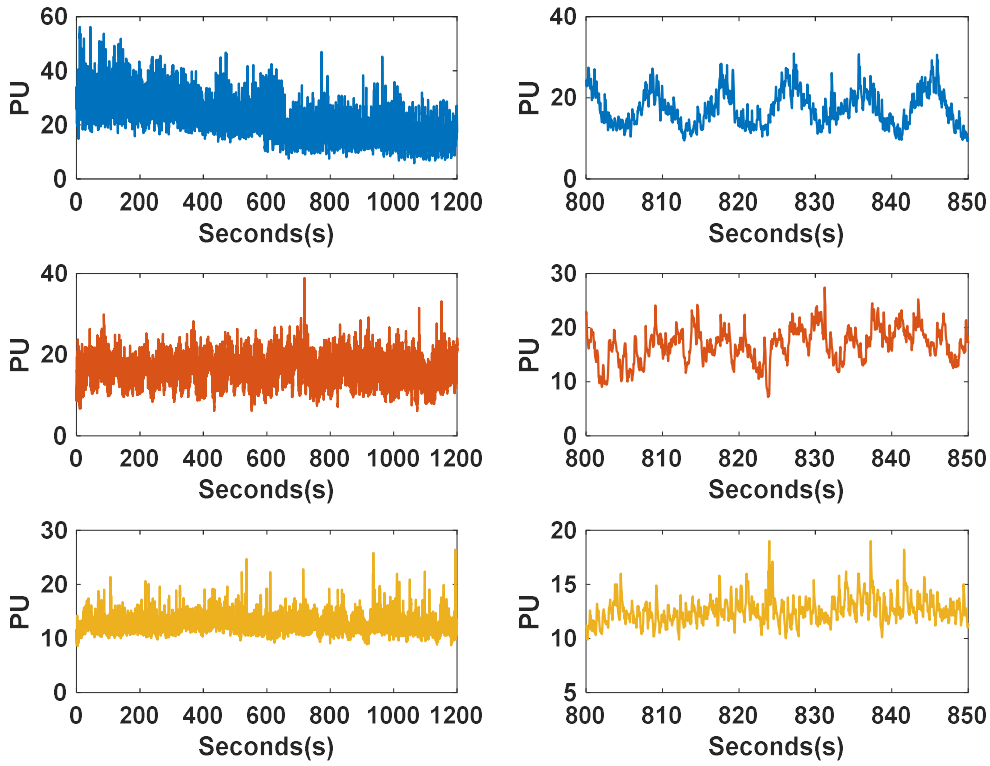

Fig. 6 Typical example of original time series (at points A1, B1, and D)

The LDF survey was conducted on several healthy subjects (4 men and 2 women). According to the LDF data, each subject corresponded to four groups of A1- A2, A1- D, B1- B2, and C1- C2. Fig. 3.4 shows two typical raw data and one reference raw data in accordance with the three positions on the forearm. It also shows that all three original time series are stable and there is no sudden change in perfusion unit (PU) However, from the enlarged version (800-850 seconds), the question is raised that whether the spontaneous oscillation of A1 may be related with the myogenic activity, and B1 appears around the 0.3 Hz oscillation signal affected by the respiration. The time series of non-acupoint C differed

from that of A1 and B1 as they exhibited disordered oscillations with no obvious myogenic and respiratory signs.

3.3 Experiment results

The experiment results involve wavelet analysis, noise analysis and averaged wavelet analysis. Typical example results for each acupoint will be provided as follows:

3.3.1 Chize (A1)

Chize is a point located at the lateral depression of the biceps tendon of the elbow joint. It is located in the so-called "lung meridian" that is traditionally used to treat cough, vomiting and diarrhea. The researchers (Bao, Xin et al. 2017) demonstrated that acupuncturing at Chize can significantly improve cough and concomitant symptoms in patients. The total efficiency is about 84.2%. This indicates that the skin blood oscillations on Chize must be more special than the non-acupuncture points.

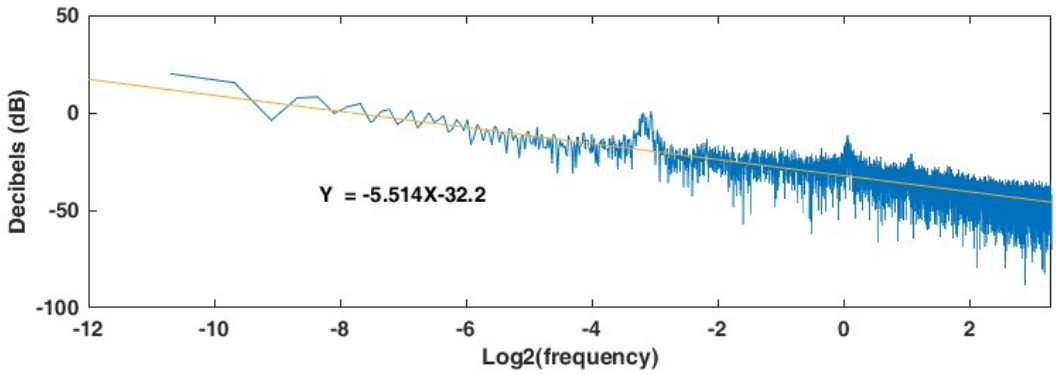

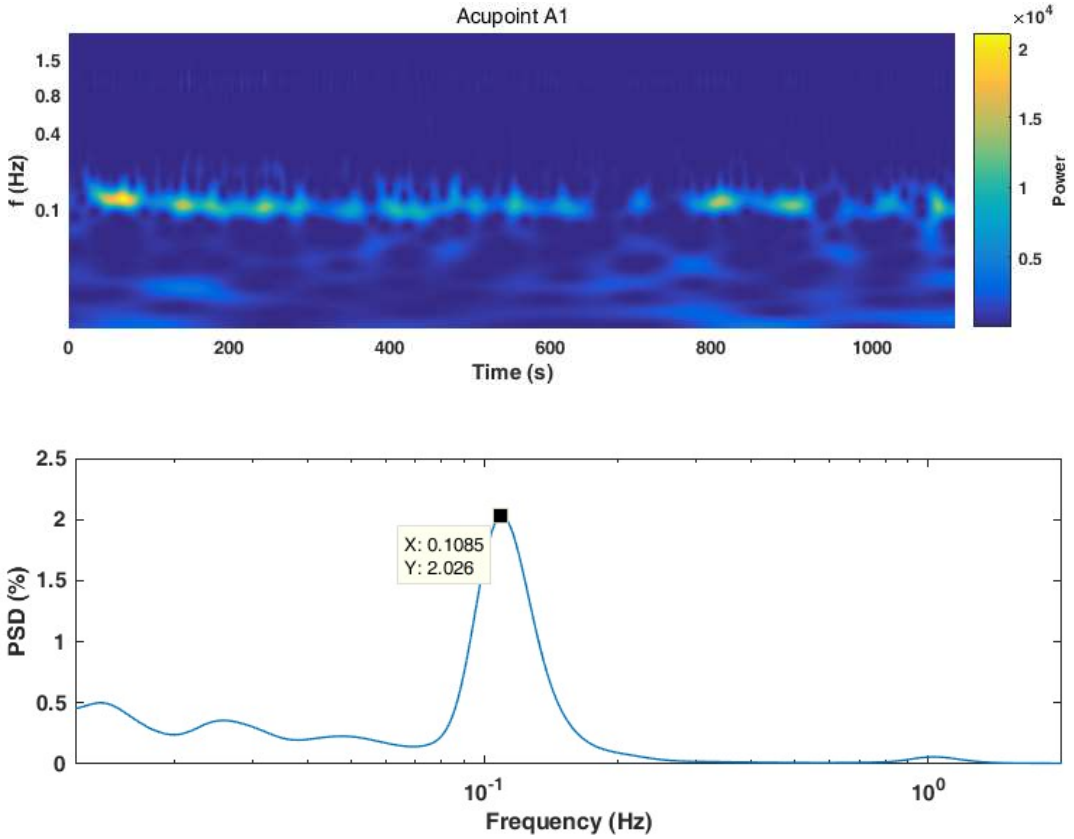

Fig. 3.5 Noise, wavelet & averaged wavelet example for Chize Acupoint

The typical example for acupoint (chize) have shown the exponent (slope) of noise analysis is 5.514 which tend to brown noise type (index = 6), and it is also obviously to see that the power of 0.1 Hz is sustainably occurred during whole experiment. The averaged wavelet figure also proved that the 0.1 Hz is dominant.

3.3.2 Kongzui (A2)

Kongzui, situated on about 23 cm above the dorsal wrist crease, are along with the same meridian as the acupoint Chize. Recently, some researchers have already found that treating acupoint Kongzui led to significant changes in the taste of the cigarettes and desire to smoke compared with the control group (Jang, Park et al. 2017).

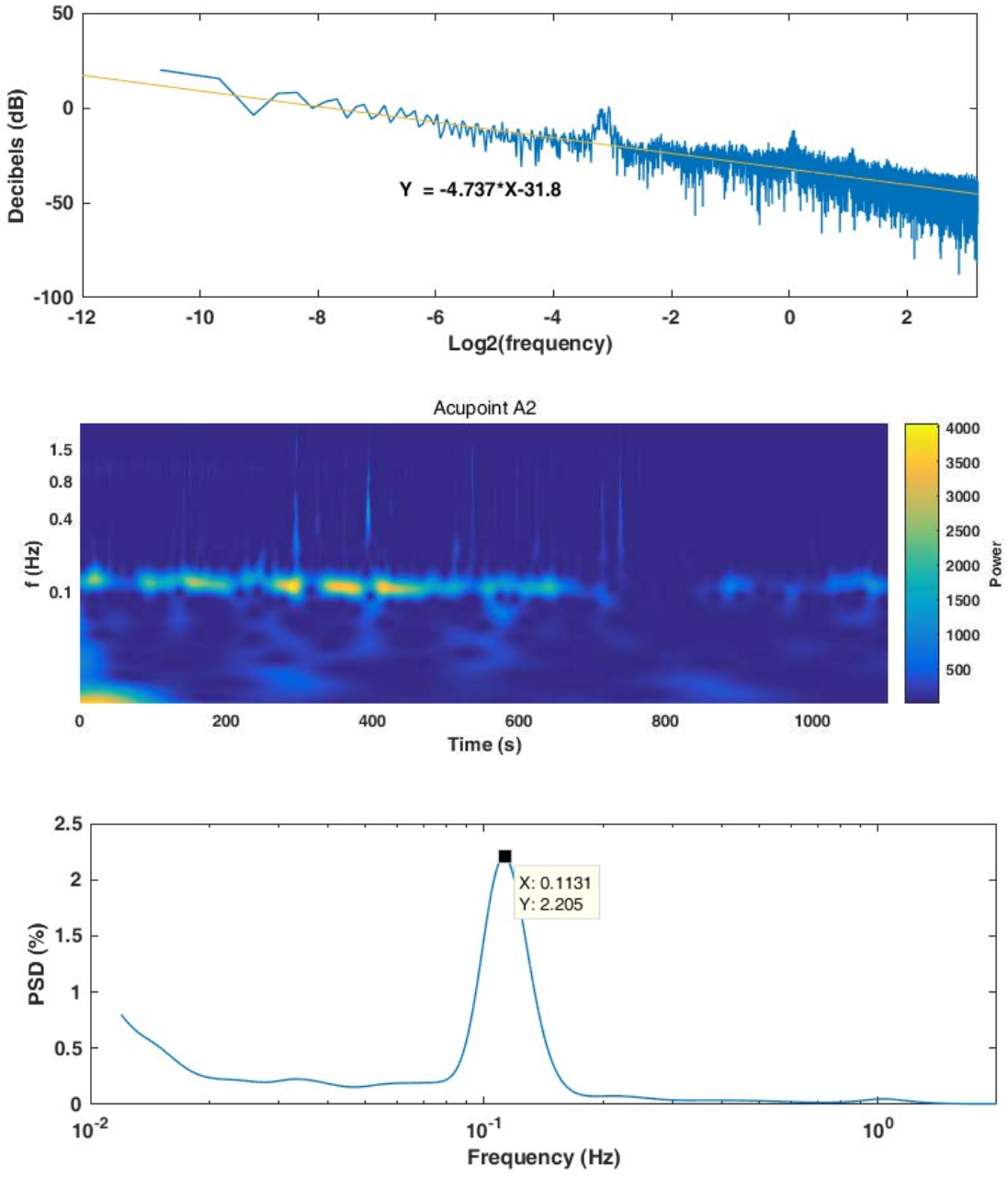

Fig. 7 Noise, wavelet & averaged wavelet example for Kongzui Acupoint

As shown above, the noise analysis has a smaller index than Chizes', but it also tends to pink noise. Both wavelet and averaged wavelet analysis results indicate that 0.1 Hz still dominates.

3.3.3 Quze (B1)

The location of Quze is the middle of the elbow fold of the ulnar side of the biceps brachii. The main function is to treat heart pain, stomach pain, vomiting, diarrhea and pain in the elbow joint. Moreover, some researcher also found out its another application, e.g., Xu et al. reported that the mean arterial pressure (MAP) and heart rate (HR) would be increased significantly after effect of electro-acupuncture on Acupoint Quze (Xu,Yu et al. 2010).

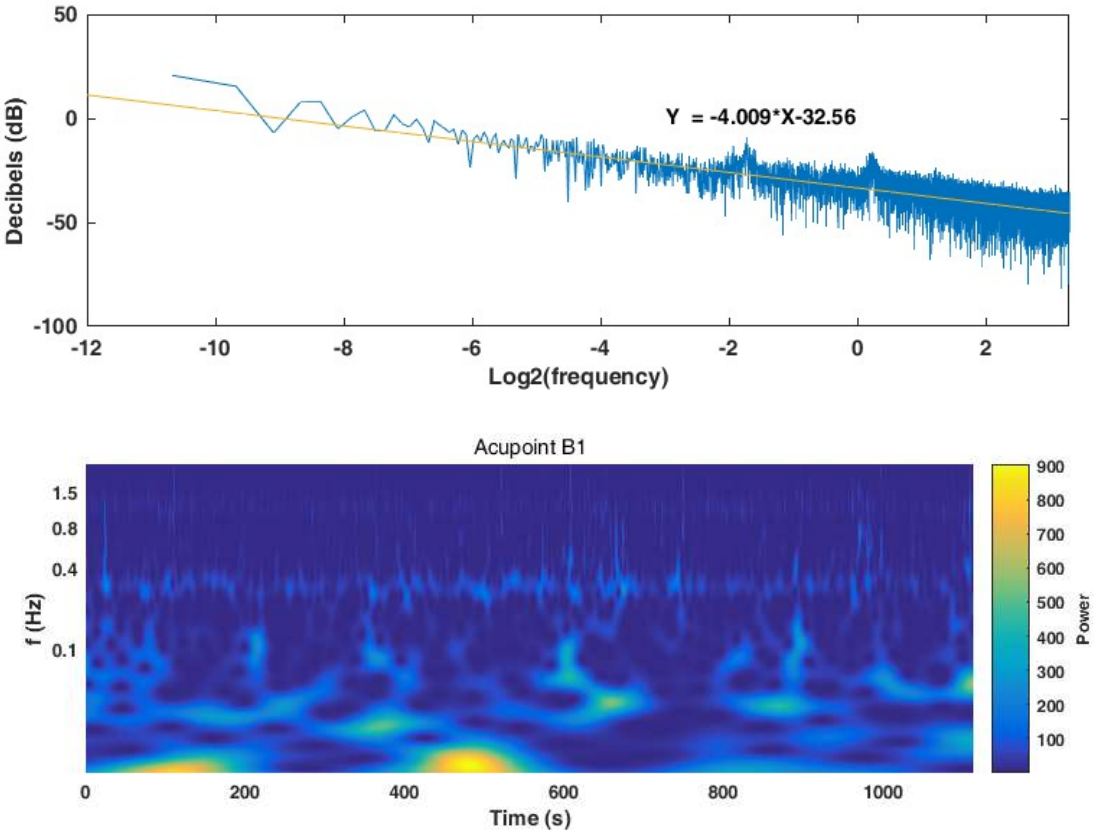

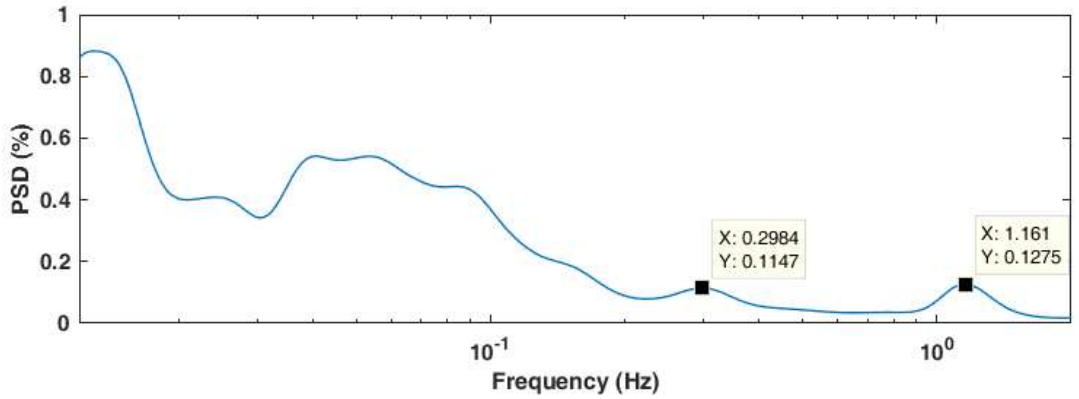

Fig. 8 Noise, wavelet & averaged wavelet example for Quze Acupoint

Compared with the two acupoints Chize & Kongzui, the exponent of noise analysis (Quze) is around 4.009 which tend to the pink noise (index = 3). From the wavelet & averaged wavelet analysis, both of the 0.3Hz & 0.1 Hz occupied the dominant place.

3.3.4 Ximen (B2)

Ximen is located on the flexor aspect of the forearm, around 16 cm proximal to wrist joint space. Due to it situated on the same as meridian with Quze, its function is also healing vomiting of blood, bleeding hemorrhoids.

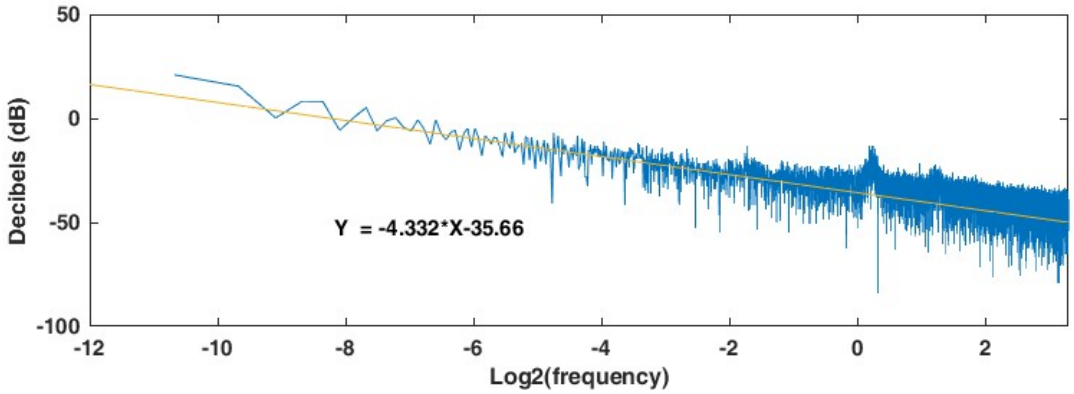

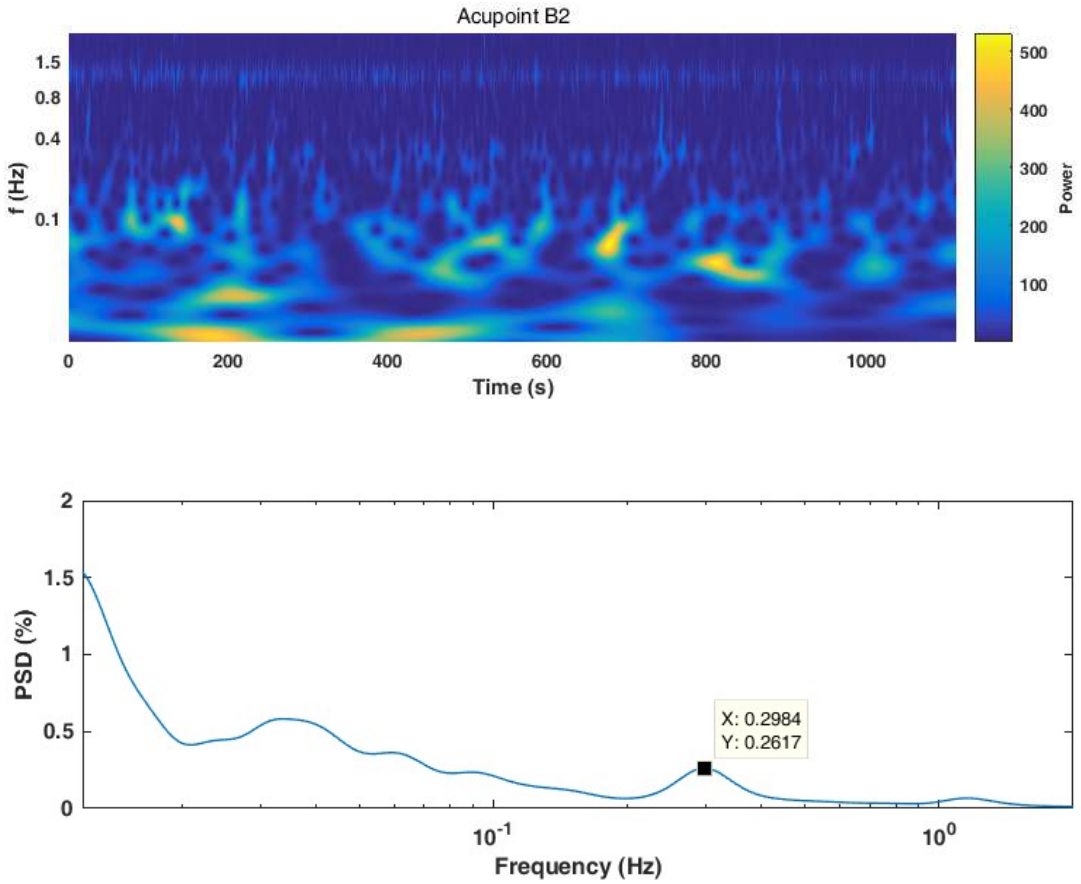

Fig.9 Noise, wavelet & averaged wavelet example for Ximen Acupoint

Though these two acupoints are along with the same meridian, the results are shown different. From the noise analysis shown in Fig. 3.8, the exponent is around 4.335 which tend to the pink noise. The dominant frequency is about 0.3 Hz displayed in wavelet and averaged wavelet analysis.

3.3.5 Shaohai (C1)

When the elbow is bent, the acupoint Shaohai is in the depression between the medial end of the transverse and cubital crease and the medial epicondyle of the humerus. The main indications are healing cardiac pain, and also for the stroke patients. Wang et al. found that the use of the electro-acupuncture to stimulate the acupoint Shaohai could heal the stroke within 6 weeks (Wang, Lin et al. 2014).

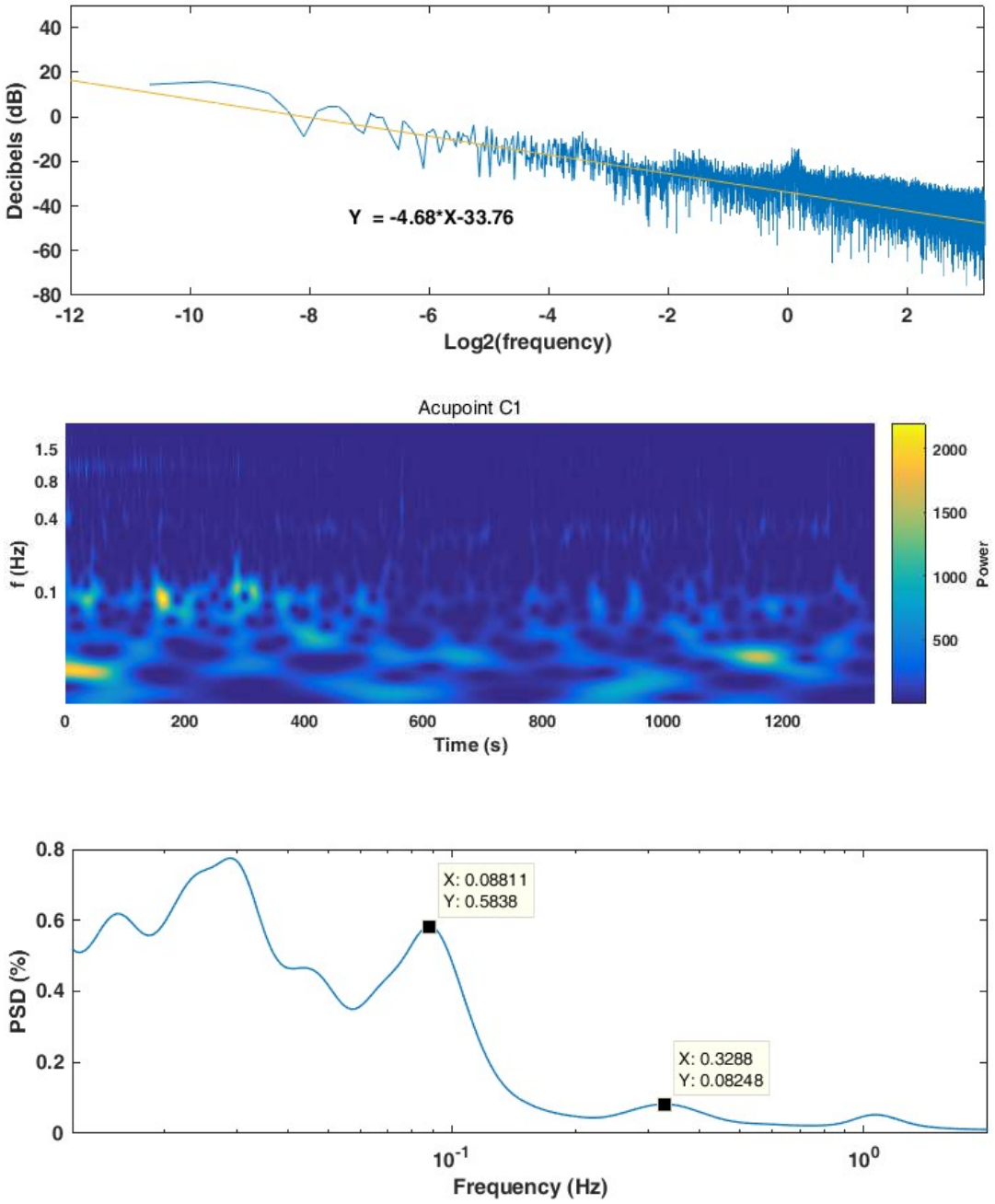

Fig. 10 Noise, wavelet & averaged wavelet example for Shaohai Acupoint

Fig. 3.9 shows that the noise analysis exponent is the same as the Chize & Kongzui noise exponent result, whereas it is shown differently based on the wavelet and averaged wavelet analysis. Obviously, the dominant frequencies within two different frequency intervals

(neurogenic & myogenic) are around 0.33 Hz, and also these two figures show significantly higher PSD in low frequency.

3.3.6 Lingdao (C2)

On the palmar aspect of the forearm, the Lingdao acupoint is on the radial side of the tendon flexor carpi ulnaris, Hong et al. discovered that the oxygen levels are higher at acupuncture points (Hong, Park et al. 2012). Using a 25-micron amperometric oxygen microsensor, they measured the partial oxygen pressure of the distal left forearm of humans. They found that the oxygen levels were significantly higher at the acupuncture points in Lingdao acupoint.

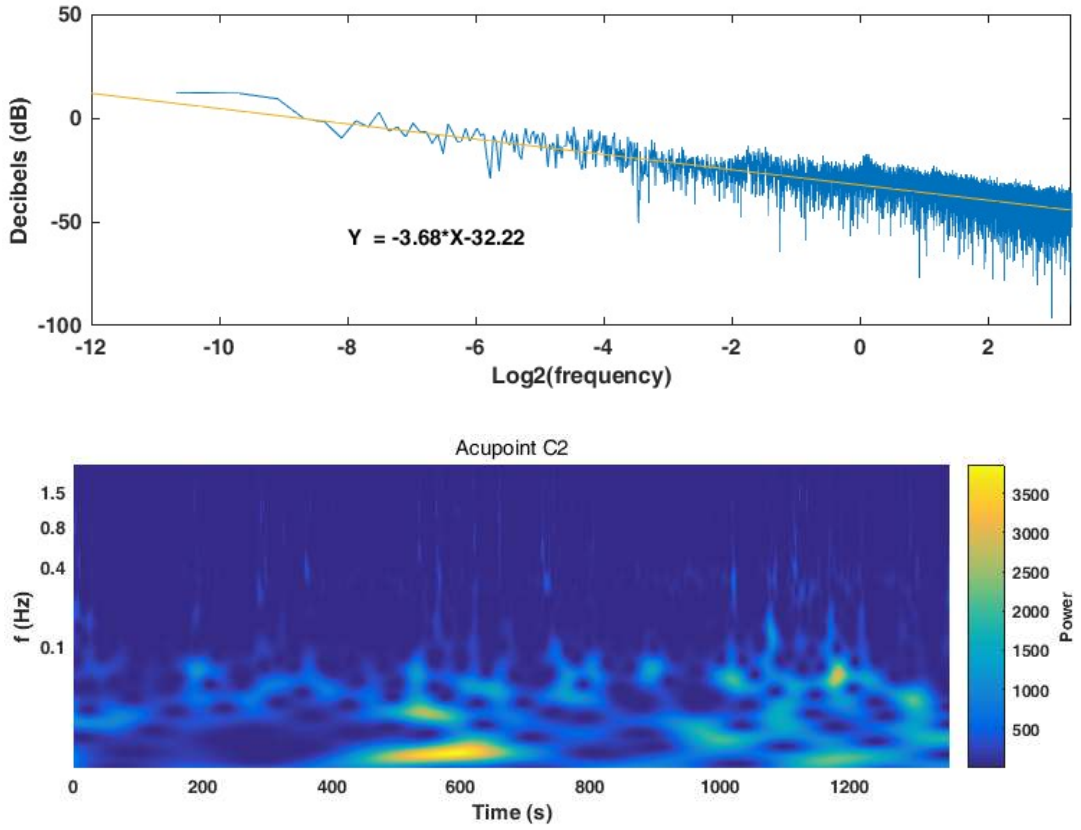

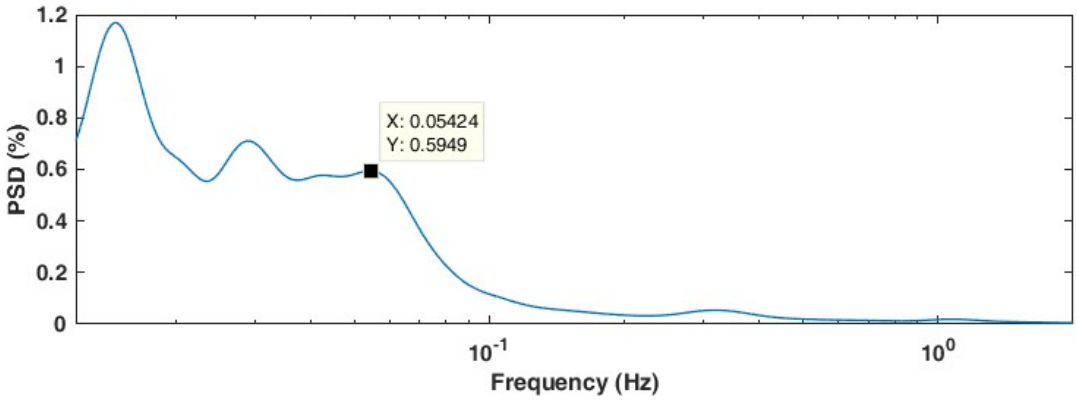

Fig. 11 Noise, wavelet & averaged wavelet example for Lingdao Acupoint

The noise analysis result (slope) is inclined to the pink noise type. The wavelet and averaged wavelet analysis result shown that there are much higher PSD within lower frequency.

3.4 Relative energy contribution analysis

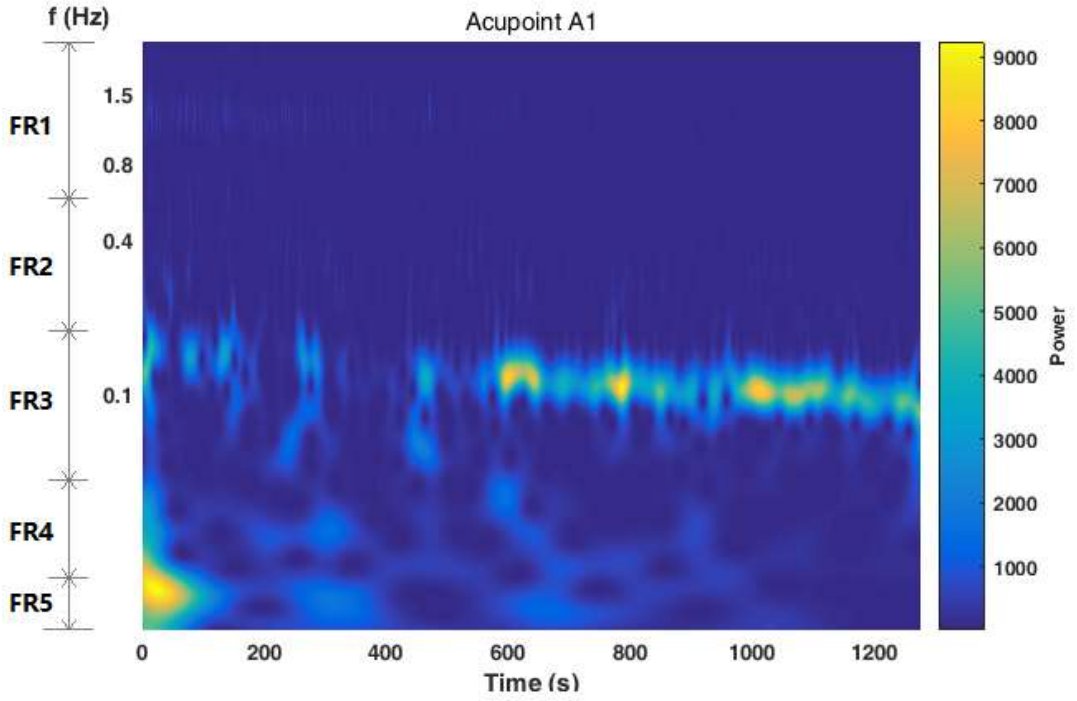

Fig. 12 Five frequency bands located in wavelet analysis result

The method named relative energy contribution analysis created by Hsiu was first used for assessing the variation of skin blood oscillation by stimulating the Hoh - Ku acupoint (Hsiu, Hsu et al. 2011) By comparison of results between the pre-stimulated and post-stimulated, the researchers have found that the relative energy from different frequency intervals will change in different situation after stimulating. In this thesis, the aim is to figure out the energy difference between acupoints and non-acupoint within different frequency intervals.. Fig. 3.11 shows an example that the whole Frequency range was divided by the Five frequency intervals which depend on the five different characteristic frequency (the heart activity related with the band 0.6 - 1.8 Hz (FR1), the respiration is corresponding to 0.2 - 0.6 Hz (FR2), the band 0.06 - 0.2 Hz is due to the myogenic activity (FR3), neurogenic also named sympathetic activity (FR4) and the endothelial activity (FR5) is associated with the band between 0.0095 - 0.02 Hz).

3. 5 Five Frequency Intervals of Relative Energy Contribution

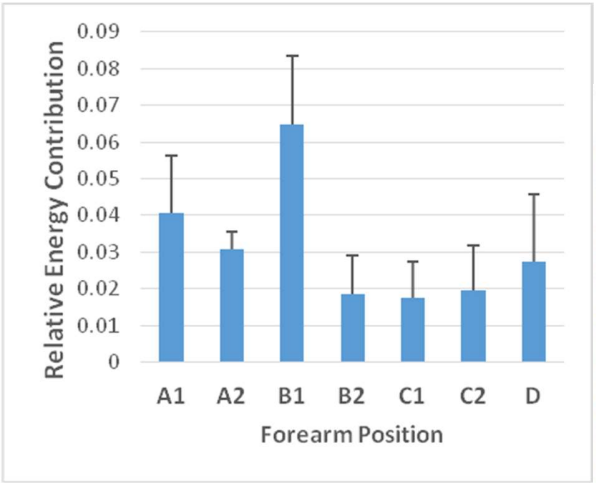

	A1	A2	B1	B2	C1	C2	D
A1	-	*	*	*	*	*	*
A2	*	-	*	*	*	*	
B1	*	*	-	*	*	*	*
B2	*	*	*	-			*
C1	*	*	*		-		*
C2	*	*	*			-	*
D	*		*	*	*	*	-

Fig. 3.12 Relative Energy Contribution for Cardiac activity, *p < 0.05

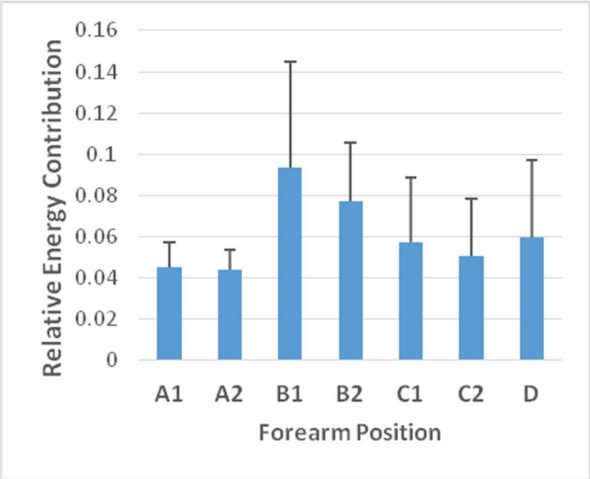

	A1	A2	B1	B2	C1	C2	D
A1	-	*	*	*	*	*	*
A2	*	-	*	*	*	*	
B1	*	*	-	*	*	*	*
B2	*	*	*	-			*
C1	*	*	*		-		*
C2	*	*	*			-	*
D	*		*	*	*	*	-

Fig. 3.13 Relative Energy Contribution for Respiration, *p < 0.05

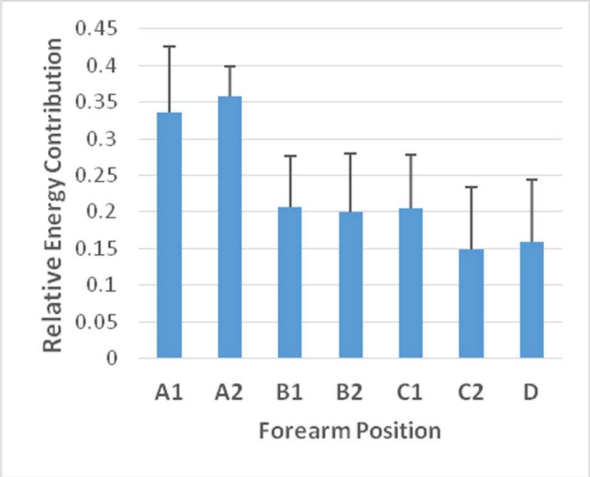

	A1	A2	B1	B2	C1	C2	D
A1	-		*	*	*	*	*
A2		-	*	*	*	*	*
B1	*	*	-			*	*
B2	*	*		-		*	*
C1	*	*			-	*	*
C2	*	*	*	*	*	-	
D	*	*	*	*	*		-

Fig. 134 Relative Energy Contribution for Myogenic, *p < 0.05

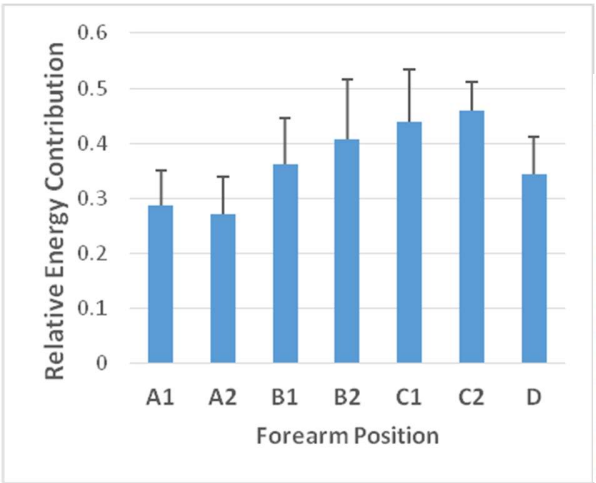

	A1	A2	B1	B2	C1	C2	D
A1	-		*	*	*	*	*
A2		-	*	*	*	*	*
B1	*	*	-	*	*	*	
B2	*	*	*	-		*	*
C1	*	*	*		-		*
C2	*	*	*	*		-	*
D	*	*		*	*	*	-

Fig. 145 Relative Energy Contribution for Neurogenic, *p < 0.05

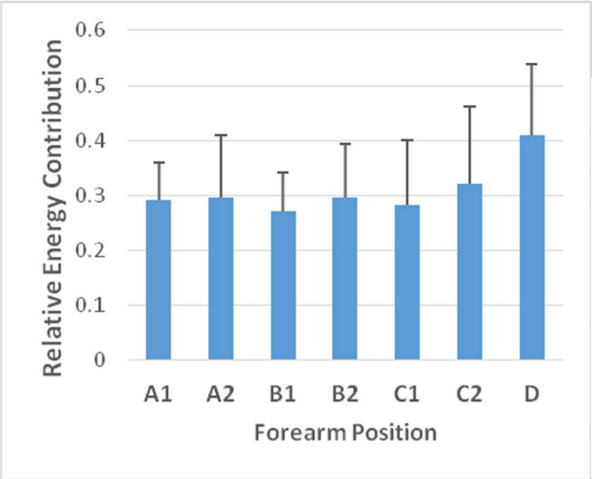

	A1	A2	B1	B2	C1	C2	D
A1	-						*
A2		-					*
B1			-				*
B2				-			*
C1					-		*
C2						-	*
D	*	*	*	*	*	*	-

Fig. 156 Relative Energy Contribution for Endothelial, *p < 0.05

Based on the percentage contribution of wavelet spectral densities, this study compared the changes in the spectra of blood-flow signals following differences between seven measured points. The Fig.3.12~3.16 show that the wavelet spectral percentage according to the five frequency intervals. Fig.3.12 shows the acupoint B1 occupied the largest percentage among FR1 (cardiac component), which has significantly difference by comparing with the rest points (*p < 0.05). For Frequency band 2 (respiration), it is clear shown that the percentages of acupoint B1 & B2 are much larger than the others (*p < 0.05), and also displayed that the acupoint B1 is still occupied the highest place within FR2 band. For the Fig.3.12 and Fig.3.13, it is obviously see that the acupoint B1 (Quze) is affected significantly by the cardiac and respiration than other points (*p <0.05). As Xu reported (Xu, Yu et al. 2010), stimulating the acupoint B1 (Quze) would increase the mean arterial pressure and heart rate. Thus, the cardiac and respiration component might be considered as the essential factors for effecting the stimulating of acupoint B1. In terms of the Fig.3.14 (Frequency band3, myogenic), it displayed different situation from Fig.3.12 & Fig.3.13. It was found that the acupoint A1&A2 have apparently higher myogenic percentage than others (*p <0.05), which are consistent with the original times series (Fig.3.4). Also, the Fig.3.14

proved that the acupoint A1&A2 occupied the similar myogenic percentage owing to the same meridian (*p > 0.05). Therefore, this conclusion may serve as a reference to compare the people with lung disease. For the neurogenic factor, the acupoint C1 and C2 hold leading position among measured points (*p < 0.05), and followed by acupoint B1 and B2. Since this study considered the non-acupoint D as the reference point which could find the differences by comparing the acupoint and non-acupoint. The results also found out some higher significances (*p > 0.05) that have similar percentage by comparing with acupoints and Non-acupoint D in first four intervals (Fig.3.12~ Fig.3.15), which are A2&D (FR1 &FR2), C2&D (FR3) and B1&D (FR4). With respect to the FR5 wavelet spectral densities in Fig.3.16, six acupoints occupied similar percentage (*p > 0.05) but much lower than non-acupoints' (D), suggesting that the endothelial cells on non-acupoint are more activity than acupoints along with forearm.

3.6 Relative Energy Contribution in Different Meridians

Depend on the theory of traditional Chinese medicine, the main function of the meridian is to transfer biological signals in order to generate communication between different parts of peripheral tissues and internal organs. The common communication mode is through the nervous system, which operates through nerve impulses at an extremely high speed for releasing neurotransmitters into synapses and with accurate point to point communication. (Zhang, Wang et al. 2016). In our study, we assumed that the acupoints situated in the same meridian could maintain the balance of communication, which suggesting the adjacent acupoints should have similar frequency characteristic within five intervals.

Fig.3.17 ~ 3.19 show that the relative energy contribution of seven points distributed on different meridians, displaying the comparison of two adjacent acupoints along with same

meridian and one reference point (D), and the data used in these figures are based on averages. From the following figures shown, it is obviously to see that the energy contribution of two adjacent acupoints on a meridian is roughly similar by comparing with the reference points. Besides, it also can be figure out that the reference point is the same trend as Fig.3.18 and Fig.3.19 in the first four intervals, with the obvious difference in the fifth interval (Endothelial).

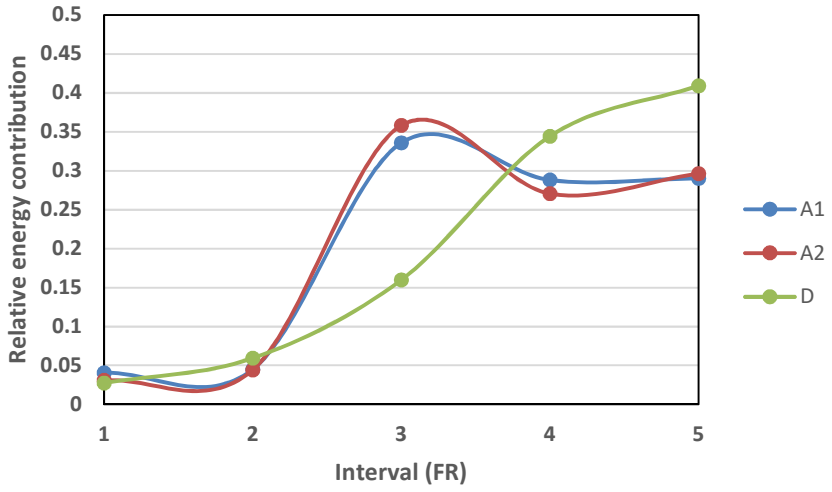

Fig. 3.17 Relative energy contribution of reference point D and acupoint A1, A2 on lung meridian

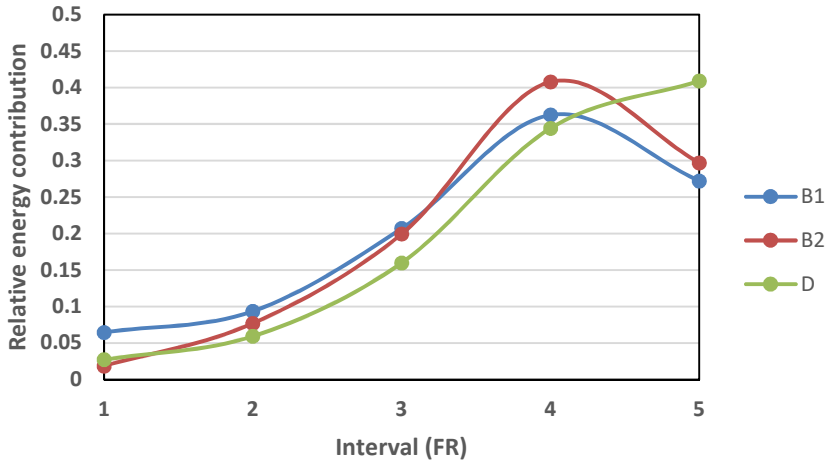

Fig. 3.18 Relative energy contribution of reference point D and acupoint B1, B2 on pericardium meridian

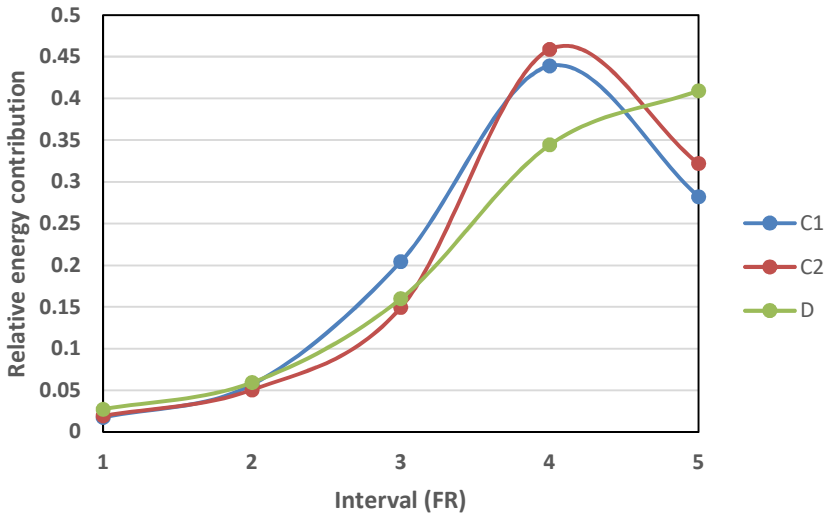

Fig. 3.19 Relative energy contribution of reference point D and acupoint C1, C2 on heart meridian

3.7 Noise analysis & SNR analysis results

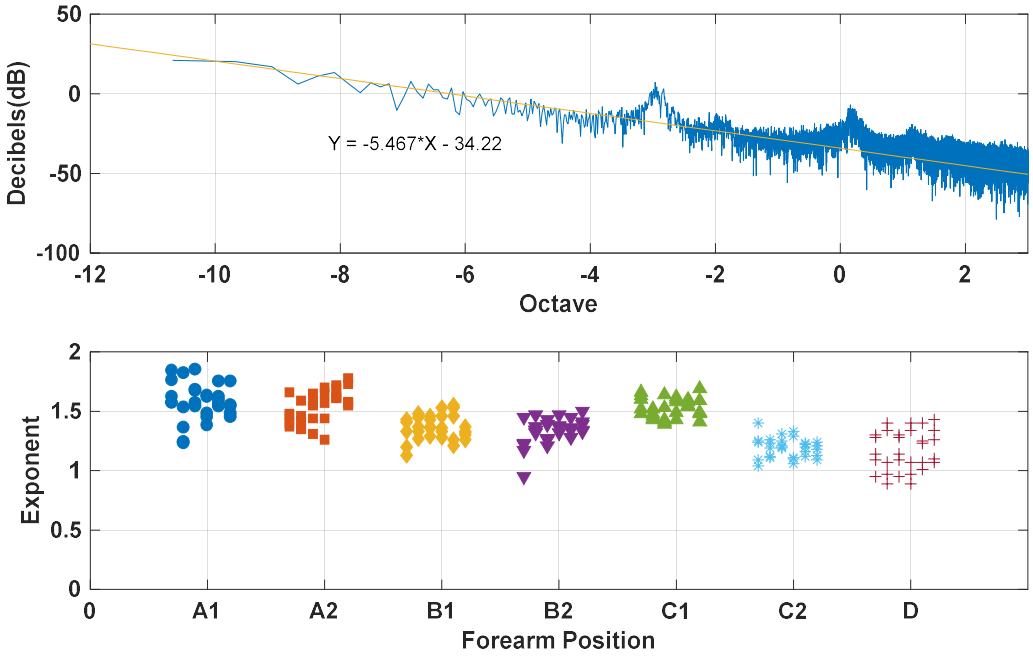

	A1	A2	B1	B2	C1	C2	D
A1	-		*	*	*	*	*
A2		-	*	*		*	*
B1	*	*	-		*	*	*
B2	*	*		-	*	*	*
C1	*		*	*	-	*	*
C2	*	*	*	*	*	-	
D	*	*	*	*	*		-

Fig. 3.20 (a) An example of noise analysis of Chize Acupoint A1, (b) The comparison of Calculated exponents based on the seven selected sites, *p < 0.05

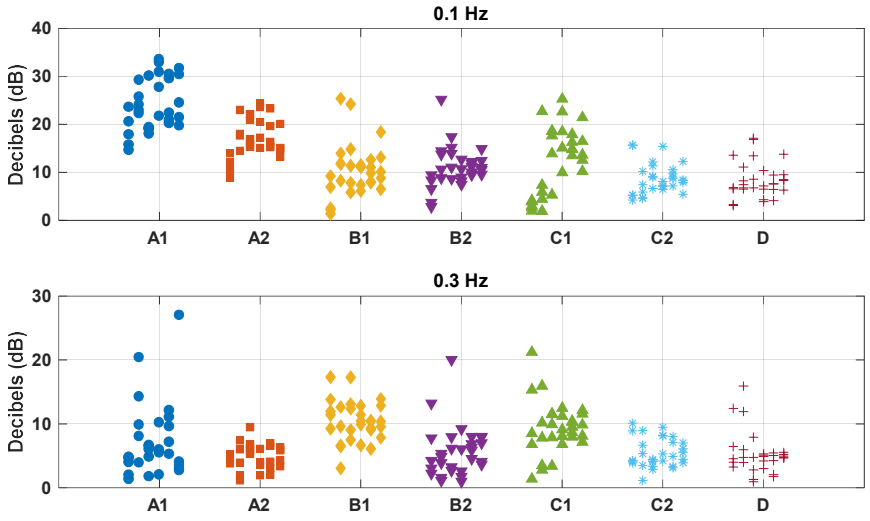

0.1Hz	A1	A2	B1	B2	C1	C2	D
A1	-	*	*	*	*	*	*
A2	*	-	*	*	*	*	*
B1	*	*	-		*		
B2	*	*		-		*	*
C1	*	*	*		-	*	*
C2	*	*		*	*	-	
D	*	*		*	*		-

0.3Hz	A1	A2	B1	B2	C1	C2	D
A1	-	*	*		*		
A2	*	-	*		*		
B1	*	*	-	*		*	*
B2			*	-	*		
C1	*	*		*	-	*	*
C2			*		*	-	
D			*		*		-

Fig. 3.21 (a) Seven SNR results for 0.1 Hz (b) Seven SNR results for 0.3 Hz, *p < 0.05

Fig.3.20 shows that the exponents (γ=slope/3) of acupoint A1 & A2 & C1 are around 1.5 which are tend to the brown noise, and for acupoint C2 & non-acupoint D, these exponents (γ) are close to the pink noise (index = 1). For brown noise type (index = 2), the time series have significantly self-similarity, which means the skin blood flow oscillation on acupoint A1 & A2 & C1 maintain a certain vibration characteristic along with time. For pink noise type, it is related with the long-term memory, C2 & D are tend to the pink noise. Combining with the meridian, the exponent of an acupoint have an extreme similarity with the adjacent acupoint along with the same meridian except heart meridian. As the Fig.3.20 shown, the exponents of lung meridian (A1, A2) are around 1.5 and pericardium meridian (B1, B2) are 1.3, indicating that these two meridians have unique characteristics in noise analysis.

For Fig.3.21, the first Figure was carried out the SNR ratio around 0.1 Hz from averaged wavelet analysis, it is observed that A1 & A2 & C1 occupied the dormant place among measured points, where its situation are similar to the Fig.3.20 In terms of the 0.3 Hz of SNR ratio, the acupoint B1 & C1 are around 10 dB ratio which are much higher than the rest points. The non-acupoint D is considered as the reference point. From the SNR analysis figure, it is shown that the value of acupoint B1 & B2 & C2 are equal to non-acupoint D among 0.1 Hz SNR ratio, for 0.3 Hz SNR ratio, A1 & A2 & B2 & C2 are equal to non-acupoint D.

Chapter 4 - Vasomotion Studies

4.1 Mechanism & physiological of Vasomotion

As the Chapter 1 mentioned, studying vasomotion in vivo allows the behavior of the vessel walls to be studied in their neutral environment, as affected by systemic and local regulatory processes. Holger Nilsson (Nilsson and Aalkjaer 2003, Aalkjær, Boedtkjer et al. 2011) suggested that it is an oscillation of vascular tone that is generated from within the vascular wall and is not a consequence of heartbeat, respiration, or neuronal input. Based on the mechanism condition, some studies have proved that the vasomotion generated within vascular wall are caused by several factors such the smooth muscle cell releasing Ca+, endothelium - niric oxide (No) - cGMP axis etc.

For the assumption of this study, part of the vasomotion may be generated from physical principle, this study believed that the vasomotion can also be produced by blood passing through vessels. In accordance with the Hagen - Poiseulle law, the oscillation of the LDF signals is proportional to Q, L is the length of a vessel segment, η is blood viscosity, ΔP is the pressure difference across the arteriole segment, and r is the arteriole radius.

$$Q = \frac{\pi \Delta P}{R} = \frac{\mathrm{r}^4 \pi \Delta P}{8 \eta L}$$

Hence, the factors causing oscillation should be related with pressure difference or cardiac pulse cycle. To verify our assumption, capturing the LDF signal time series from the signal vessel could be a convenience method.

4.2 Simulated Experiment of Vasomotion

In accordance with the Hagen - Poiseulle law, a simulated experiment was designed, keeping the radius, viscosity, length and pressure difference as the constant value. The infusion apparatus could be regarded as the cardiac heart. This because that the drip water frequency is same as the velocity of pulse, and the tube of infusion apparatus is regard as the single vessel. To avoid other factors in the outcome, the water played as blood flow through the single vessel. The setup of simulated experiment is shown as below (Fig.4.1).

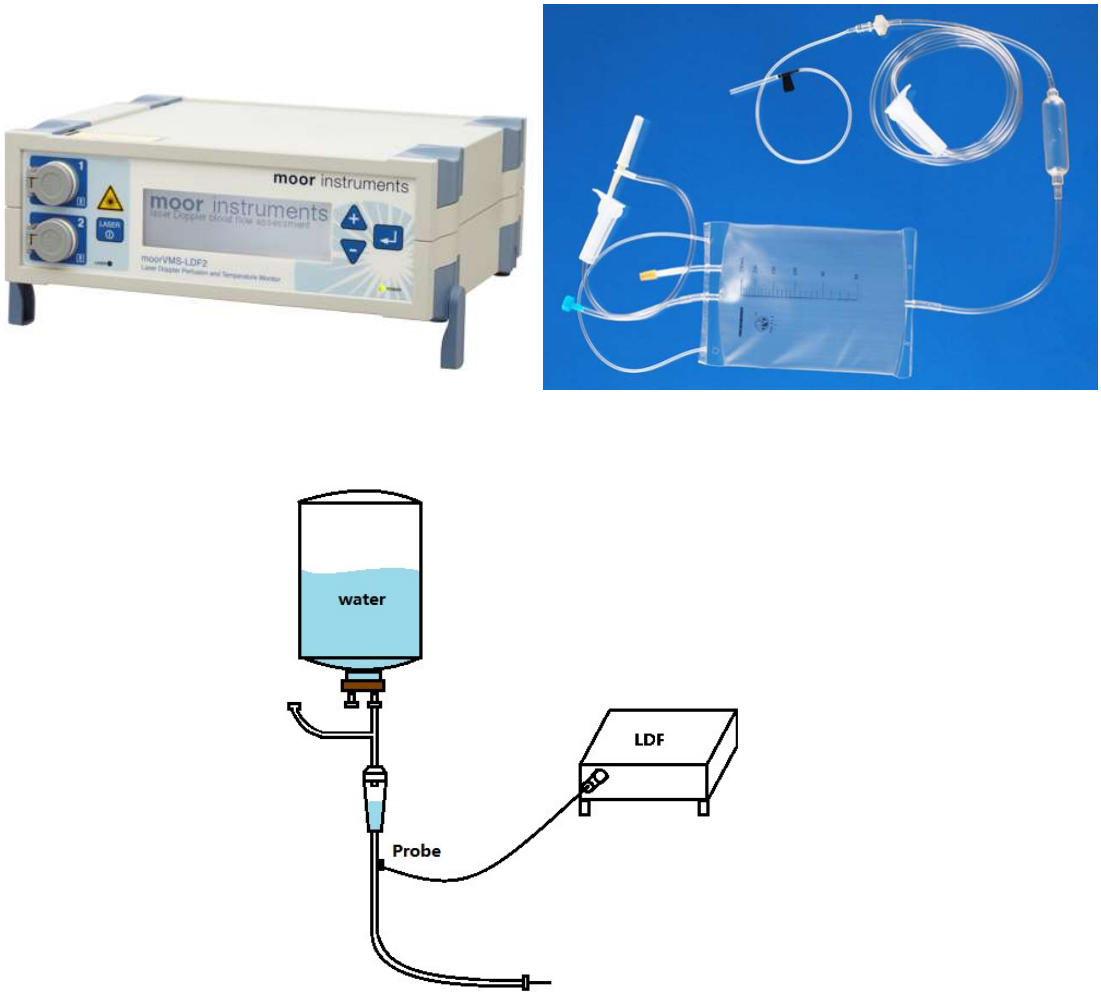

Fig. 4.1 (a) Laser Doppler Flowmetry (LDF) and Infusion apparatus (b) Basic structure of simulated experiment

During the experiment, the drip referred to as the cardiac heart frequency was controlled around 1 Hz. The experiment was carried out repeatedly by nine times, and each lasted for an hour. The Figure 4.2 shows an example of original time series for simulated experiment.

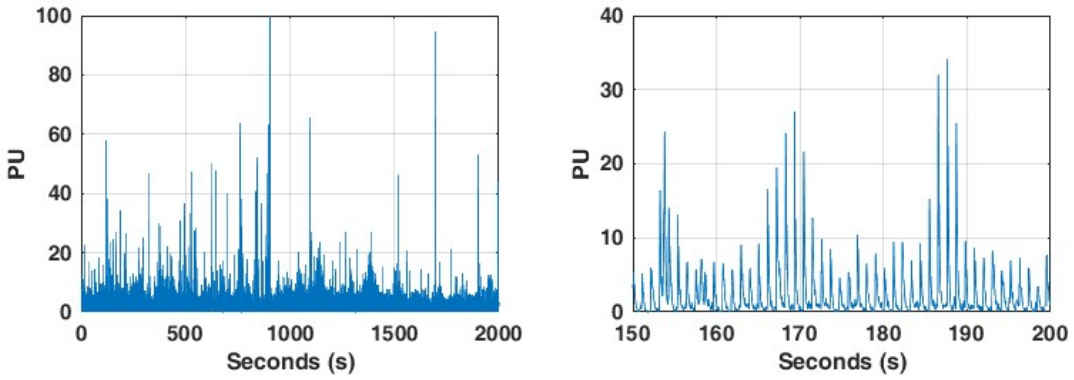

Fig. 4.2 Original time series of simulated experiment and zoom in figure

It is suggested that the vasomotion occurred in this time series, and the right figure shown the enlarged view. The displayed pattern is similar to the cardiac heartbeat, which means that the simulated experiment is in line with the physiological condition. Depending on the different droplet frequency setting, the rest simulated experiments would be shown as following.

4.2.1 Simulated Experiment 1

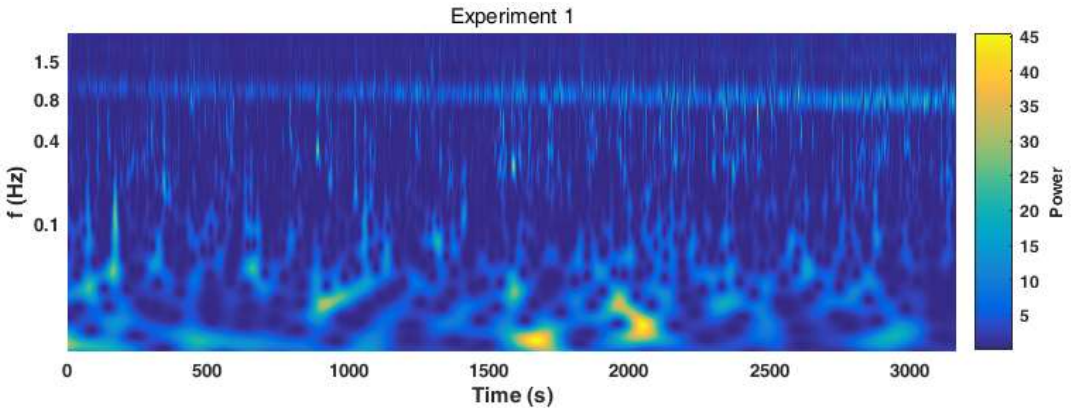

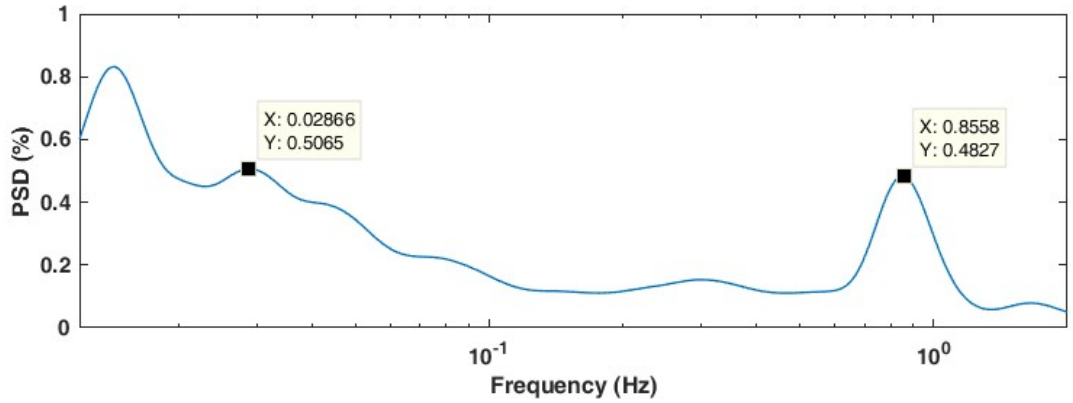

Fig. 4.3 wavelet & averaged wavelet analysis for Experiment 1

4.2.2 Simulated Experiment 2

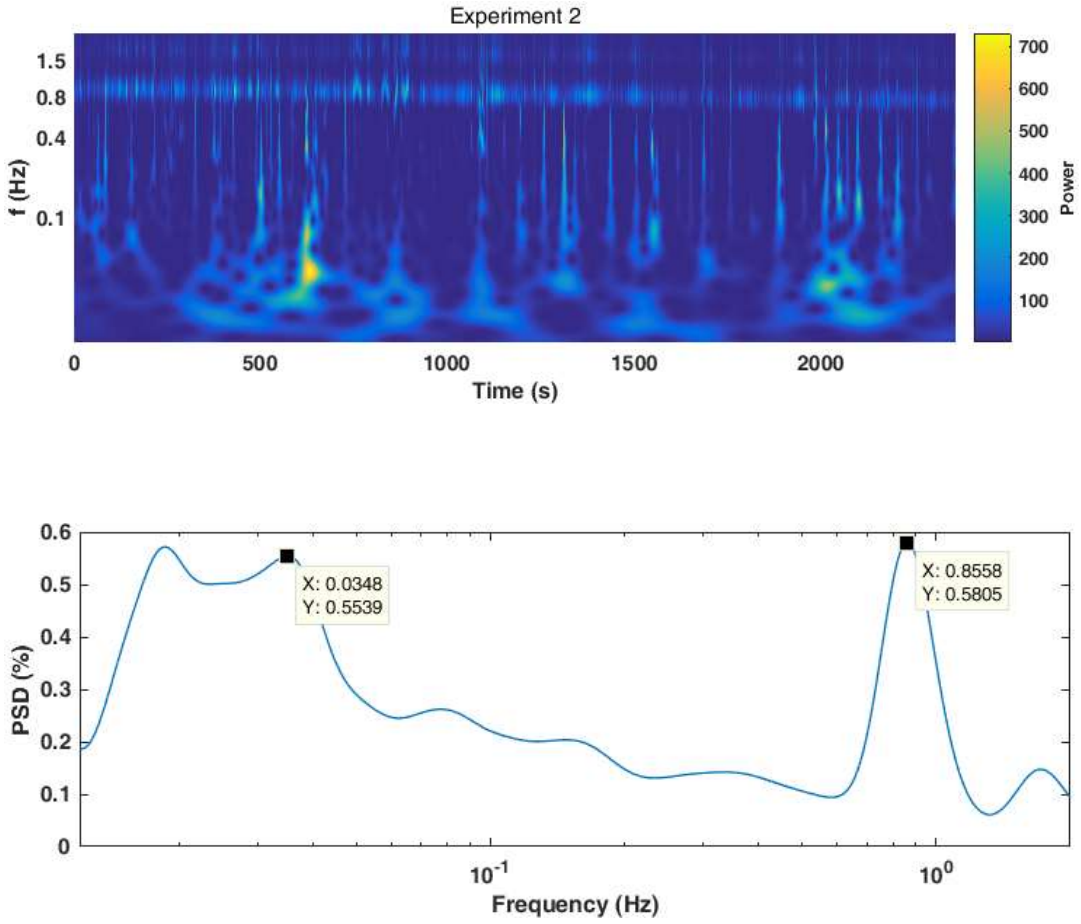

Fig. 4.4 wavelet & averaged wavelet analysis for Experiment 2

4.2.3 Simulated Experiment 3

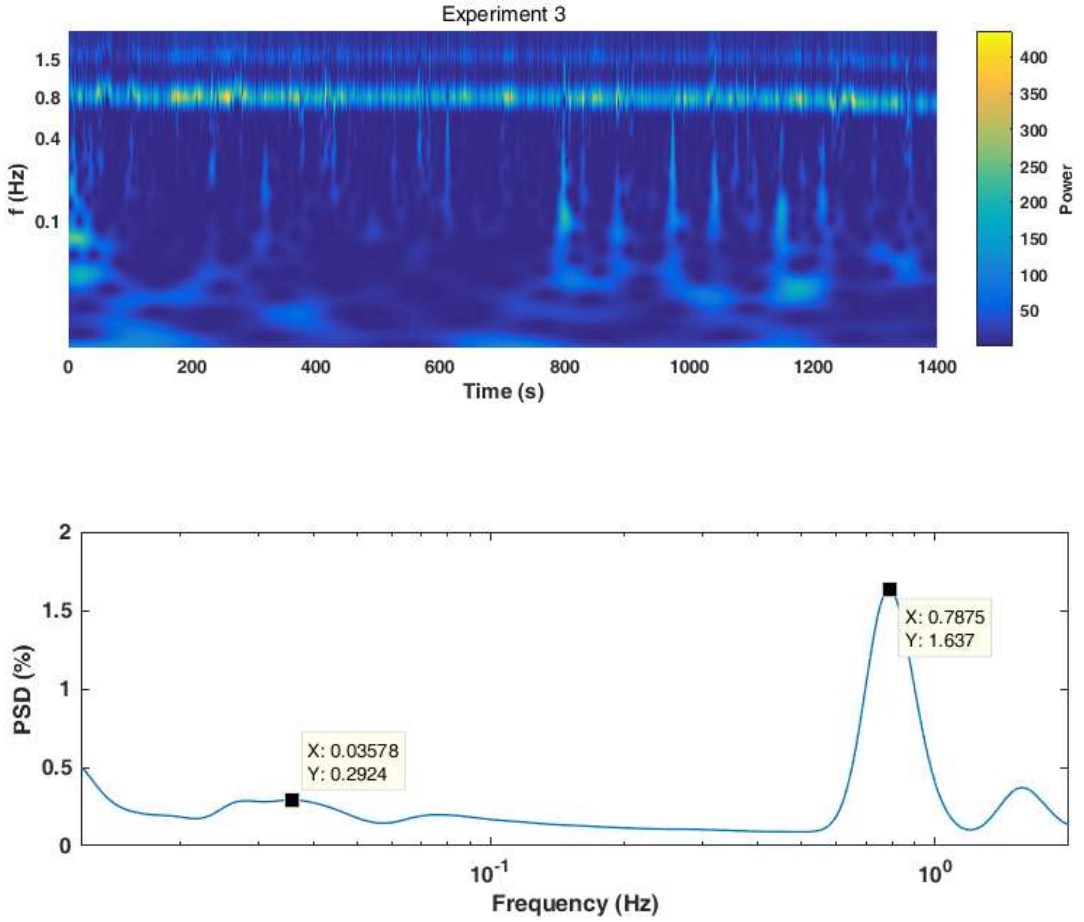

Fig. 4.5 wavelet & averaged wavelet analysis for Experiment 3

4.2.4 Simulated Experiment 4

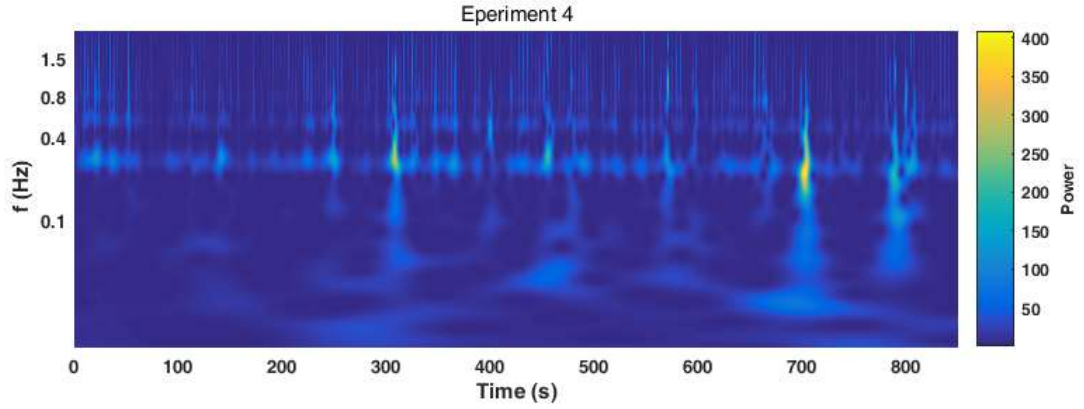

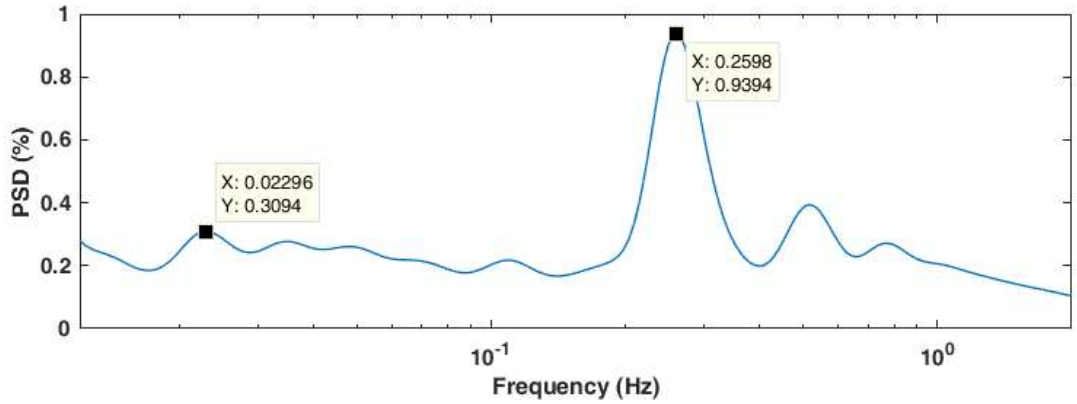

Fig. 4.6 wavelet & averaged wavelet analysis for Experiment 4

4.2.5 Simulated Experiment 5

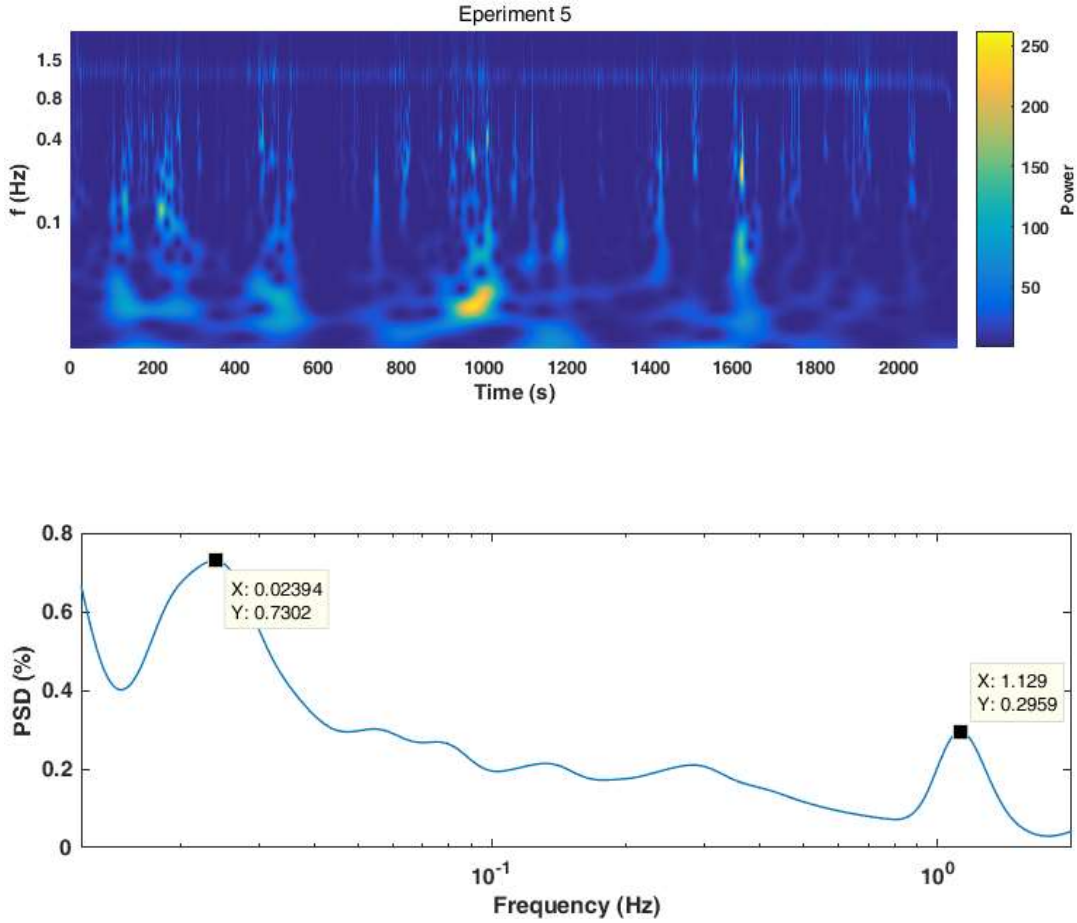

Fig. 4.7 wavelet & averaged wavelet analysis for Experiment 5

4.2.6 Simulated Experiment 6

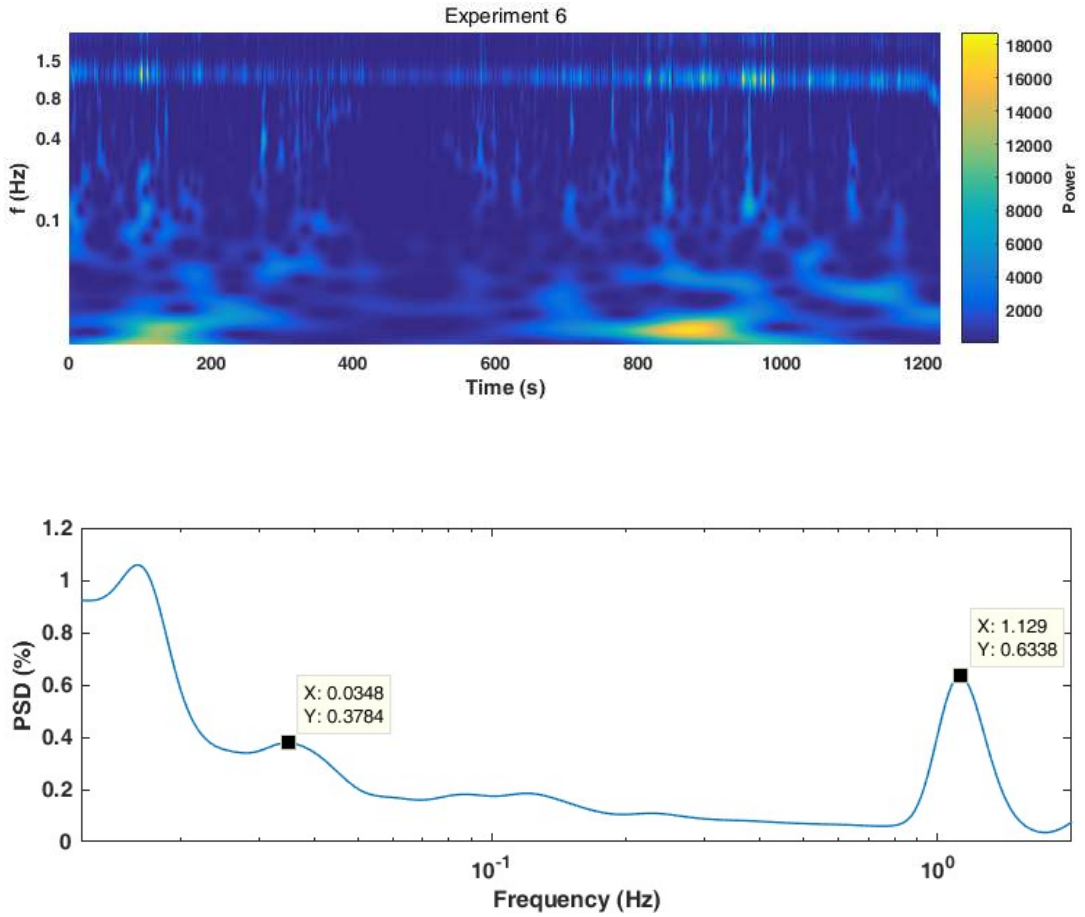

Fig. 4.8 wavelet & averaged wavelet analysis for Experiment 6

4.2.7 Simulated Experiment 7

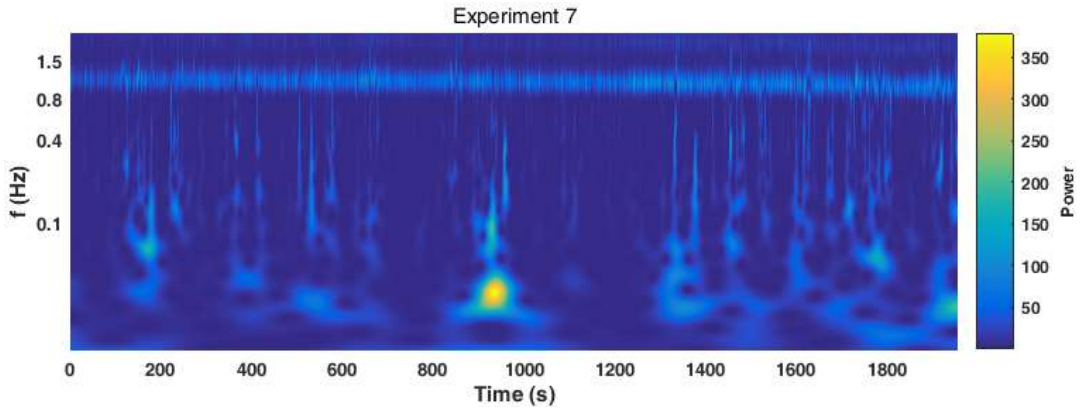

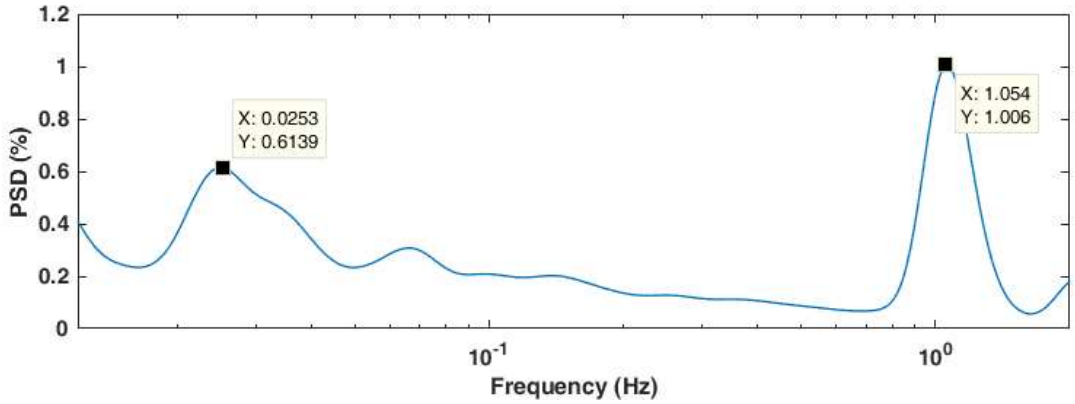

Fig. 4.9 wavelet & averaged wavelet analysis for Experiment 7

4.2.8 Simulated Experiment 8

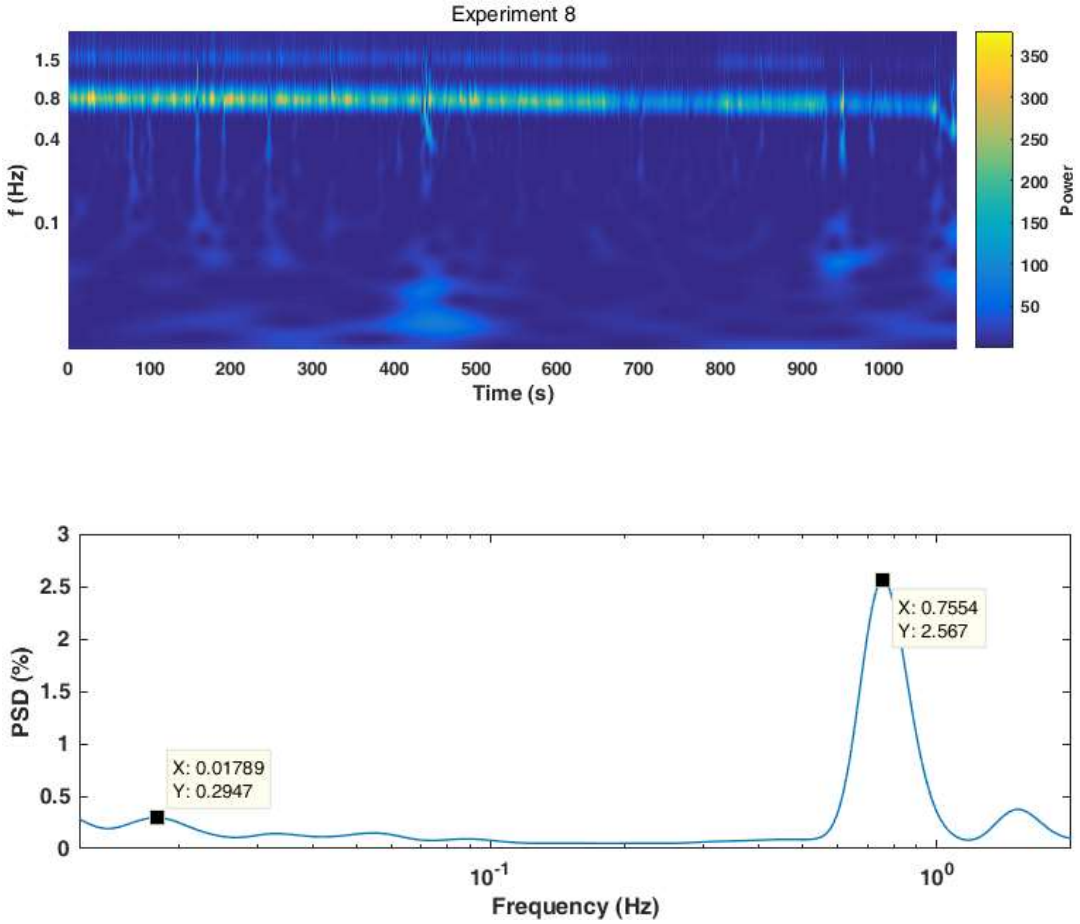

Fig. 4.10 wavelet & averaged wavelet analysis for Experiment 8

4.2.9 Simulated Experiment 9

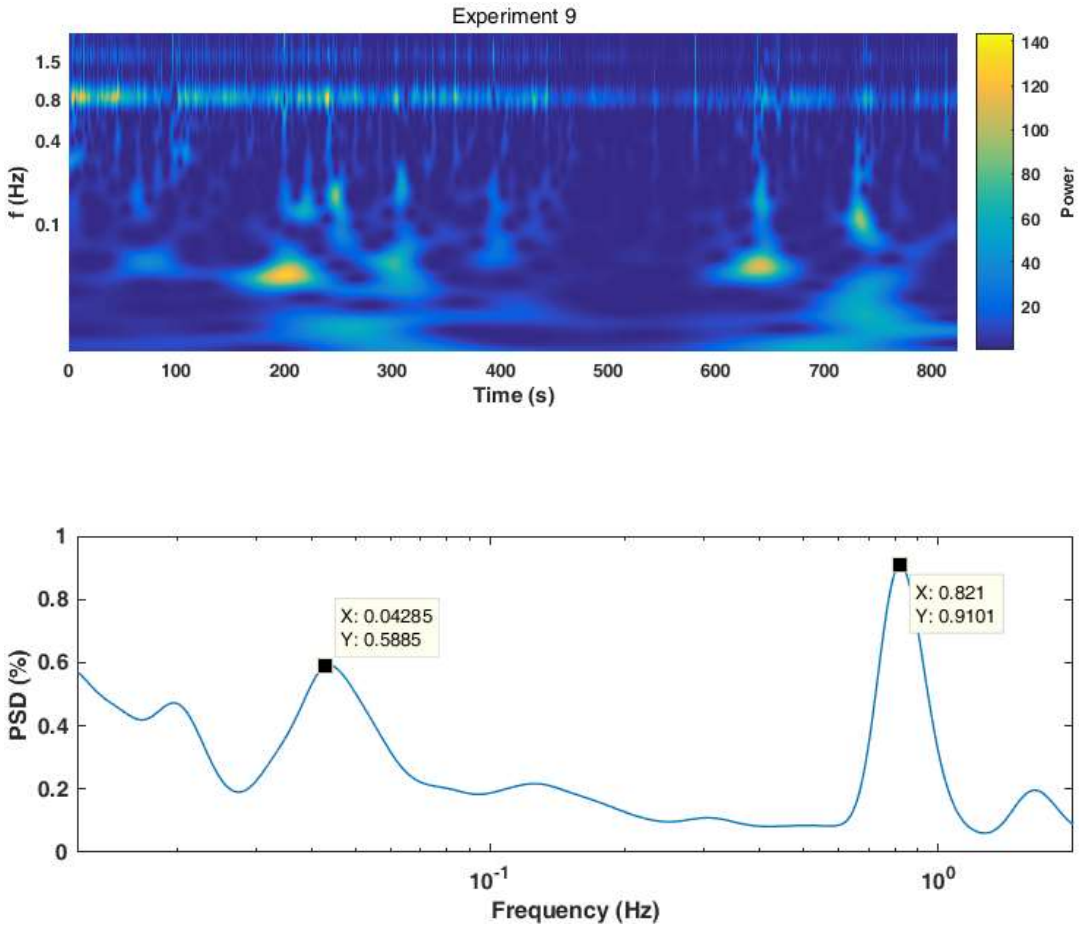

Fig.4.11 wavelet & averaged wavelet analysis for Experiment 9

4.2.10 Simulated Results

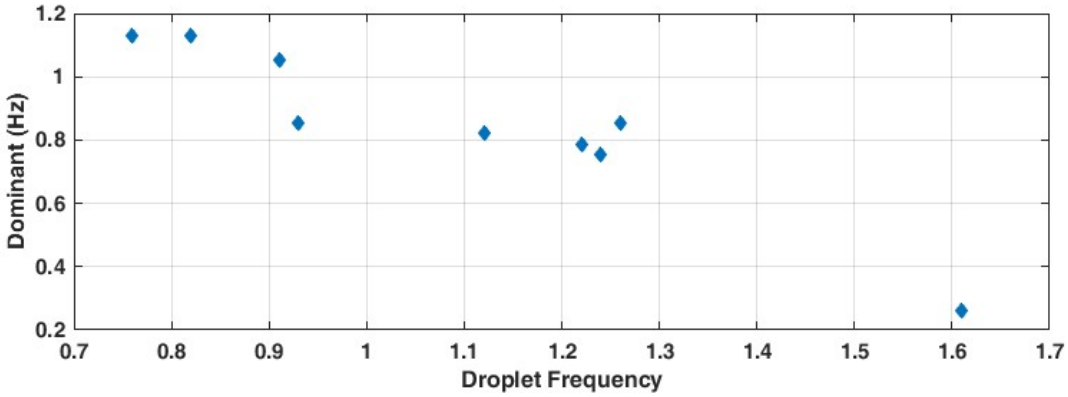

Fig.4.12 The dominant frequency changed with the droplet frequency

Within the average dominant frequency is around 1 Hz. The dominant frequency is decreased with the droplet frequency which shown in Fig. 4.12. It can be explained that the drip chamber could control the droplet frequency during the whole experiment. Besides, the dominant frequency is not an extreme value but the largest value within specific range. This can explain that the different falling velocity of droplet occurred in the experiment with the constant pressure.

Fig. 4.13 obviously shows that the primary lower frequency focuses on around 0.02 Hz ~ 0.04 Hz, which not changed with the droplet frequency. Recalling the previous experiment parameter settings and Hagen - Poiseulle law, the simulated experiment controls the unchanged parameters include (vessel radius, length of the segment, viscosity (water), and pressure difference). Hence, the only factor would be the falling velocity of droplet.

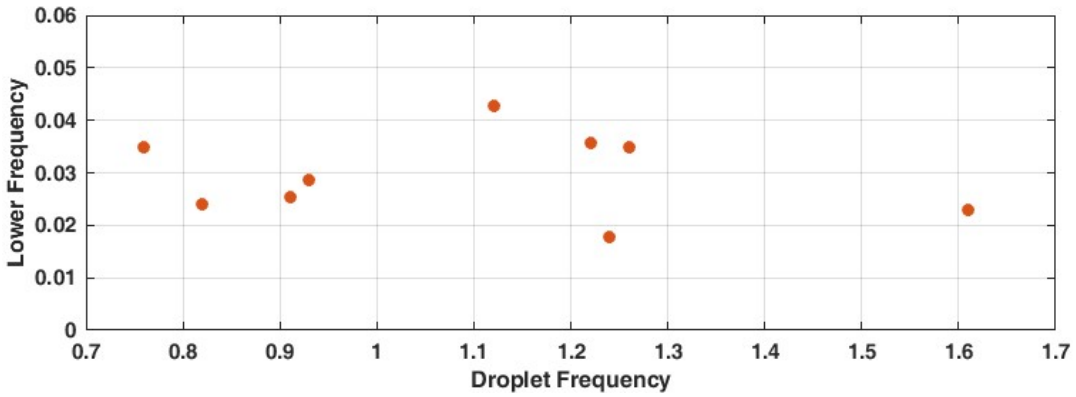

Fig. 4.13 Lower frequency changed with droplet frequency

Hence, it is assumed that the falling velocity of droplet is the same as the velocity of pulse in human body. To verify the assumption of this study, a point upon radial artery situated on wrist was selected (Fig. 4.14). This is because that the other blood vessels are not very

dense at this selected point, it has a greater ability to measure the signal from the signal vessel.

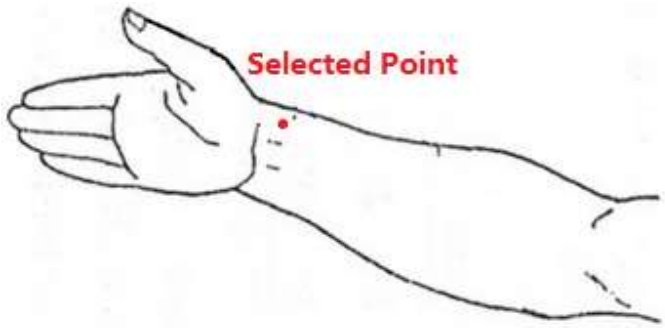

Fig. 4.14 Selected point on forearm

4.3 Pulse Experiment

Five healthy subjects (25±3 years old) were recruited by this experiment, which were also asked to refrain from consuming caffeine in the 2h before the test and not to take any medication three days before the experiment. Each subject would be measured twice by attaching LDF probe on selected point. The sampling rate was 40 Hz and the measure time was around 10 min.

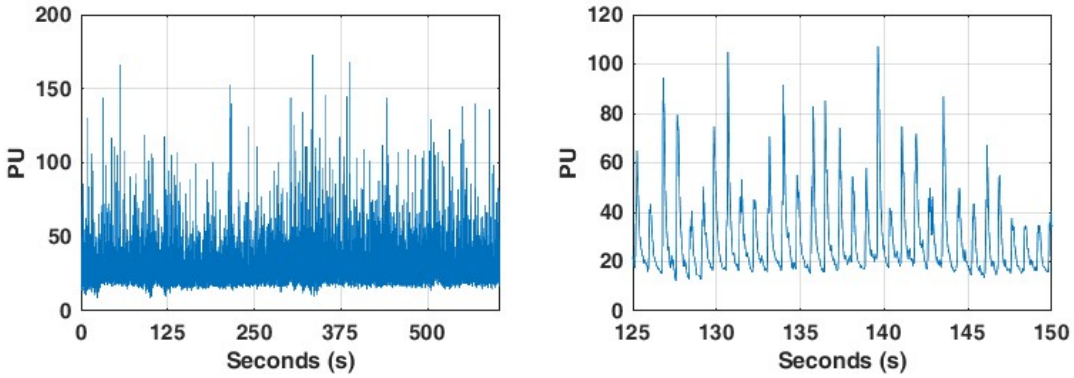

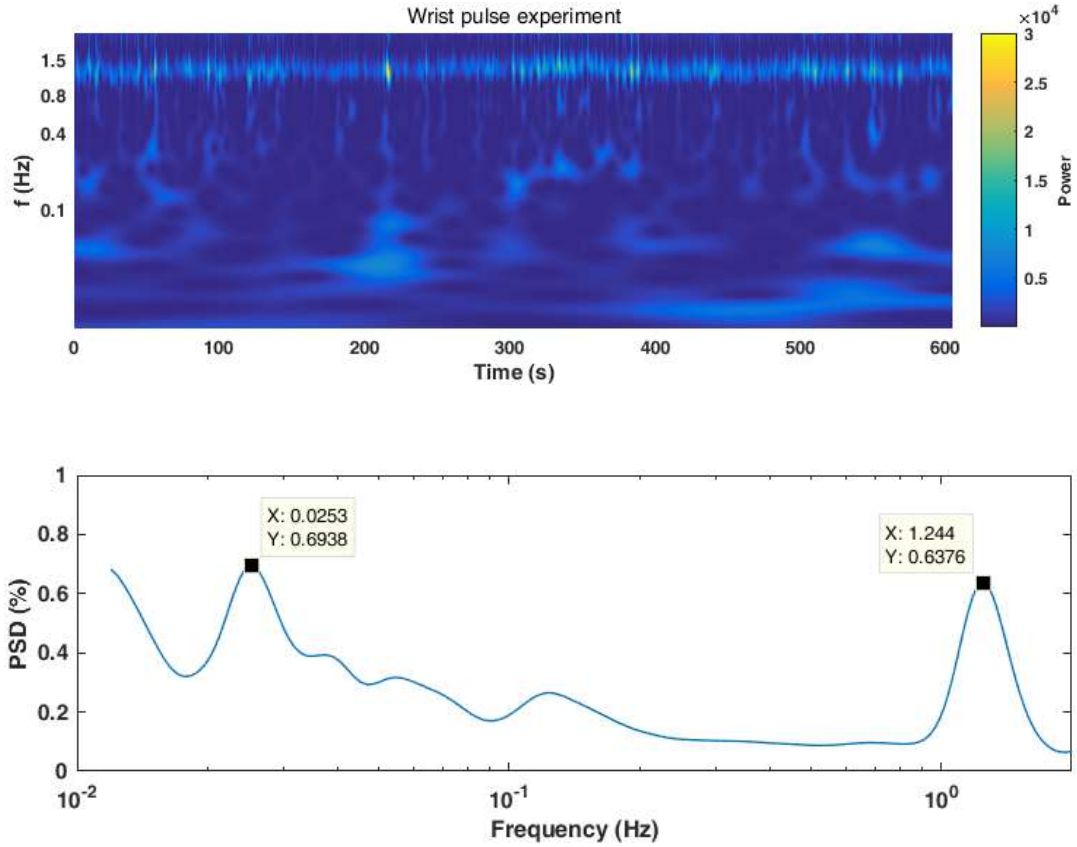

Fig. 1615 An example of selected point include original time series & wavelet & averaged wavelet analysis

4.3.1 Pulse Experiment Results

Table 2 Ten experiment results

Experiment No.	Dominant (Hz)	Low Frequency (Hz)
1-1	1.244	0.0253
1-2	1.334	0.0275
2-1	1.262	0.0389
2-2	1.262	0.0333
3-1	1.371	0.0249
3-2	1.352	0.0246
4-1	1.194	0.0261

4-2	1.194	0.0179
5-1	1.039	0.0189
5-2	1.039	0.0362

After the experiment, it could be found that the results of each subjects' two experiments were basically the same included dominant frequency (cardiac activity) and lower frequency. As mentioned in Chapter 1, the vasomotion with a frequency ranging between 0.01 to 0.3 Hz are detected by the isolated artery from various species [66, 67]. Hence, it was found that the produced lower frequency is around 0.02 - 0.03 Hz partly should related with neurogenic interval (0.021 - 0.052 Hz), and the rest part are derived from the cardiac pulse changed periodically. This is the reason why the neurogenic interval took up the second place in averaged wavelet analysis figure.

4.3.2 Pulse & Simulated Experiment Comparison

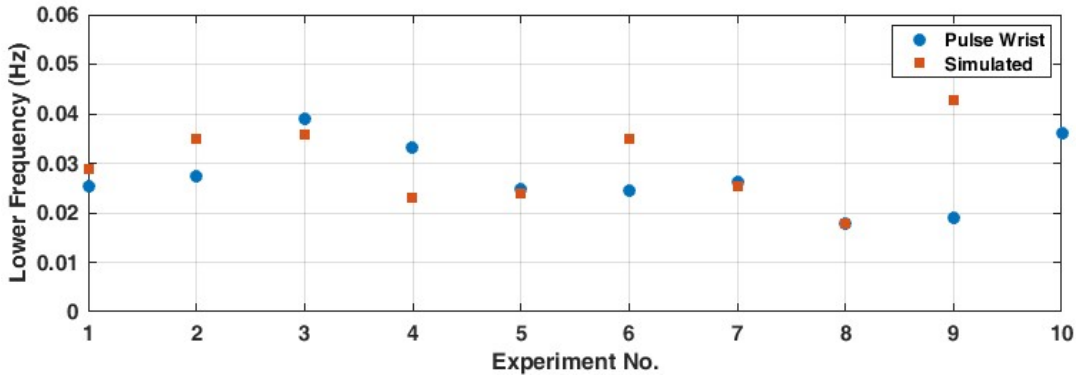

Fig. 1716 Comparison with pulse wrist and simulated results

Combining with the lower frequency results from two experiments would be displayed in the Figure. The results are basically the same in both two groups. The results are all focused on the 0.03 Hz, suggesting that the cardiac pulse changed periodically indeed exists in the blood stream, and it produced 0.03 Hz lower frequency.

Chapter 5 - Computation Modeling of Vasomotion (Myogenic)

5.1 Modeling of Vasomotion

For the analysis of the observed mechanism of observed changes in the LDF spectroscopic measurements for Chize (A1) (Chapter 3), a series of theoretical models was employed to develop a nonlinear model of microvascular spontaneous (vascular) oscillations. Koenigsberger et al. developed a dynamic model of the molecular mechanism of this myogenic oscillation. (2005). Arciero and Secomb improved the model on the basis of the original. The developed phenomenological model reflects the oscillation of arteriolar diameter and blood flow under the tension of the vessel wall and shares the stress. In these models, vascular motion involves the oscillatory contraction of vascular smooth muscle (VSM) in the arteriolar wall, which is caused by the interaction between the mechanical tension of the vessel wall and the dynamics of tone generation in the VSM.

In this study, a version of the vasomotion model developed in Arciero and Secomb was used and extended to consider the myogenic oscillation of arteriolar wall caused by synchronous calcium oscillation of VSM. Subsequently, the cardiac pulse changed periodically factor was added, leading to the production of 0.03 Hz to the created model to make it more practical.

5.2 Creating Model by Equations

A theoretical model is conducted by the length-tension characteristics of vessel walls containing vascular smooth muscle (VSM). Arciero and Secomb (Arciero and Secomb 2012) pointed out that increasing the intravascular pressure and shear stress of luminal wall would result in the arteriolar constriction (myogenic response) and arteriolar dilation, respectively. Starting with the tension equation in the vessel wall, T_{tot} (D) is the tension generated by the VSM in the vessel wall, defined by its passive T_{pass} (D) and active T_{act} (D) components, and A (D) is the degree of VSM activation or tone (ranges from 0 and 1):

$$T_{\text{tot}}(D) = T_{pass}(D) + A(D)T_{act}(D)$$

Where T_{pass} (D) and T_{act} (D):

$$T_{\text{pass}}(D) = C_{pass}\exp(C'_{pass}(\frac{D}{D_0}-1))$$

$$T_{act}(D) = C_{act}\exp(-\frac{D/D_0 - C'_{act}}{C''_{act}})$$

T_{pass} (D) is an exponential function of diameter due to the circumferential stretch increased rapidly. D_0 presents the passive diameter of the vessel within an intraluminal pressure **(13.3 kPa)**. C_{pass} and C'_{pass} represent the passive tension at D_0 and the steepness of the curve. For the active tension (T_{act}), it is derived from a Gaussian function of diameter, and represents the property of tension at various smooth muscle lengths. The rest parameters named C_{act}, C'_{act} and C''_{act} are represented by the peak magnitude, peak location and the curve width of the Gaussian, respectively.

In terms of the activation function, a value (A_{tot}) is taken from 0 to 1 under steady-state condition. This value could be defined as a sigmoidal function of a stimulus S combined by various response mechanisms:

$$A_{\text{tot}}(S) = (1 + e^{-S})^{-1}$$

Where

$$S = C_{myo}T - C_{shear}\tau + C'_{tone}$$

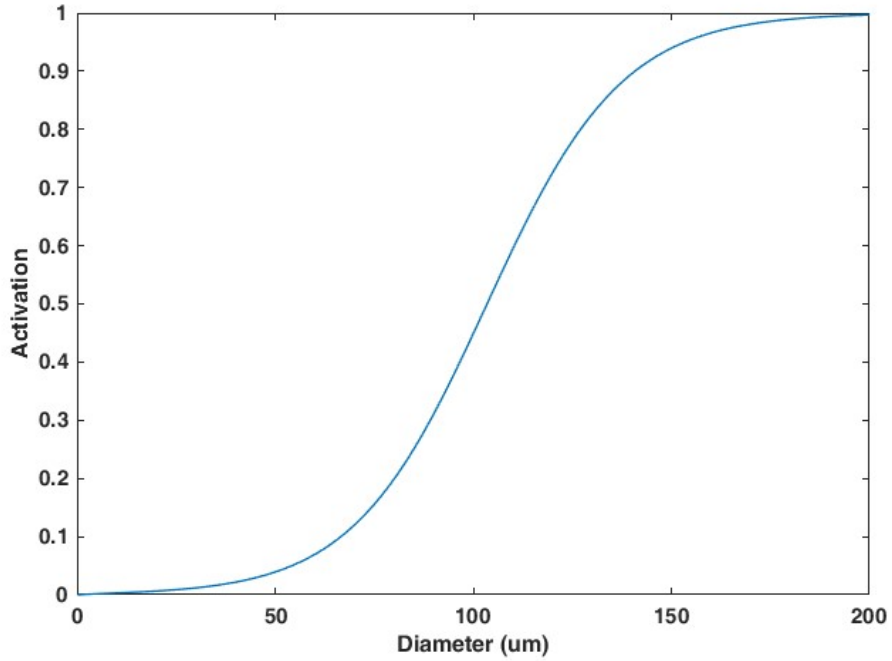

Fig. 5.1 Activation - diameter phase plane

From the above equation, the first term C_{myo} in function S corresponds to the myogenic response to the wall tension. The second term C_{shear} presents the shear-dependent response and C'_{tone} is a constant. Tension (T) of VSM is generated by intravascular pressure, and the wall share stress (τ) results from the blood flow in small vessels.

Under the non-steady conditions, two Ordinary Differential Equations (ODEs) (Arciero and Secomb 2012) describe: (1) The change in arterial diameter D and (2) The dynamics of force generation within the VSM:

$$\frac{\mathrm{d}D}{dt} = \frac{1}{\tau_d}\frac{D_0}{T_0}(T(D) - T_{tot}(D))$$

$$\frac{dA}{dt} = \frac{1}{\tau_a}(A(D) - A_{tot}(D))$$

Where T (D) =PD/2 represents the wall tension due to intra-vascular pressure (P) in accordance with Laplace's law. D_0 and T_0 are constant values of vessel diameter and tension (Table 3). In order to reproduce low-frequency spontaneous oscillations, the time scales τ_d and τ_a are determined by 5s and 60s, respectively (Arciero and Secomb 2012).

Table 3 Parameters of theoretical model (Arciero and Secomb, 2012)

Parameters	Parameters values	Parameters	Parameters values
ΔP	120 kdyn/cm^2	C''_{act}	0.3
C_{Pass}	1.04 kdyn/cm	C_{myo}	0.01 cm/dyn
C'_{act}	8.3	C_{shear}	0.03 cm^2/dyn
D_0	156 μm	τ	8 dyn/cm^2
C_{act}	1.6 kdyn/cm	C'_{tone}	-5.7

C'_{act}	0.68

It is assumed that myogenic oscillations of small arteries and arterioles containing VSMs are generated by synchronous calcium oscillations in smooth muscle cells (SMCs), forcing oscillations of vessel diameter. To describe these myogenic oscillations of the vascular diameter, additional tension Tm was introduced into T_{tot} Equation in the form of forcing oscillatory function of amplitude Am and frequency fm:

$$T_{\mathrm{m}} = A_m \sin(2\pi f_m t)$$

Frequency of the myogenic oscillation in the model was taken as f_m =0.11Hz corresponding to the typical LDF signal from Chize acupoint shown in Fig.5.2

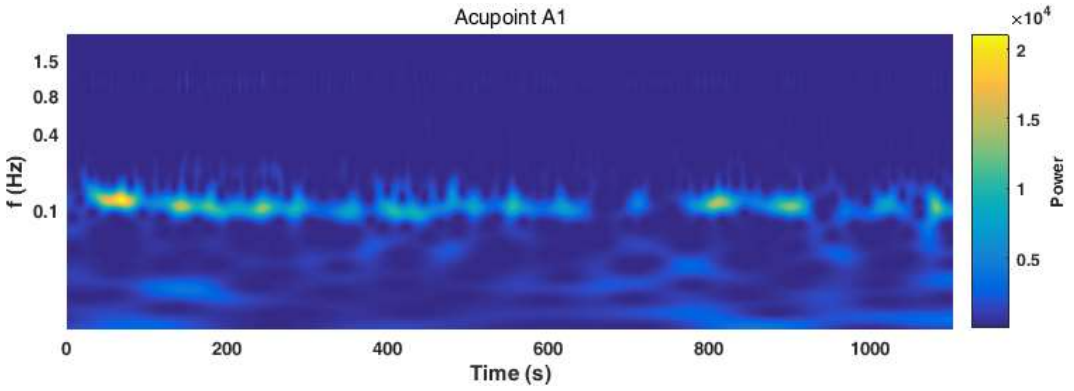

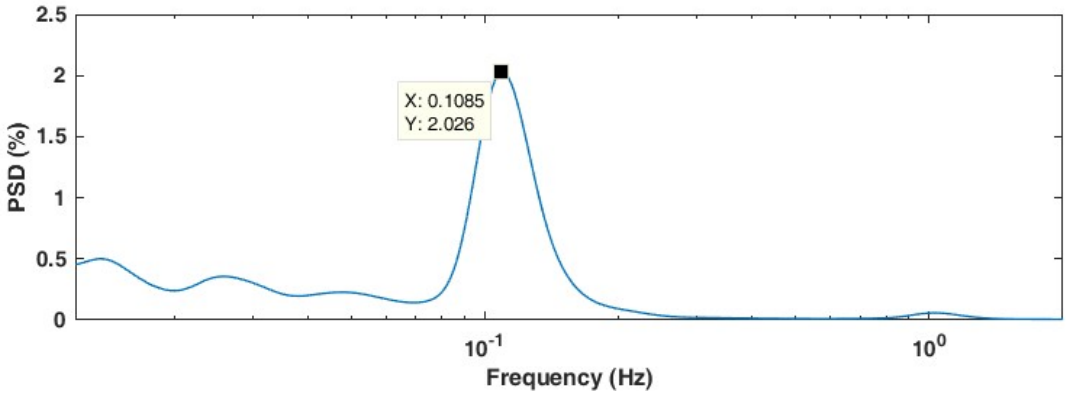

Fig. 5.2 wavelet & averaged wavelet analysis of Chize (A1)

In the model, it is suggested that oscillations of the LDF signals result from the oscillations of the platelet velocity induced by active oscillations of the arteriole radius. In accordance with the Hagen - Poiseuille law:

$$Q = \frac{\pi \Delta P}{R} = \frac{\mathrm{r}^4 \pi \Delta P}{8 \eta L}$$

Arteriole radius oscillations cause fluctuations in the hydraulic viscous resistance of an arteriole, which have an inverse relation with the fourth power of the arteriole radius r, the oscillation of the LDF signals, proportional to Q, is defined by the active oscillation of the arteriole radius r.

5.3 The Initial Theoretical Model

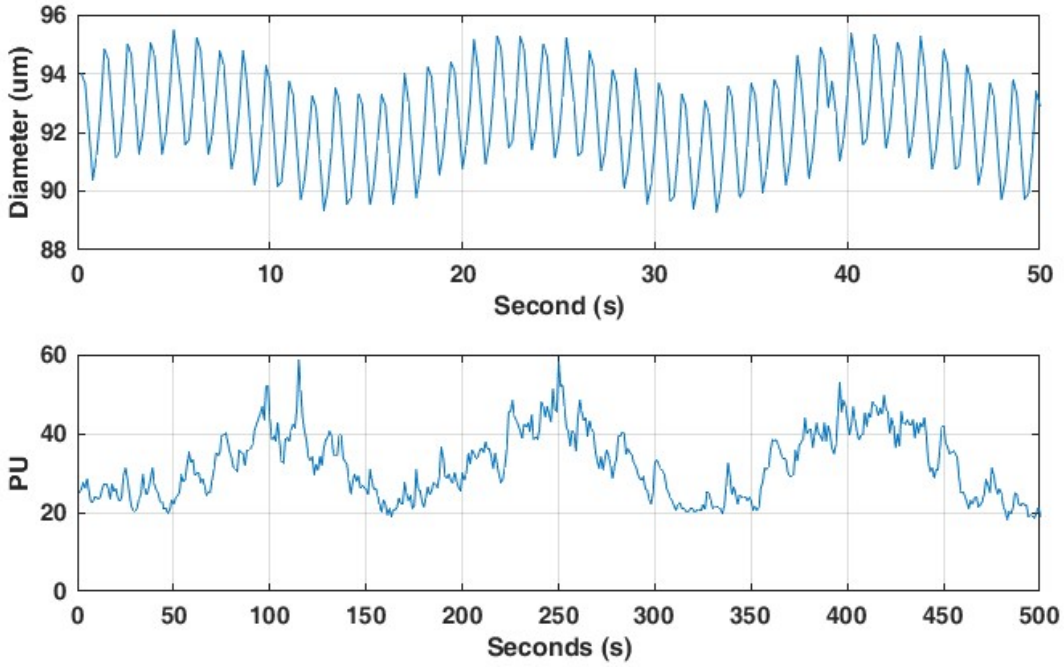

Fig.5.3 Comparison with theoretical model and LDF time series of Chize (A1)

Fig. 5.3 gives an example for vasomotion in the large arteriole with Amplitude is equal to 1 and a piece of real LDF signal from acupoint Chize (A1). It can be seen that the pattern of two Figures are roughly same. The only difference is that the radius of the simulated vessel is constant due to the pressure difference across the arteriole segment. According to the results obtained in Chapter 4, the real vasomotion should involve physiological and physical mechanism, so the physical mechanism would produce the lower frequency around 0.03 Hz. Based on the created model, we added the 0.03 Hz into the T_{tot} Equation. (As shown in Fig. 5.4&5.5)

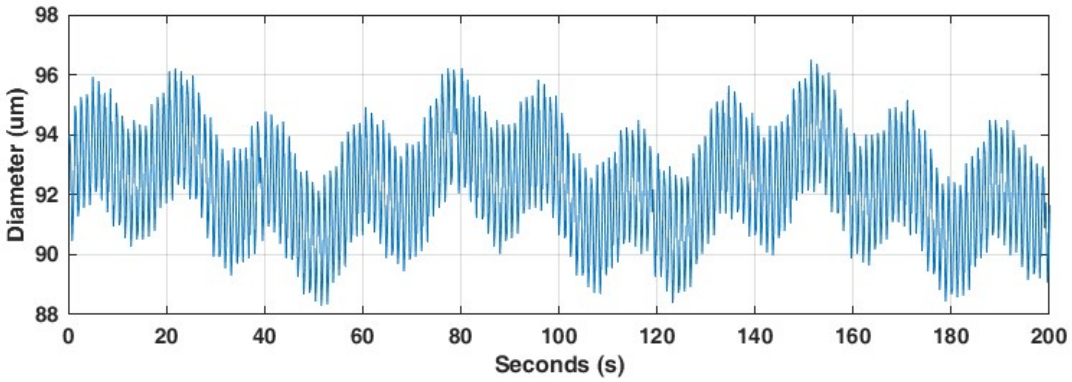

Fig. 5.4 Time series of Theoretical model

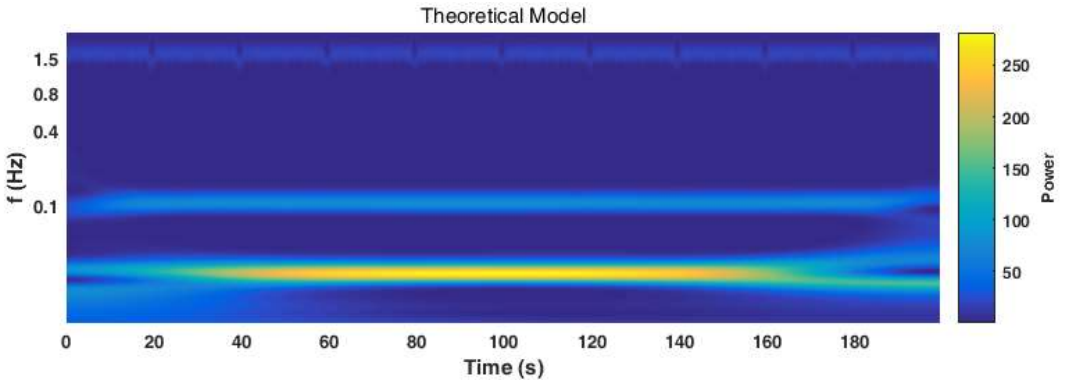

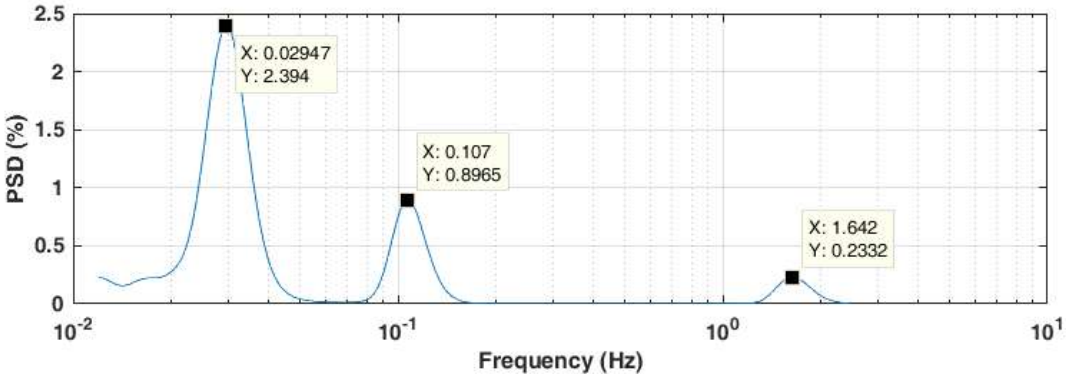

Fig. 5.5 Wavelet & averaged wavelet analysis of Theoretical model

Chapter 6 - Concluding Remarks

6.1 Discussion & Conclusion

The acupoints were discovered in China thousands of years ago. They exist in all parts of the body. The doctor of traditional Chinese medicine used a specific needle to insert the acupoint on skin, which is called acupuncture. According to the stimulation by needling, the acupuncture used most commonly for pain relief including low back pain, shoulder stiffness and knee pain.

For the assumption of this study, the differences between Acupoint and non-acupoint were considered related to the skin blood oscillation. Accordingly, the experiment selected seven measured points (six acupoints and one non-acupoint) on forearm. Based on the measured results, we used the several methods to figure out the differences. From relate energy contribution in wavelet, the acupoint B1 is obviously associated with the heart activity in FR1, which occupied the dominant place. In accordance with the TCM theory, the acupoint B1 (quze) acupuncture is for healing the cardiac pain, palpitation. Thus, the skin blood flow oscillation under B1 could reflect the cardiac activity. Moreover, the FR2 associated with the respiration shows that the RECs of acupoint B1 & B2 are much higher than rest measured points. Thus, needling on B1 & B2 acupoint also increase the respiration better than other points. In terms of the FR3, the Figure shows that the A1 & A2 have remarkable myogenic component (~0.1 Hz). The myogenic mechanism is arteries and arterioles react to an increase or decrease of blood pressure to keep the blood flow. Thus, the A1 & A2 could serve as a predicting point for high blood pressure. For FR4, the acupoint C1 (shaohai) have more sensitivity neurogenic component, The TCM theory also reported that the

acupuncture of shaohai is employed for treating neurasthenia, intercostal neuralgia, ulnar nerve neuralgia, etc. As a result, almost of the REC results are consistent with the TCM theory.

From the noise analysis results, the exponent value of seven measured points shown that the acupoint A1 & A2 & C1 are equally around 1.5, tending to the brown noise. This can also be explained that the skin blood flow oscillation of these three acupoints follow a certain oscillation rule. Combining with the SNR analysis, it can be observed that the SNR 0.1 Hz situation is the same as the noise analysis. Obviously, 0.1 Hz energy could impact the noise analysis type, whereas 0.3 Hz energy is irrelevant with the noise analysis.

According to the different blood oscillations of the skin in different positions of the forearm, we believe that vasomotion is not only caused by mechanism conditions (e.g., smooth muscle cell releasing Ca+, endothelium - niric oxide (No) - cGMP axis, etc.) but also dependent on some physical factors. From the beginning of the simulation experiment (infusion device combined with LDF device), the blood flow through a single vessel can be simulated. Besides, this simulated experiment simplifies all parameter and makes all parameters constant except the falling speed of droplet. After nine experiments based on different droplet frequencies, this study found that the lower frequency around 0.03 Hz would be produced all the time. Accordingly, to verify our assumption, we compare the simulated results with the signals captured from pulse wrist also by using LDF. Consequently, both of the two experimental results displayed significantly value of PSD of lower frequency (0.03 Hz). This suggests that the cardiac pulse changed periodically do produce the lower frequency 0.03 Hz not only generated by the neurogenic interval.

Furthermore, according to the previous studies, the myogenic model composed of multiple parameters creates a new research area in future. On Chapter 5, we only take the Chize acupoint as an example due to the higher myogenic component occupied. Based on the conclusion drawn in the fourth chapter, 0.03 Hz was added to the original basis to make the model more practical. The aim of the future work is to build a model of each acupoint or non-acupoint, each acupoint model have its own specific feature so that the common point can be found between acupoints.

6.2 Future Work

In general, the current progress have provided some results and research methods for deep understanding the role of vasomotion in forearm acupoints. To thoroughly understand this problem, there are still a lot of work to do in the future. We suggest the future work as following:

6.2.1 Comparison of acupoints and non - acupoints on arm

- Recruiting more volunteers to compare performance of vasomotion in studied acupoints at different ages.
- We also need to recruit patients with hypertension and diabetes to measure acupoints and non-acupoints on their arms.
- Explore out other acupoints that have not been researched along with arm, calculate their correlation and signal feature of oscillating signal within lower frequency range.
- Seeking the cooperation with local acupuncture experts, and compare the vasomotion results of forearm acupoints by using acupuncture stimulated.

6.2.2 Mathematical modelling

- Establish the corresponding healthy subject mathematical model for rest acupoints according to their specific frequency characteristic. The established model would be considered as the reference standard of healthy person.

- Compare the calculated mathematical model with the actual data of patient (hypertension, diabetes) on specific acupoint. We can predict potential diseases from the different outcome of spectral analysis.

Reference

Aalkjær, C., D. Boedtkjer and V. Matchkov (2011). "Vasomotion - what is currently thought?" Acta Physiologica **202**(3): 253–269.

Aalkjaer, C. and H. Nilsson (2005). "Vasomotion: cellular background for the oscillator and for the synchronization of smooth muscle cells." British Journal of Pharmacology **144**(5): 605-616.

Addison, P. S. (2016). "The Illustrated Wavelet Transform Handbook." Science Engineering Medicine & Finance Institute of Physics Publishing.

Ahn, A. C., A. P. Colbert, B. J. Anderson, Ø. G. Martinsen, R. Hammerschlag, S. Cina, P. M. Wayne and H. M. Langevin (2008). "Electrical properties of acupuncture points and meridians: A systematic review." Deutsche Zeitschrift Fuer Akupunktur **51**(3): 48-49.

Aird, M., M. Coyle, D. M. Cobbin and C. Zaslawski (2000). "A study of the comparative accuracy of two methods of locating acupuncture points." Acupuncture in Medicine **18**(1): 15-21.

AnetaStefanovska (1999). "Physics of the human cardiovascular system." Contemporary Physics **40**(1): 31-55.

Arciero, J. C. and T. W. Secomb (2012). "Spontaneous oscillations in a model for active control of microvessel diameters." Mathematical Medicine & Biology A Journal of the Ima **29**(2): 163.

Avogaro, A. and S. V. de Kreutzenberg (2005). "Mechanisms of endothelial dysfunction in obesity." Clinica Chimica Acta **360**(1-2): 9-26.

Bajrovic, F., M. Cencur, M. Hozic, S. Ribaric and A. Stefanovska (2000). "The contribution of lumbar sympathetic neurones activity to rat's skin blood flow oscillations." Pflügers Archiv **439**(1): r158-r160.

Bao, D. P., H. E. Xin, X. M. Pang and P. Han (2017). "Therapeutic Observation of Electroacupuncture plus Nasal Irrigation for Upper Airway Cough Syndrome." Shanghai Journal of Acupuncture & Moxibustion.

Berliner, M. N. (1997). "Skin microcirculation during tapwater iontophoresis in humans: cathode stimulates more than anode." Microvascular Research **54**(1): 74.

Bertuglia, S., A. Colantuoni, G. Coppini and M. Intaglietta (1991). "Hypoxia- or hyperoxia-induced changes in arteriolar vasomotion in skeletal muscle microcirculation." Am J Physiol **260**(2): 362-372.

Bocchi, L., A. Evangelisti, M. Barrella, L. Scatizzi and M. Bevilacqua (2010). "Bocchi L, Evangelisti A, Barrella M, et al. Recovery of 0.1 Hz microvascular skin blood flow in dysautonomic diabetic (type 2) neuropathy by using Frequency Rhythmic Electrical Modulation System (FREMS)." Medical Engineering & Physics **32**(4): 407-413.

Boggett, D., J. Blond and P. Rolfe (1985). "Laser Doppler measurements of blood flow in skin tissue." Journal of Biomedical Engineering **7**(3): 225-232.

Bollinger, A., A. Yanar, U. Hoffmann and U. K. Franzeck (2015). "Is High-Frequency Flux Motion due to Respiration or to Vasomotion Activity?1." Przegląd Lekarski **60 Suppl 6**(2): 60-64.

Bouskela, E. and W. Grampp (1992). "Spontaneous vasomotion in hamster cheek pouch arterioles in varying experimental conditions." American Journal of Physiology **262**(2): 478-485.

Bracic, M. and A. Stefanovska (1998). "Wavelet-based analysis of human blood-flow dynamics." Bulletin of Mathematical Biology **60**(5): 919-935.

Chen, G., H. Suzuki and A. H. Weston (1988). "Acetylcholine releases endothelium ‐ derived hyperpolarizing factor and EDRF from rat blood vessels." British journal of pharmacology **95**(4): 1165-1174.

Cines, D. B., E. S. Pollak, C. A. Buck, J. Loscalzo, G. A. Zimmerman, R. P. McEver, J. S. Pober, T. M. Wick, B. A. Konkle and B. S. Schwartz (1998). "Endothelial cells in physiology and in the pathophysiology of vascular disorders." Blood **91**(10): 3527-3561.

Cleaver, O. and D. A. Melton (2003). "Endothelial signaling during development." Nature medicine **9**(6): 661.

Clemson, P. T. and A. Stefanovska (2014). "Discerning non-autonomous dynamics." Physics Reports **542**(4): 297-368.

Colantuoni, A., S. Bertuglia and M. Intaglietta (1984). "Quantitation of rhythmic diameter changes in arterial microcirculation." Am J Physiol **246**(2): 508-517.

Costa, C. and R. Virag (2009). "The endothelial–erectile dysfunction connection: An essential update." The journal of sexual medicine **6**(9): 2390-2404.

Coyle, M., M. Aird, D. M. Cobbin and C. Zaslawski (2000). "The Cun measurement system: an investigation into its suitability in current practice." National Municipal Review **18**(1): 10-14.

Cracowski, J. L., C. T. Minson, M. Salvatmelis and J. R. Halliwill (2006). "Methodological issues in the assessment of skin microvascular endothelial function in humans." Trends in Pharmacological Sciences **27**(9): 503.

Cracowski, J. L. and M. Roustit (2016). "Current Methods to Assess Human Cutaneous Blood Flow: An Updated Focus on Laser‐Based‐Techniques." Microcirculation **23**(5): 337-344.

Dolger, H. (1950). "Vascular complications of diabetes mellitus." Bulletin of the New York Academy of Medicine **26**(12): 779.

Eliseyeva, M. R. (2013). "Endothelium: a long road from mystery to discovery." International J Biomedicine **3**(1): 9-11.

Endemann, D. H. and E. L. Schiffrin (2004). "Endothelial dysfunction." Journal of the American Society of Nephrology **15**(8): 1983-1992.

Favero, G., C. Paganelli, B. Buffoli, L. F. Rodella and R. Rezzani (2014). "Endothelium and its alterations in cardiovascular diseases: life style intervention." BioMed research international **2014**.

Félétou, M. and P. M. Vanhoutte (1996). "ENDOTHELIUM - DERIVED HYPERPOLARIZING FACTOR." Clinical and experimental pharmacology and physiology **23**(12): 1082-1090.

Fishman, A. P. (1982). "Endothelium: a distributed organ of diverse capabilities." Annals of the New York Academy of Sciences **401**(1): 1-8.

Florey, L. (1966). "The endothelial cell." Br Med J **2**(5512): 487-490.

Frelin, C., A. Ladoux and G. D'angelo (2000). "Vascular endothelial growth factors and angiogenesis."

Furchgott, R. F. and J. V. Zawadzki (1980). "The obligatory role of endothelial cells in the relaxation of arterial smooth muscle by acetylcholine." nature **288**(5789): 373.

Germain, A. M., M. C. Romanik, I. Guerra, S. Solari, M. S. Reyes, R. J. Johnson, K. Price, S. A. Karumanchi and G. Valdés (2007). "Endothelial dysfunction: a link among preeclampsia, recurrent pregnancy loss, and future cardiovascular events?" Hypertension **49**(1): 90-95.

Gilden, D. L. (2001). "Cognitive emissions of 1/f noise." Psychological Review **108**(1): 33-56.

Goldman, D. and A. S. Popel (2001). "A Computational Study of the Effect of Vasomotion on Oxygen Transport from Capillary Networks." Journal of Theoretical Biology **209**(2): 189.

His, W. (1865). Die Häute und Höhlen des Köpers: academisches Programm, Schweighauser.

Holden, J. G. (2005). "Gauging the fractal dimension of response times from cognitive tasks."

Hong, M., S. S. Park, Y. Ha, J. Lee, K. Yoo, G. J. Jhon, M. Suh and Y. Lee (2012). "Heterogeneity of Skin Surface Oxygen Level of Wrist in Relation to Acupuncture Point." Evidence-Based Complementray and Alternative Medicine,2012,(2012-5-16) **2012**(3): 106762.

Hsiu, H., W.-C. Hsu, C.-L. Hsu and S.-M. Huang (2011). "Assessing the effects of acupuncture by comparing needling the hegu acupoint and needling nearby nonacupoints by spectral analysis of

microcirculatory laser Doppler signals." Evidence-Based Complementary and Alternative Medicine **2011**.

Hu, S., K. Maslov and L. V. Wang (2009). "Noninvasive label-free imaging of microhemodynamics by optical-resolution photoacoustic microscopy." Optics Express **17**(9): 7688.

Iatsenko, D., P. V. Mcclintock and A. Stefanovska (2015). "Nonlinear mode decomposition: A noise-robust, adaptive decomposition method." Physical Review E Statistical Nonlinear & Soft Matter Physics **92**(3): 032916.

Ignarro, L. J., G. M. Buga, K. S. Wood, R. E. Byrns and G. Chaudhuri (1987). "Endothelium-derived relaxing factor produced and released from artery and vein is nitric oxide." Proceedings of the National Academy of Sciences **84**(24): 9265-9269.

Jaffe, E. A., R. L. Nachman, C. G. Becker and C. R. Minick (1973). "Culture of human endothelial cells derived from umbilical veins. Identification by morphologic and immunologic criteria." The Journal of clinical investigation **52**(11): 2745-2756.

Jang, S., S. Park, B. H. Jang, Y. L. Park, J. A. Lee, C. S. Cho, H. Y. Go, Y. C. Shin and S. G. Ko (2017). "Study protocol of a pragmatic, randomised controlled pilot trial: clinical effectiveness on smoking cessation of traditional and complementary medicine interventions, including acupuncture and aromatherapy, in combination with nicotine replacement therapy." Bmj Open **7**(5): e014574.

Jones, T. W. (1852). "Discovery That the Veins of the Bat's Wing (Which are Furnished with Valves) are Endowed with Rythmical Contractility, and That the Onward Flow of Blood is Accelerated by Each Contraction." Abstracts of the Papers Communicated to the Royal Society of London **6**: 147-149.

Julien, C. (2006). "The enigma of Mayer waves: Facts and models." Cardiovascular Research **70**(1): 12.

Kaiser, G. (2011). A friendly guide to wavelets, s.n.].

Kalogeris, T., C. P. Baines, M. Krenz and R. J. Korthuis (2012). Cell biology of ischemia/reperfusion injury. International review of cell and molecular biology, Elsevier. **298:** 229-317.

Kastrup, J., J. Bülow and N. A. Lassen (1989). "Vasomotion in human skin before and after local heating recorded with laser Doppler flowmetry. A method for induction of vasomotion." International Journal of Microcirculation Clinical & Experimental **8**(2): 205.

Kaufman, A. G. and M. Intaglietta (1985). "Automated diameter measurement of vasomotion by cross-correlation." International Journal of Microcirculation Clinical & Experimental **4**(1): 45-53.

Keselbrener, L. and S. Akselrod (1996). "Selective discrete Fourier transform algorithm for time-frequency analysis: method and application on simulated and cardiovascular signals." IEEE transactions on bio-medical engineering **43**(8): 789.

Koenigsberger, M., R. Sauser, D. Seppey, J. L. Bény and J. J. Meister (2008). "Calcium dynamics and vasomotion in arteries subject to isometric, isobaric, and isotonic conditions." Biophysical Journal **95**(6): 2728-2738.

Kvandal, P., S. A. Landsverk, A. Bernjak, A. Stefanovska, H. D. Kvernmo and K. A. Kirkebøen (2006). "Low-frequency oscillations of the laser Doppler perfusion signal in human skin." Microvascular Research **72**(3): 120-127.

Kvandal, P., A. Stefanovska, M. Veber, H. D. Kvernmo and K. A. Kirkebøen (2003). "Regulation of human cutaneous circulation evaluated by laser Doppler flowmetry, iontophoresis, and spectral analysis: importance of nitric oxide and prostaglandines." Microvascular Research **65**(3): 160-171.

Kvernmo, H. D., A. Stefanovska and K. A. Kirkebøen (2003). "Enhanced endothelial activity reflected in cutaneous blood flow oscillations of athletes." European Journal of Applied Physiology **90**(1-2): 16-22.

Kvernmo, H. D., A. Stefanovska, K. A. Kirkebøen and K. Kvernebo (1999). "Oscillations in the Human Cutaneous Blood Perfusion Signal Modified by Endothelium-Dependent and Endothelium-Independent Vasodilators ☆." Microvascular Research **57**(3): 298.

Landsverk, S. A., P. Kvandal, A. Bernjak, A. Stefanovska and K. A. Kirkeboen (2007). "The effects of general anesthesia on human skin microcirculation evaluated by wavelet transform." Anesthesia & Analgesia **105**(4): 1012-1019.

Landsverk, S. A., P. Kvandal, T. Kjelstrup, U. Benko, A. Bernjak, A. Stefanovska, H. Kvernmo and K. A. Kirkeboen (2006). "Human skin microcirculation after brachial plexus block evaluated by wavelet transform of the laser Doppler flowmetry signal." Anesthesiology **105**(3): 478-484.

Lehtipalo, S., O. Winsö, L. O. Koskinen, G. Johansson and B. Biber (2000). "Cutaneous sympathetic vasoconstrictor reflexes for the evaluation of interscalene brachial plexus block." Acta Anaesthesiologica Scandinavica **44**(8): 946.

Lo, S. Y. (2002). "Meridians in acupuncture and infrared imaging." Medical Hypotheses **58**(1): 72-76.

Malpas, S. C. (1998). "The rhythmicity of sympathetic nerve activity." Progress in Neurobiology **56**(1): 65-96.

Mandelbrot, B. B. (1999). "Multifractals and 1/f noise." Springer Verlag New York.

Mehta, D. and A. B. Malik (2006). "Signaling mechanisms regulating endothelial permeability." Physiological reviews **86**(1): 279-367.

Moncada, S., R. Gryglewski, S. Bunting and J. Vane (1976). "An enzyme isolated from arteries transforms prostaglandin endoperoxides to an unstable substance that inhibits platelet aggregation." Nature **263**(5579): 663.

Nachman, R. L. (2012). "Endothelium: from cellophane to orchestral maestro." The Journal of clinical investigation **122**(3): 796-797.

Nilsson, H. and C. Aalkjaer (2003). "Vasomotion: mechanisms and physiological importance." Molecular Interventions **3**(2): 79.

Olufsen, M. S., C. S. Peskin, W. Y. Kim, E. M. Pedersen, A. Nadim and J. Larsen (2000). "Numerical simulation and experimental validation of blood flow in arteries with structured-tree outflow conditions." Annals of biomedical engineering **28**(11): 1281-1299.

Orden, G. C. V., H. Kloos and S. Wallot (2011). "Living in the Pink : Intentionality, Wellbeing, and Complexity." Philosophy of Complex Systems: 629-672.

Palmer, R. M., A. Ferrige and S. Moncada (1987). "Nitric oxide release accounts for the biological activity of endothelium-derived relaxing factor." Nature **327**(6122): 524.

Pappano, A. J. and W. G. Wier (2012). Cardiovascular Physiology E-Book: Mosby Physiology Monograph Series, Elsevier Health Sciences.

Pearce, J. (2007). "Malpighi and the discovery of capillaries." European neurology **58**(4): 253-255.

Peng, H., V. Matchkov, A. Ivarsen, C. Aalkjaer and H. Nilsson (2001). "Hypothesis for the initiation of vasomotion." Circulation Research **88**(8): 810-815.

Pohl, U., J. Holtz, R. Busse and E. Bassenge (1986). "Crucial role of endothelium in the vasodilator response to increased flow in vivo." Hypertension **8**(1): 37-44.

Rajan, V., B. L. Varghese, Tg and W. Steenbergen (2009). "Review of methodological developments in laser Doppler flowmetry." Lasers in Medical Science **24**(2): 269-283.

ROSS, G., E. Stinson, J. t. SCHROEDER and R. Ginsburg (1980). "Spontaneous phasic activity of isolated human coronary arteries." Cardiovascular research **14**(10): 613-618.

Rossi, M., A. Bradbury, A. Magagna, M. Pesce, S. Taddei and A. Stefanovska (2011). "Investigation of skin vasoreactivity and blood flow oscillations in hypertensive patients: effect of short-term antihypertensive treatment." Journal of hypertension **29**(8): 1569-1576.

Rossi, M., E. Matteucci, M. Pesce, C. Consani, F. Galetta, O. Giampietro and G. Santoro (2013). "Study of skin vasomotion in type 1 diabetic patients and of its possible relationship with clinical and laboratory variables." Clinical Hemorheology & Microcirculation **53**(4): 357.

Rossi, M., M. Nannipieri, M. Anselmino, M. Pesce, E. Muscelli, G. Santoro and E. Ferrannini (2011). "Skin vasodilator function and vasomotion in patients with morbid obesity: effects of gastric bypass surgery." Obesity Surgery **21**(1): 87-94.

Roustit, M. and J. L. Cracowski (2012). "Non ‐ invasive Assessment of Skin Microvascular Function in Humans: An Insight Into Methods." Microcirculation **19**(1): 47-64.

Rücker, M., O. Strobel, B. Vollmar, F. Roesken and M. D. Menger (2000). "Vasomotion in critically perfused muscle protects adjacent tissues from capillary perfusion failure." American Journal of Physiology Heart & Circulatory Physiology **279**(2): H550.

Safar, P. and P. Kochanek (2000). "Cerebral blood flow promotion after prolonged cardiac arrest." Critical care medicine **28**(8): 3104-3106.

Sakurai, T. and N. Terui (2006). "Effects of sympathetically induced vasomotion on tissue-capillary fluid exchange." American Journal of Physiology Heart & Circulatory Physiology **291**(4): H1761.

Schmidt, J. A., P. Borgström, G. P. Firestone, W. P. Von, M. Intaglietta and A. Fronek (1993). "Periodic hemodynamics (flow motion) in peripheral arterial occlusive disease." Journal of Vascular Surgery **18**(2): 207.

Shepherd, A. P. (1990). History of Laser-Doppler Blood Flowmetry, Springer US.

Sheppard, L. W., V. Vuksanović, P. V. Mcclintock and A. Stefanovska (2011). "Oscillatory dynamics of vasoconstriction and vasodilation identified by time-localized phase coherence." Physics in Medicine & Biology **56**(12): 3583-3601.

Shiogai, Y. (2010). "Nonlinear dynamics of cardiovascular aging." Physics Reports **488**(2-3): 51.

Siegel, G., G. Meyer-Rath, E. Ermilov, M. Rodríguez, M. Malmsten, P. Claesson, R. Saunders, R. Hetzer and B. Lindman (2015). "Flow sensing in the cardiovascular system." Colloids and Surfaces A: Physicochemical and Engineering Aspects **480**: 318-327.

Slaaf, D. W., G. J. Tangelder, H. C. Teirlinck and R. S. Reneman (1987). "Arteriolar vasomotion and arterial pressure reduction in rabbit tenuissimus muscle." Microvascular Research **33**(1): 71-80.

Söderström, T., A. Stefanovska, M. Veber and H. Svensson (2003). "Involvement of sympathetic nerve activity in skin blood flow oscillations in humans." American Journal of Physiology Heart & Circulatory Physiology **284**(5): H1638.

Stam, F., C. van Guldener, C. G. Schalkwijk, P. M. ter Wee, A. J. Donker and C. D. Stehouwer (2003). "Impaired renal function is associated with markers of endothelial dysfunction and increased inflammatory activity." Nephrology Dialysis Transplantation **18**(5): 892-898.

Stefanovska, A., M. Bračič and H. D. Kvernmo (1999). "Wavelet analysis of oscillations in the peripheral blood circulation measured by laser Doppler technique." IEEE transactions on bio-medical engineering **46**(10): 1230-1239.

Stefanovska, A., L. W. Sheppard, T. Stankovski and P. V. E. Mcclintock (2011). "Reproducibility of LDF blood flow measurements: Dynamical characterization versus averaging." Microvascular Research **82**(3): 274.

Stergiopulos, N., C.-A. Porret, S. De Brouwer and J.-J. Meister (1998). "Arterial vasomotion: effect of flow and evidence of nonlinear dynamics." American Journal of Physiology-Heart and Circulatory Physiology **274**(6): H1858-H1864.

Stern, M. D. (1975). "In vivo evaluation of microcirculation by coherent light scattering." Nature **254**(5495): 56-58.

Stern, M. D., D. L. Lappe, P. D. Bowen, J. E. Chimosky, H. G. Jr, H. R. Keiser and R. L. Bowman (1977). "Continuous measurement of tissue blood flow by laser-Doppler spectroscopy." Am.j.physiol **232**(4): H441.

Steyers, C. M. and F. J. Miller (2014). "Endothelial dysfunction in chronic inflammatory diseases." International journal of molecular sciences **15**(7): 11324-11349.

Ticcinelli, V., R. Martini and A. Bagno (2014). "Preliminary study of laser doppler perfusion signal by wavelet transform in patients with critical limb ischemia before and after revascularization." Clinical Hemorheology & Microcirculation **58**(3): 415-428.

Tong, X.-K., N. Nicolakakis, A. Kocharyan and E. Hamel (2005). "Vascular remodeling versus amyloid β-induced oxidative stress in the cerebrovascular dysfunctions associated with Alzheimer's disease." Journal of Neuroscience **25**(48): 11165-11174.

Tsai, A. G. and M. Intaglietta (1993). "Evidence of flowmotion induced changes in local tissue oxygenation." Int J Microcirc Clin Exp **12**(1): 75-88.

Urbančič-Rovan, V., A. Bernjak, A. Stefanovska, K. Ažman-Juvan and A. Kocijančič (2006). "Macro- and microcirculation in the lower extremities—possible relationship." Diabetes research and clinical practice **73**(2): 166-173.

van Leeuwenhoek, A. (1800). The select works of anthony van leeuwenhoek: containing his microscopical discoveries in many of the works of nature, translator.

Vane, J. R., E. E. Änggård and R. M. Botting (1990). "Regulatory functions of the vascular endothelium." New England Journal of Medicine **323**(1): 27-36.

Veber, M., A. Bandrivskyy, P. B. Clarkson, P. V. Mcclintock and A. Stefanovska (2004). "Wavelet analysis of blood flow dynamics: effect on the individual oscillatory components of iontophoresis with pharmacologically neutral electrolytes." Physics in Medicine & Biology **49**(8): N111-117.

Vesna Vuksanović, L. W. S., Aneta Stefanovska (2008). "Nonlinear relationship between level of blood flow and skin temperature for different dynamics of temperature change." Biophysical Journal **94**(10): 78-80.

Wagenmakers, E. J., S. Farrell and R. Ratcliff (2004). "Estimation and interpretation of 1/falpha noise in human cognition." Psychon Bull Rev **11**(4): 579-615.

Wang, B. H., C. L. Lin, T. M. Li, S. D. Lin, J. G. Lin and C. Li-Wei (2014). "Selection of acupoints for managing upper-extremity spasticity in chronic stroke patients." Clinical Interventions in Aging **9**(default): 147-156.

Xu, B., X. C. Yu, C. Y. Chen, L. L. Wang, J. L. Liu, Z. S. Liu, J. H. Gao, X. J. Chang and L. Chen (2010). "[Relationship between efficacy of electroacupuncture and electroacupuncture stimulation of different acupoints and different tissue layers of acupoint area in hypotension plus bradycardia rats]." Acupuncture Research **35**(6): 422.

Yanagisawa, M., H. Kurihara, S. Kimura, Y. Tomobe, M. Kobayashi, Y. Mitsui, Y. Yazaki, K. Goto and T. Masaki (1988). "A novel potent vasoconstrictor peptide produced by vascular endothelial cells." nature **332**(6163): 411.

Young, J. (1929). Malpighi's “De pulmonibus.”, SAGE Publications.